Republic of Iraq

Ministry of Higher Education and Scientific Research

University of Babylon

College of Science

Department of Physics

Theoretical and Experimental Investigations on Some Characteristics of Organic Material Doped with Nanoparticles for Recent Applications

A Thesis

Submitted to the Council of the College of Science / University of Babylon in Partial Fulfillment of the Requirements for the Degree of Doctor in Philosophy of Sciences in Physics

By

Huda Bukheet Hasan Atiaa

B.Sc. in Physics (2005)

M.Sc. in Physics (2011)

Supervised by

Prof. Dr. Hayder M. Abduljalil **Prof. Dr. Ahmed H. Mohaisen**

2022 A.D **1443 A.H**

Dedication

To :

Soul of my present absent husband, Muhammad, may God have mercy upon him…

My Love and Hope…Dear Mother

My Sweet kids…Mustafa ,Ruqiya ,Redha and Karar

with my love

My Brothers and Sisters with My Great Love

Huda

Supervisor Certification

We certify that this thesis entitled (***Theoretical and Experimental Investigations on Some Characteristics of Organic Material Doped with Nanoparticles for Recent Applications***)was prepared by (***Huda Bukheet Hasan*** **Atiaa)** under our supervision at Department of Physics, College of Sciences, University of Babylon, as a partial fulfillment of the requirements of Ph.D. degree in the theoretical physics.

Supervisors

Signature :

Name: **Dr. Hayder M. Abduljalil**
Title : Professor
Address:

Department of Physics
College of Science
University of Babylon

Date : / 7 / 2022

Signature :

Name: **Dr. Ahmed H. Mohaisen**
Title : Professor
Address:

Department of Physics
College of Education for Pure Science
University of Babylon

Date : / 7 / 2022

Certification of the Head of Physics department

In view of the available recommendation, I forward this thesis for debate by the Examining Committee.

Signature:

Name: **Dr. Abdulazeez O. Mousa Al-Ogaili**

Title: Professor

Date: / 7 / 2022

جمهورية العراق
وزارة التعليم العالي والبحث العلمي
جامعة بابل
كلية العلوم
قسم الفيزياء

استقصاءات نظرية وعملية على بعض الخصائص لمادة عضوية مشوبة بجسيمات نانوية للتطبيقات الحديثة

اطروحة مقدمة إلى مجلس كلية العلوم - جامعة بابل

وهي جزء من متطلبات نيل درجة الدكتوراه في فلسفة علوم الفيزياء

من قبل

هدى بخيت حسن عطية

بكالوريوس علوم فيزياء (2005)

ماجستير علوم فيزياء (2011)

بإشراف

أ .د. حيدر محمد عبد الجليل

أ. د. احمد هاشم محيسن

١٤٤٣ هـ

٢٠٢٢ م

بِسْمِ اللَّهِ الرَّحْمَنِ الرَّحِيمِ

إِنَّا فَتَحْنَا لَكَ فَتْحًا مُّبِينًا ۞ لِّيَغْفِرَ لَكَ اللَّهُ

مَا تَقَدَّمَ مِن ذَنبِكَ وَمَا تَأَخَّرَ وَيُتِمَّ نِعْمَتَهُ عَلَيْكَ

وَيَهْدِيَكَ صِرَاطًا مُّسْتَقِيمًا ۞ وَيَنصُرَكَ اللَّهُ

نَصْرًا عَزِيزًا ۞

صدق الله العلي العظيم

سورة الفتح آية (١-٣)

Acknowledgments

First, I should like to express my deep thanks to the Almighty God, ALLAH JALA JALALAH, for what I have been.

I extend my thanks and gratitude to my professors and my supervisors for this research Prof. Dr. Hayder M. Abduljalil and Prof. Dr. Ahmed H. Mohaisen Who did not hesitate to give a helping hand and advices. I am grateful to the Dean of the college of science and the chairman of physics department for their help.

Special thanks are due to Prof .Dr. Nahida Bukheet Hasan and Asst. Prof. Dr. Hind A. Mohammed Roof for their encouragement and help.

huda

Examining Committee Certificate

We certify that we have read this thesis entitled " ***Theoretical and Experimental Investigations on Some Characteristics of Organic Material Doped with Nanoparticles for Recent Applications*** **"** and as an examining committee, examined the Ph.D. student " ***Huda Bukheet Hasan Atiaa***" in its content and that, in our opinion it meets the standards of a thesis for the degree of Doctor of Science of Philosophy in the theoretical physics.

Signature:
Name: **Dr. Abdulazeez O. Mousa Al-Ogaili**
Title: Professor
Address: Department of Physics/ College of Science / University of Babylon
Date: / / 2022
(Chairman)

Signature:
Name: **Dr. Shurooq Sabah Abed Al-Abbas**
Title: Professor
Address: Dep. of Physics /College of Education for Pure Science/University of Babylon
Date: / / 2022
(Member)

Signature:
Name: **Dr. Amera Abo Al-Sood**
Title: Professor
Address: Dep. of Physics / College of Science / University of Babylon
Date: / / 2022
(Member)

Signature:
Name: **Ansam Jameel Talib**
Title: Assistant Professor
Address: Dep. of Physics/ College of Science/ University of Thi-Qar
Date: / / 2022
(Member)

Signature:
Name: **Dr. Hussein Hakim Abed**
Title: Assistant Professor
Address: Dep. of Physics/ College of Science/ University of Babylon
Date: / / 2022
(Member)

Signature:
Name: **Dr. Hayder M. Abduljalil**
Title: Professor
Address: Dep. of Physics/ College of Science/ University of Babylon
Date: / / 2022
(Member and Supervisor)

Signature:
Name: **Dr. Ahmed H. Mohaisen**
Title: Professor
Address: Dep. of Physics/ College of Education for Pure Science / University of Babylon
Date: / / 2022
(Member and Supervisor)

Approved by the college committee on graduate studies:

Signature:
Name: Dr. Faez Ali Rashid Almaamori
Title: Professor.
Address: Dean of the College of Sciences / University of Babylon
Date: / / 2022

الخلاصة

تم استقصاء الدراسات النظرية والتجريبية للخصائص التركيبية والبصرية للمتراكبات النانوية ($PEO-CuO-In_2O_3$) و ($PEO-NiO-In_2O_3$) وتطبيقاتها في التحفيز الضوئي ومضادات البكتيريا. تم إجراء الحسابات النظرية للخصائص الهيكلية والإلكترونية والبصرية باستخدام طريقة DFT في برنامج Gaussian 09من خلال استخدام المعلمات الوظيفية الهجينة الثلاثة Lee-Yang-Parr B3LYP لمستوى الكثافة الوظيفية لنظرية دالة الكثافة جنبًا إلى جنب مع مجموعات أساس .SDD.ان حسابات حالات الانتقال والاطياف المرئية – فوق البنفسجية للهياكل المدروسة تم اجراؤها من خلال استخدام نظرية دالة الكثافة المعتمدة على الزمن. تم تحضير المركبات النانوية ($PEO-CuO-In_2O_3$) و (PEO-$NiO-In_2O_3$) تجريبيا بطريقة صب المحلول. تمت دراسة تأثير تراكيز الجسيمات النانوية In_2O_3 على الخصائص التركيبية والبصرية لمركبات (PEO-CuO) و (PEO-NiO) النانوية. أظهرت النتائج استرخاء جيد للمركبات النانوية من استعمال طريقة دالة الكثافة النظرية المستخدمة. تتوافق القيم المحسوبة للمعلمات الهندسية للمركبات النانوية بشكل جيد مع الدراسات النظرية. الطاقة الكلية مستقلة عن الجسيمات النانوية في المركبات النانوية وتعتمد فقط على عدد الإلكترونات في كل مركب نانوي. من النتائج المحسوبة ، أظهرت النتائج أن المركبات النانوية المدروسة أظهرت عدم استقرار المدار الجزيئي السفلي غير المشغول واستقرار المدار الجزيئي العلوي المشغول ، وكلاهما يتغير بشكل كبير ليشير إلى أن الهياكل المختلفة تلعب أدوارًا مهمة في الخصائص الإلكترونية. تضمنت الخصائص الهندسية تحسين الأمثلية الهندسية (الروابط والزوايا).أما بالنسبة للخصائص الإلكترونية فقد تضمنت (جهد التاين ، الالفة الالكترونية ، الصلابة الكيميائية ، المرونة الكيميائية ، الكهروسالبية ، الطاقة الكلية ، فجوة الطاقة وكثافة الحالات) بالإضافة إلى الخواص الطيفية التي تضمنت (الأشعة تحت الحمراء والأشعة فوق البنفسجية المرئية). أظهرت النتائج أن زيادة عدد ذرات المركبات النانوية كان له تأثير مباشر على جميع خواص البنية المدروسة. حيث تؤدي زيادة عدد ذرات المركبات النانوية إلى تقليص فجوة الطاقة بشكل تدريجي وجدير بالملاحظة. أظهرت النتائج التجريبية والنظرية للخواص البصرية للمتراكبات النانوية (PEO-$CuO-In_2O_3$) و($PEO-NiO-In_2O_3$) زيادة الامتصاصية، معامل الامتصاص، معامل الخمود، معامل الانكسار، ثوابت العزل الحقيقي والخيالي والتوصيلية البصرية للمتراكبات النانوية (PEO-CuO) و (PEO-NiO) بزيادة تراكيز الجسيمات النانوية In_2O_3. وان النفاذية وفجوة الطاقة يقلان بزيادة تراكيز

الجسيمات النانوية In_2O_3. المتراكبات النانوية ($PEO-CuO-In_2O_3$)و($PEO-NiO-In_2O_3$) تمتلك امتصاصية عالية في المنطقة فوق البنفسجية.

أظهرت نتائج تطبيقات التحفيز الضوئي للبوليمر (PEO) والمركبات النانوية أن امتصاصية صبغة الميثيلين البرتقالية انخفض بزيادة تراكيز الجسيمات النانوية In_2O_3 ومع زيادة وقت التشعيع حيث كان أفضل نشاط تحفيزي ضوئي للمركبات النانوية ($PEO-CuO-In_2O_3$) و ($PEO-NiO-In_2O_3$) 90٪ و 87٪ على التوالي خلال 90 دقيقة بتركيز 5.4wt% من جسيمات In_2O_3 . تزداد نسب التحلل الضوئي للمركبات النانوية مع زيادة وقت التشعيع. أظهرت النتائج أن نشاط التحفيز الضوئي للمركبات النانوية قد زاد مع زيادة تركيز In_2O_3 NPs. أظهرت تطبيقات التحلل الضوئي انحلال جيدًا وانتشارًا عاليًا وتشتتًا للجسيمات النانوية.

اختبرت المتراكبات النانوية ($PEO-CuO-In_2O_3$)و($PEO-NiO-In_2O_3$) كمضادات لبكتيريا موجبة غرام (بكتيريا سيريوس العصويه) وسالبة غرام (السالمونيلا) أظهرت النتائج زيادة منطقة التثبيط بزيادة تراكيز الجسيمات النانوية In_2O_3. وكذلك الحال بالنسبة لغيرها من الخواص التي تنسجم تماما مع النتائج النظرية والتجريبية السابقة. وقد تم مقارنة جزء من النتائج التي تم الحصول عليها عمليا مع النتائج المقابلة لها نظريا وقد كان هناك تقارب كبير بينهما وهذا هو الهدف الاساسي والجوهري لهذا العمل.

Summary

The theoretical and experimental studies for the structural and optical properties of (PEO-CuO-In_2O_3) and (PEO-NiO-In_2O_3) nanocomposites and their applications in photocatalysis and anti-bacterial have been investigated. The theoretical calculations of structural, electronic and optical properties are carried out by employing the DFT method at the Gaussian 09 program by employing the hybrid functional three parameters Lee-Yang-Parr B3LYP level of density functional theory DFT together with SDD basis sets .The calculations of transition states and UV-VIS spectra of the studied structures are carried out by employing the time dependent TD-DFT. The (PEO-CuO-In_2O_3) and (PEO-NiO-In_2O_3) nanocomposites have been prepared experimental by solution cast method. The effect of In_2O_3 nanoparticles concentrations on the structural and the optical properties of (PEO-CuO) and (PEO-NiO) nanocomposites have been studied . The results showed good relax was obtained for the nanocomposites from used DFT theoretical method. The theoretical calculated values of geometrical parameters of the nanocomposites are in good agreement with previous studies theoretical. The total energy is independent on the nanoparticles in the nanocomposites, it depends only on the number of electrons in each nanocomposite. the electronic properties included the (Ionization potential ,Electron affinity, Chemical hardness ,Chemical softness, Electronegativity, Total energy, energy gap, Electrophilicity and density of states) as well as spectral properties, which included (IR and UV-Visible) The results showed that increase the number of atoms of the nanocomposites had a direct effect on all the properties of the studied structure. Where increase the number of atoms of the nanocomposites leads to decrease the energy gap gradually and noteworthy. The

experimental results of optical properties for (PEO-CuO- In_2O_3) and (PEO-NiO-In_2O_3) nanocomposites showed that the absorbance, absorption coefficient, extinction coefficient, refractive index, real, imaginary dielectric constants and optical conductivity of (PEO-CuO-In_2O_3) and (PEO-NiO-In_2O_3) nanocomposites were increased with an increase in In_2O_3 nanoparticles (In_2O_3 NPS) concentrations. The transmittance and energy band gap were decreased with an increase in In_2O_3 nanoparticles (In_2O_3NPS) concentrations. The (PEO-CuO-In_2O_3) and (PEO-NiO-In_2O_3) nanocomposites have high absorbance in the UV region.

The results of photocatalysis applications for (PEO) polymer and nanocomposites show that the absorbance of methylene orange dye decreased with adding In_2O_3 nanoparticles concentrations and with an increase in the time of the irradiation where the best photocatalytic activity for (PEO-CuO-In_2O_3) and (PEO-NiO-In_2O_3) nanocomposites was 90% and 87% respectively within 90 minutes at concentration 5.4%wt of In_2O_3 nanoparticles. The photodegradation percentages for nanocomposites increase with the increase the time of the irradiation. The results show that the photocatalytic activity of nanocomposites was increased with increase the concentration of In_2O_3 NPs. The photodegradation applications showed good degradation, high diffusion and dispersion of nanoparticles.

The results of antibacterial applications for (PEO-CuO- In_2O_3) and (PEO-NiO-In_2O_3) nanocomposites which tested against gram positive (Bacillus cereus) and gram-negative (Salmonella) showed that the inhibition zone was increased with increase the concentrations of In_2O_3 nanoparticles (In_2O_3 NPS).

Contents

List of Symbols and Abbreviations

Symbol	Description
PEO	Poly Ethylene Oxide
CuO	Copper Oxide
NiO	Nickel Oxide
In_2O_3	Indium Oxide
$\hbar$	The Reduced Planck Constant
∇^2	The laplacian Operator
V (r, t)	potential Energy
$\widehat{H}$	The Hamiltonian Operator
$\psi(\vec{r}, \vec{R})$	The Total Wave Function
E_{tot}	The Total Energy
m_e	Electronic Mass
$\widehat{T}_e$	The Electronic Kinetic Energy Operator
$\widehat{T}_n$	The Nuclear Kinetic Energy Operator
$\widehat{V}_{ne}$	The Attractive Interactions between Nuclei and Electrons Operator
$\widehat{V}_{ee}$	The Repulsive Electron– Electron Interactions Operator
$\widehat{V}_{nn}$	The Repulsive Nucleus- Nucleus Interactions Operator
$Z_{A,B}$	The Atomic Number of Atoms A and B
m_A	The Mass of Atom A

r_{AB}	The Distance between Nuclei A and B
r_{iA}	The Distance between Nucleus A and Electron i
r_{ij}	The Distance between Electrons i and j
ψ_e	The Electronic Wave Function
E_e	The Electronic Energy
V_{ext}	The External Potential
E_{nuc}	The Constant Nuclear Repulsion
E_0	The Ground-State Energy
Φ	The Trial Function
N	The Number of Electrons
$\hat{H}^{core}$	The Core Hamiltonian Operator
$\langle H_{ii} \rangle$	Expectation Value of Core Hamiltonian
M	Atomic Nuclei
Z_μ	The Charge of Nucleus
$r_{\mu 1}$	The Distance between Nucleus μ and Electron 1
J_{ij}	Coulomb Integral
K_{ij}	Exchange Integral
$\hat{F}$	The Fock Operator
S_{rs}	The Overlap Elements
F_{rs}	Fock Matrix Element

ϕ_s	A Linear Combination of Atomic Orbitals (Basis Functions)
$\rho(r)$	Electron Density
$\rho_0(x,y,z)$	The Ground State Electron Density
ρ_t	Trial Electronic Density
$F_{HK}[\rho]$	Hohenberg-Kohn Operator
$V_{ext}(r)$	External Potential
$v(\vec{r}_i)$	The External Potential for the Attraction of Electron i to the Nuclei
ψ_i	Wave Function Molecular Orbitals
X^{STO}	Slater Wave Function
ξ	The Orbital Exponent
$Y_{lm}(\theta,\varphi)$	The Spherical Harmonics Functions
X^{GTO}	Gaussian Wave Function
E_{HOMO}	Energy of the Highest Occupied Molecular Orbital
E_{LUMO}	Energy of the Lowest Unoccupied Molecular Orbital
E_g	Energy Gap
K	Chemical Potential
X	Electronegativity
η	Chemical Hardness

S	Chemical Softness
DFT	Density Functional Theory
HF	Hartree–Fock
IR	Infrared Ray
UV	Ultra-Violet
UV-Vis	Ultraviolet-Visible
MOs	Molecular Orbitals
SCF	Self-Consistent Field
KS	Kohn–Sham
LCAOs-MO	Linear Combination of Atomic Orbitals- Molecular Orbital
LDA	Local Density Approximation
LSDA	Local Spin Density Approximation
G09	Gaussian 09
GV5	Gauss view 5.0.8
HOMO	Highest Occupied Molecular Orbital
LUMO	Lowest Unoccupied Molecular Orbital
ESP	Electrostatic Potential
TED	Total Electron Density
IP	Ionization Potential

EA	Electron Affinity
ZPE	Zero Point Energy
I_T	Transmitted Intensity Beam
I_A	Absorbed light Intensity
I_o	Incident Intensity of light
α	Absorption Coefficient
A_0	Absorbance
K_B	Boltzman Constant
n^*	Complex Refractive Index
E_g^{opt}	Optical Energy Gap
k	Extinction Coefficient
υ	Frequency
ε_1	Real Dielectric Constant
E_g^{opt}	Optical Energy Gap
ε_1	Real Dielectric Constant
ε_2	Imaginary Dielectric Constant
C	Light Speed in Vacuum
n	Refraction Index
R_0	Reflectance

E_{ph}	Photon Energy
t	Thickness of the Sample
L	Length
P	Total Dipole Moment
T_0	Transmittance
UV	Ultraviolet Spectrum
λ	Wavelength of Photon
σ	Optical Conductivity
MO	Methylene orange
A_1	Absorption after irradiation
DP	Degradation percentage

List of Figures

List of Tables

1.1 Introduction

Nanoscience and nanotechnology have gained a lot of attention in recent years. Quantum dots and Nano crystals of metals, semiconductors, oxides, and other materials, as well as one-dimensional nanostructures like nanotubes and nanowires, are important Nano objects. These nanomaterials' synthesis, characterization, and uses are all being studied in depth. Single molecule electronics based on nanotubes and nanowires, Nano catalysis and biological sensors employing Nano crystals or nanotubes are examples of novel nanomaterial uses that are emerging. One-dimensional nanostructures of materials have received great attention since the discovery of the carbon nanotubes. Nanomedicine refers to the application of nanotechnology to improve human health and well-being. The use of nanotechnology in various sectors of therapeutics has revolutionized the field of medicine where nanoparticles of dimensions ranging between 1–100 nm are designed and used for diagnostics, therapeutics and as biomedical tools for research. With the use of these instruments, it is now possible to deliver therapy at the molecular level, curing the disease and assisting in the research of disease causation. Nanotechnology is an essentially interdisciplinary field that has piqued the interest of scientists and engineers in recent years. Nanomaterials can be found in nature and have been a component of the environment since the formation of our planet roughly 4.5 billion years ago [1].

In order to manufacture and understand new forms of rubber, plastic, adhesives, coatings and fibers, polymer science was invented in the world's leading industrial laboratories. Soon after, polymer science came into contact with academic life [2]. A polymer is a big molecule with hundreds or thousands of atoms that is made up of one, two, or sometimes more tiny (monomers) kinds

of the molecule linked together in a chain or network of structures [3]. One of the most important means of developing new materials is polymer blending with a combination of properties and excellent than the individual polymer components. It's one of the more active methods for increasing amorphous content while decreasing crystalline content. Polymer materials are often insulators that are combined with conductive fillers to improve conductivity [4]. In the future years, polymers will continue to expand. All polymer indicator growth is dependent on the synthesis of new polymers, as well as their physical and chemical changes. Improved manufacturing techniques will also result in lower-cost goods [5]. Polymer/nanocomposite materials are gaining popularity because they offer new potential for designing flexible materials with improved optical, mechanical, and electrical properties [6].

Polymers are made up of big organic molecules and small structural components (monomers) that are joined together in a polymerization process. Thousands of atoms are joined by covalent chemical bonds in each molecule. Molecules in a polymer are attracted to one another by forces that vary depending on the polymer type. Polymers are made up of large, coupled molecules that are difficult to regulate, but which can be ordered into a linear chain. Polymers have crystalline and non-crystalline areas in the solid state[7].

1.2 Nanocomposites

A nanocomposite is a multiphase solid material where one of the phases has one, two or three dimensions of less than 100 nanometers (nm), or structures having nano-scale repeat distances between the different phases that make up the material. In the broadest sense this definition can include porous media, colloids, gels and copolymers, but is more usually taken to mean the solid combination of a bulk matrix and nanodimensional phase (s) differing in properties due to

dissimilarities in structure and chemistry. The mechanical, electrical, thermal, optical, electrochemical, catalytic properties of the nanocomposites will differ distinctly from that of the component materials. Size limits for these effects have been proposed, <5 nm for catalytic activity, <20 nm for making a hard magnetic material soft, <50 nm for refractive index changes, and <100 nm for achieving super paramagnetism, mechanical strengthening or restricting matrix dislocation movement[8].

1.3 Polymer nanocomposites

Many academics have been interested in polymer nanocomposites in recent years because of their ability to change mechanical, electrical, and optical properties. This novel class of materials has benefited EM detectors, optical integrated circuits, automobiles, drug delivery, sensors, injection molded products, membranes, adhesives, coatings, fire-retardants, medical devices, aircraft, packaging materials, consumer goods, and other applications. Several metal oxide nanoparticles have been used as filler materials in various polymeric systems to offer physio-chemical characteristics that are vastly different from those of the virgin polymer [9]. These advanced nanocomposites have many advantages such as low cost production and the possibility of device fabrication on large scale and flexible substrates [10]. Developing nanocomposites could be a solution to adjust the properties of individual nanomaterials appropriately like, optical, electrical, thermal and mechanical properties [11]. In particular, nanoparticles represent as advanced technological materials because of their attractive electrical/electronic properties and high refractive index[12]. Nanocomposites of organic and inorganic materials can possess advantages of both organic polymers (dielectric, ductility, flexibility) and inorganic materials

(high thermal stability, rigidity, strength, high refractive index, hardness), thus have many applications [13].

1.4 The Properties of the Used Materials

1.4.1 Poly Ethylene Oxide (PEO)

Polyethylene oxide polymer is a semi-crystalline and linear polymer [14] with high molecular weight polymers that have the common structure: [$(OCH_2CH_2)n$]. In which (n) is the degree of polymerization, ranges from (2000 to over 100,000). With a molecular formula of [15]:

$$[C2n+2H_4n+_6O_{n+2}]$$

Polyethylene oxide is a nonionic homopolymer of ethylene oxide with a high molecular weight ranging from (600,000 to 4,000,000) g/mol. Because of its polar nature, it may create diverse composites in a variety of solvents. It's a white to off-white powder that comes in a variety of grades, each with a different viscosity profile of an aqueous isopropyl alcohol solution. It may contain a suitable antioxidant. Figure (1.1) shows the chemical structure of PEO's repeating unit . Polyethylene oxide was chosen because it is non-toxic, abundant, low-cost, and water-soluble, as well as being environmentally benign.

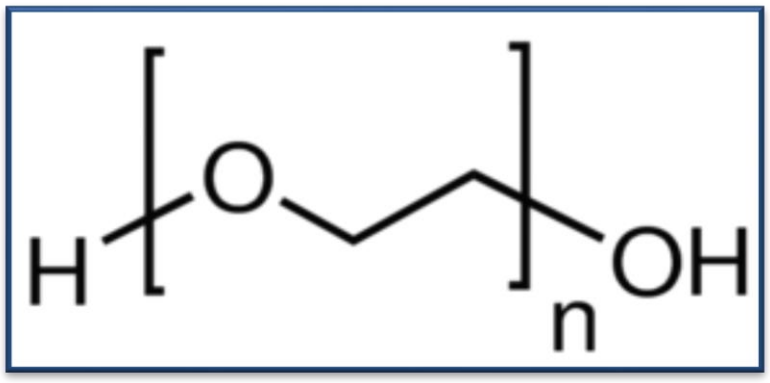

Figure (1.1): Chemical structure of polyethylene oxide[16].

Polyethylene oxide polymers are utilized in a wide range of applications and are classified into two groups based on their molecular weight. Since 1930, liquid and waxy polymers with molecular weights of (6000-8000) g/mol have been commercially accessible and are frequently utilized in medicinal, cosmetic, sizing, and humectant formulations. High polymers with molecular weights of (100,000) g/mol and above are relatively new products that have been commercialized in the last few years (1960). The unusual solubility and thermoplastic properties of these materials influence their applications [16].

1.4.2 Copper Oxide Nanoparticles (CuONPs)

In the last few years, the synthesis of transition of metal oxide nanostructures with different sizes and morphologies has attracted the great attention of the researchers because of their potential applications in different fields[17]. CuO has attracted much attention. CuO is a p-type semiconductor material with small band gap energy about 1.2 eV at room temperature. It has been shown that CuO can be used in high temperature superconductors, gas sensor, magnetic storage media, catalysis and field emitters [18]. It is one of the hardest materials due to high melting and boiling points. Unlike other MOSs which crystallize in a cubic rock salt structure with possible rhombohedral distortions, CuO has a lower-symmetry monoclinic cell [19]. Copper Oxide Nanoparticles (CuONPs) have a high importance according to their ability to effectively interact with light through dint of surface plasmon resonance (SPR). CuONPs are now very involved in electrical, catalytic, optical antibacterial and mechanical characterization because of their wide range of applications[20]. Figure (1.2) shows the crystal structure of Copper Oxide.

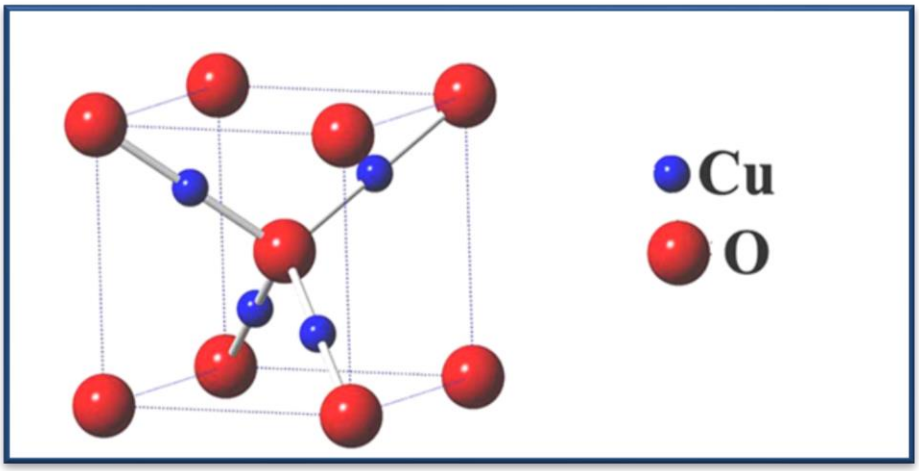

Figure (1. 2):The crystal structure of copper oxide (CuO)[21].

1.4.3 Nickel Oxide Nanoparticles (NiO NPs)

Metal oxide semiconductors (MOS) structures are future availability for electronic and optoelectronic applications. One of this structures is nickel oxide, NiO is a p-type transparent semiconductor with a wide band gap of 3.6 - 4.0 eV [22]. Nickel oxide is considered as the possibility applicants in the engineering nano materials synthesis for multifunctional fields owing the good dispersion capacity in the polymeric system. NiO is starting joint into the matrix of polymer for improving the polymer nanocomposites with enhanced dielectric and electrical characteristic[23]. With regard to its magnetic ordering, the bulk crystal of NiO exhibits antiferromagnetism (AFM) with a relatively high Neel temperature T_N ~523 K. Because of the volume effect, the quantum size effect, the surface effect and the macroscopic quantum tunneling effect, NiO NPs are expected to possess many improved properties as compared to those of the bulk sized NiO particles. In recent years, NiO NPs have many applications in catalysis, battery cathodes, gas sensors, electrochromic films, transparent

conducting films and dye-sensitized photocathodes[24] figure (1.3) shows the crystal structure of nickel oxide.

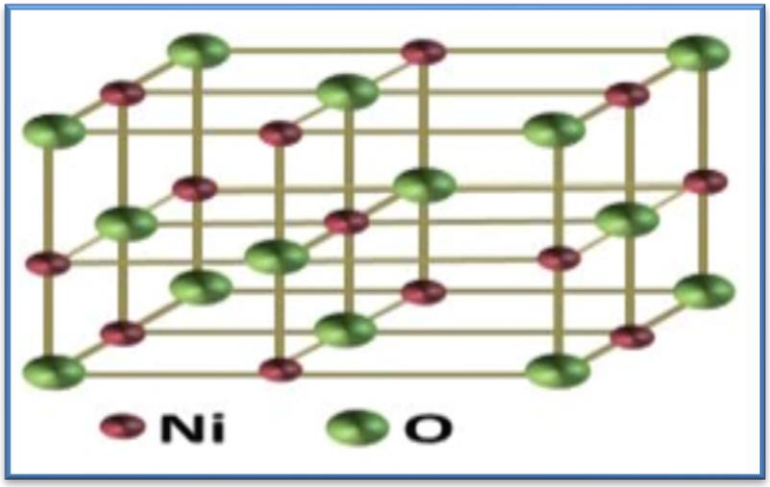

Figure (1. 3):Shows the face centered cubic (fcc) crystal structure of nickel oxide (NiO) [25].

1.4.4 Indium OxideNanoparticles (In_2O_3NPs)

Indium oxide (In_2O_3) is an important n-type semiconductor with band gap (≈ 3.6 eV). Single crystal In_2O_3 has cubic bixebyte structure (also called as c-type rare-earth oxide structure) with lattice parameter of $10.117A^0$. The electronic properties of the material makes it suitable for various solid state devices such as solar cells, sensors, electrocatalyst and nanoscale transistors [26,27] etc. Transparent, conducting indium trioxide or tin-doped indium oxide (ITO) has been exploited in various applications ranging from flat panel displays and electrochemical windows to modern solar cells, because of its superior optical and electrical properties. Thin transparent films prepared on this basis have remarkably high transmittance in the visible region, high infrared reflectance, and close to metallic electric conductivity [28]. Figure (1.4) shows the crystal structure of Indium Oxide.

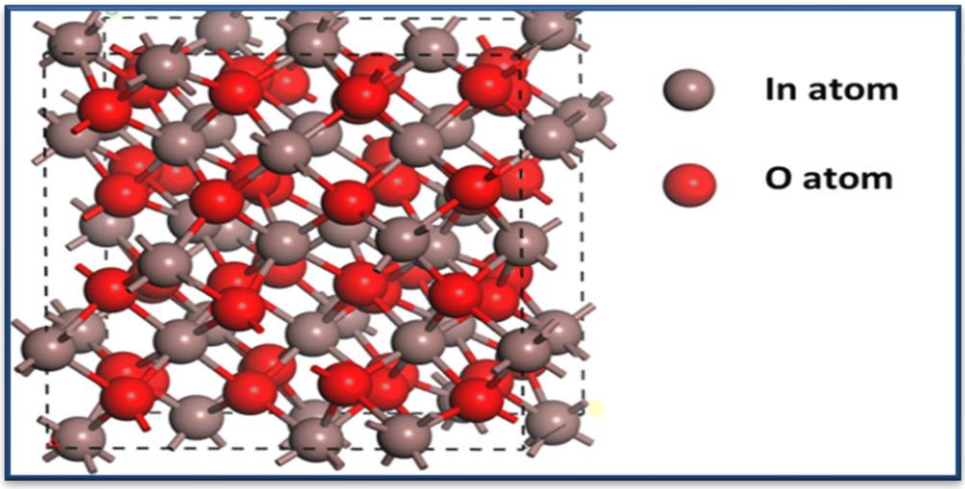

Figure(1. 4): The crystal structure of indium oxide (In_2O_3) [29].

1-5 Literature Survey

Nanocomposites have a wide range of medical and industrial uses. Electrical and optical properties, as well as their applicability to various chemicals and nanoparticles, have been studied in the past.

Mohan *et. al*, [30] in (2007) studied the optical and electrical properties of pure and doped PEO polymer electrolyte films. The optical absorption studies were made in the wavelength range (200-600) nm on pure and $NaFeF_4$ doped PEO film. They found that optical energy gap (both direct and indirect) showed a decreasing trend with increasing dopant concentration. The direct band gaps for undoped film was decreased from 4.54 eV to 3.63 eV and $NaLaF_4$ doped PEO film was decreased from 3.74 eV to 3.54 eV while the indirect band gaps was reduced from 4.43 eV to 3.38 eV for undoped film and from (3.52 eV to 3.26) eV $NaFeF_4$ doped PEO film. The absorption edge was observed at 4.62 eV for undoped while it ranged from 3.86 to 3.61 eV for $NaFeF_4$ doped films.

Kumar *et. al*, [31] in (2011) studied effects of complexation of NaCl salt with polymer blend (PEO/PVP) electrolytes on ionic conductivity and optical

energy band gaps. UV-Vis absorption spectra in wavelength region 200–800 nm, were used to evaluate the optical properties like direct and indirect optical energy band gaps. They found that the optical band gaps decreased with the increase of (Na+) ion concentration. The optical band gaps (both direct and indirect) decreases from 4.87 eV and 4.63 eV to 4.61 eV and 4.30 eV respectively.

Kesavan *et. al*, [32] in (2013) studied on poly(vinyl pyrrolidone) based solid polymer blend electrolytes complexed with various lithium salts. The complexation of the prepared simples was confirmed by Fourier transform infrared analysis. They found that the SEM images of the PEO/PVP/LiN[CF_3SO_2]2 sample show the presence of a number of pores and surface roughness of the sample. The maximum conductivity value was found to be 1.08×10^{-5} $(S.cm)^{-1}$ for the film at room temperature. Ultra violetvisible analysis reveals that the values of the band gap energies were changed with the addition of various lithium salts. The direct and indirect band gap values decreased from 4.35 eV and 4.32ev to 4.24 eV and 4.03 eV, respectively.

Abdullah *et. al*, [33] in (2015) examined the complexion formation in PVA/PEO/$CuCl_2$ solid polymer electrolyte. The solid polymer electrolyte films PVA/PEO/$CuCl_2$ were prepared by a solution casting method, and are characterized by FTIR, UV-Vis spectroscopy. They found that the values of optical band gap (direct and indirect) decreased from 5.26 eV and 3.71eV to 2.58 eV and 1.53 eV, respectively as the concentrations of $CuCl_2$ increases. This indicates the creation of localized states in the band gap as a result of the compositional disorder. The optical conductivity increases with increase $CuCl_2$ concentration attributed to the reducing the crystalline phase which provide the conducting pathways for the mobility of ions as well as polymer segments.

Ahmed Hashim *et.al*, [34] in (2017) studied prepared the polyvinyl alcohol–starch-copper oxide nanocomposites for humidity sensors applications at different temperatures and copper oxide nanoparticles concentration. The electrical and optical properties of nanocomposites have been studied. Results showed that the electrical conductivity increases with increasing of copper oxide nanoparticles concentration. The optical studies showed that the absorbance increase and energy band gap decreases with increase the copper oxide nanoparticles concentration. The results of humidity sensors applications showed that the electrical resistance of polyvinyl alcohol–starch-copper oxide nanocomposites decreases with increase the humidity and temperatures.

Choudhary *et. al*, [35] in (2017) studied the morphological, structural, dielectric and electrical properties of PEO–ZnO nanodielectric films. They found that the scanning electron microscopy (SEM) images of these films show that the morphology of pristine PEO aggregated spherulites changes into fluffy, voluminous and highly porous with dispersion of ZnO nanoparticles into the PEO matrix.

Abdelrazek *et. al*, [36] in (2018) studied the structural, optical, morphological and thermal properties of PEO/PVP blend containing different concentrations of biosynthesized Au nanoparticles. They found that the FTIR studies confirmed the complexation between the polymer blend and Au nanoparticals through the interaction between Au nanoparticals and the polar groups of polymer blend. Absorption spectra for PEO/PVP/Au nanocomposites showed the appearance of peaks in the visible region which is a characteristic for Au NPs. The values of optical parameters for nanocomposite films were enhanced due to Au NPs addition within the polymeric matrix. The optical energy gap value decreases from 4.86 eV for pure PEO/PVP to 2.46 eV for

sample 0.72 wt.%. Such a decrease may be attributed to the chemical bonding formation between blend chains and Au NPs, which is responsible for the localized states. The surface morphology changes from rough to smooth revealed an increase for amorphous region within the polymeric matrix due to the existence of Au NPs.

M. T. Ramesan *et.al,* [37] in (2019) described the preparation, characterization and electrical properties of polyindole (PIN) /phenothiazine (PTZ) blend nanocomposite with different contents of nickel oxide (NiO) nanoparticles. Ultraviolet–Visible spectroscopy and Fourier transform infrared spectroscopic characterizations were carried out to investigate the extent of chemical interactions between PIN/PTZ blend and NiO nanoparticles. Morphological studies carried out using scanning electron microscopy and transmission electron microscopy showed the formation of globular composite particles with a size in 15–25 nm range.

M. M. Abutalib and A. Rajeh [38] in (2019) studied Zinc oxide nanoparticles (ZnO NPs) had been synthesized via sol-gel and the silver nanoparticles (Ag NPs) had been synthesized via chemical synthesis. A series of polyacrylamide and polyethylene oxide (PAM/PEO) blend films doped with ZnO NPs and various concentrations of Ag NPs were prepared by the solution casting method. The FTIR spectra studies indicate the structural changes taking place in the nanocomposites which confirmed the compatibility between ZnO/Ag NPs and pure blend. The optical energy gap decreases by the addition of ZnO and Ag nanoparticles. It has been viewed that the conductivity raised with addition of the ZnO/Ag NPs due to an increase in the number of charges carrier. The dielectric constant reduces with a raise in the frequency for the samples prepared.

M. O. Farea *et.al*, [39] in (2020) prepared films of polyethylene oxide and sodium alginate polymer blend (50/50 wt%) embedded with different quantities of Au nanoparticles with size 3–32 nm were made using the casting process. The nanocomposite films were examined by FT-IR spectroscopy, UV/Vis spectroscopy, and dielectric parameter measurements. From the Fourier transform infrared spectra it seems that the intensity of the FT-IR bands decreased which depicted the existence of the interaction between (PEO/SA) virgin polymer and gold nanoparticles. The optical properties of the polymer composite were examined by ultraviolet-visible techniques. In a direct transition the optical energy gap of the prepared films is decreased from 4.73 to 2.92 eV and in an indirect transition decreased from 2.95 to 1.50 eV. The dielectric and electrical spectra of the obtained films were examined via dielectric broadband spectroscopy. The electrical and dielectric measurements are appropriate for the use of the polymer nanocomposite films in the fabrication of electroactive materials.

Angham Hazim1 *et.al*, [40] in (2020) a theoretical study to investigate the electronic structure and optimized geometry for pure PMMA and PMMA doped with ZrO2, Al_2O_3 and Pt nanoparticles for electronics devices. The studied structures are initially relaxed by employing the hybrid functional three parameter Lee–Yang–Parr B3LYP density functional theory at Gaussian 09 package of programs and Gaussian view 5.0.8 program. The PMMA is origin molecule before adding nanoparticles, also this work includes calculations of the electronic properties which contain total energy, energy of highest occupied molecular orbital, energy of lowest unoccupied molecular orbital, energy gap, ionization potential, electronic affinity, hardness, softness, electronegativity and electrophilic index. The geometrical optimization of PMMA has been found in

good agreement with the experimental data due to its relaxed geometrical parameters. The electronic variables, such as, IE, EA, χ, S, H and ω are computed by the orbital vertical (Koopmans theorem), the nanocomposites studied need small energy to become cation due to ionization potential is smaller than original PMMA, but the electronic affinity are larger than the original PMMA. So, the hardness for nanocomposites was lowering values as compared with PMMA, therefore all the new molecules are softer, and this reduces the resistance of a species to lose electrons, and the total energy of the studied PMMA was decreased with added nanoparticles to the pure PMMA, total energy is a reflection of, binding energy of each sheet. The results showed that the nanoparticles added to PMMA reduces the energy gap. All nanoparticles constructed in this work have energy gap lower than that of original PMMA and the (PMMA–ZrO_2–Pt) nanocomposites have the lowest value of energy gap. These results refer to construct new structures with new electronic properties to use it for modern electronics fields.

Aseel Hadi ***et.al*** , [41] in (2020) investigated Fabrication of polyvinyl alcohol (PVA)–polyethylene oxide (PEO) blend doped with tin dioxide (SnO_2) nanocomposites has been investigated for flexible electrical and optical applications. The prepared nanocomposites have low cost, lightweight, flexible, high corrosion resistance, good optical and electrical properties. These properties of fabricated nanocomposites make it useful for different optoelectronics applications such as: sensors, solar cells, transistors, diodes, capacitors, energy storage etc. The structural, optical and electrical properties of (PVA–PEO–SnO_2) nanocomposites have been studied. The experimental results of optical properties for (PVA–PEO–SnO_2) nanocomposites showed that the nanocomposites have higher absorbance in UV region at wavelength range (200–280) nm. This

behavior makes the nanocomposites may be used for optoelectronics applications. The absorbance, absorption coefficient, extinction coefficient, refractive index, real and imaginary dielectric constants and optical conductivity of polymer blend are increased with the increase in SnO_2 nanoparticles concentrations while the transmittance and energy band gap are decreased with the increase in SnO_2 nanoparticles concentrations. The decrease in energy band gap is useful for different optoelectronics devices industries.

Eman S. Mansora *et.al*, [42] in (2020) studied the endless introduction of toxic dyes through industrialization has worsened the dyes pollution in the environment. As a consequence, the need for the effective removal of such dyes has become more crucial than before. Recently, polymeric membranes for dye adsorption are gaining tremendous attention. In this context, they synthesized the polyethylene oxide/polyaniline (PEO/PANI) composite membrane by a very simple and cost effective approach for the first time. The removal of methyl orange (MO) dye onto pure PEO and composite membrane was conducted utilizing batch mode. The results proposed that the uptake efficiency of PEO after hybridization with PANI is more than two times higher than that of the unmodified PEO membrane under the same experimental conditions. The effect of changing the adsorbent dose (1.5, 2, 2.5, 3 g/L), pH (3, 5, 6.5, 9, 11), and dye concentration (2.5, 5, 7.5, 10 mg/L) on the adsorption performance of the composite membrane was studied. The reusability studies proved that within 50 min of adsorption period the PEO/PANI composite membrane can retain 99% removal percentage for 8 cycles. This indicates that the low cost composite membrane has a good recyclability, which represents a crucial feature for the sorption technique to remove dyes from wastewater streams. The results revealed improved the dye rejection by 82.5% compared to that of the pure PEO film

Dana S. Muhammed *et.al*, [43] in (2020) studied the structure and optical properties of polyethylene oxide (PEO) doped with tin titanate ($SnTiO_3$) nano-filler by UV-Vis spectroscopy as non-destructive techniques. PEO-based composed polymer electrolytes inserted with $SnTiO_3$ nano-particles (NPs) were synthesized through the solution cast technique. The change from crystalline phase to amorphous phase of the host polymer was established by the lowering of the intensity and broadening of the crystalline peaks. The optical constants of PEO/$SnTiO_3$ nano-composite (NC), such as, refractive index (n), optical absorption coefficient (α), dielectric loss (ε_i), as well as dielectric constant (ε_r) were determined for pure PEO and PEO/$SnTiO_3$ NC. From these findings, the value of n of PEO altered from 2.13 to 2.47 upon the addition of 4 wt.% $SnTiO_3$NPs. The value of εr also increased from 4.5 to 6.3, with addition of 4 wt.% $SnTiO_3$. The fundamental optical absorption edge of the PEO shifted toward lower photon energy upon the addition of the $SnTiO_3$ NPs, confirming a decrement in the optical band gap energy of PEO. The band gap shifted from 4.78 eV to 4.612 eV for PEO-doped with 4 wt.% $SnTiO_3$.

Hind Ahmed and Ahmed Hashim [44] in (2021) studied the electronic properties and optimized geometry for (PVA-PEO-SiC)(56Atom) by using DFT at B3LYP level with bases set LanL2DZ for electronic, photonic and optic applications. The electronic characteristic which contain total energy, cohesive energy, HOMO, LUMO), ionization potential, energy gap, softness, electronic affinity, hardness, electronegativity and electrophilicity. The spectroscopic properties (IR and UV) for (PVA-PEO-SiC)(56Atom)were investigated at the same large level of theory. The results indicate to the PVA-PEO-SiC have excellent optical and electronic properties with low energy band gap which make it suitable for various optoelectronics applications.

M.M. Abutalib and A. Rajeh,[45] in (2021) studied the sol-gel technique was used to syntheses TiO_2 nanoparticles and different methods were used to characterize the nanoparticles (Ag and TiO_2) including UV–Vis spectroscopy Also, new nanocomposites were prepared using the solution casting method. The prepared films were characterized by different analytical methods. The absorption peak of the silver nanoparticles shown by the UV–visible spectrum was around 430 nm. Meanwhile, the degree of amorphicity of the Cs/PEO blend was increased as a result of adding Ag and TiO_2 NPs. It was evident through the FTIR spectroscopy that there was an interaction between the functional groups of the polymer blend and the Ag/TiO_2 nanofiller It was also evident from the results that the antibacterial activity of the pure Cs/PEO blend was increased as a result of doping Ag/TiO_2 nanoparticles to the polymer blend. The activity index (%) of the antibacterial activity at sample blend + (0.3%) Ag + (0.8%) TiO_2 of the E. coli, S. aureus, C. Albicans, A. niger was 32, 45.8, 77.8, and 92 (%) respectively. Thus, these results indicate the applicability and potential of the nanocomposites for use in food packaging applications.

Al-Muntaser, A. A., *et al,* [46] in (2022) prepared nanocomposite films of PVP/PEO containing of MoO_3 nanoplates by using a casting procedure. The DFT/FT-IR results have established the miscibility and the interaction between PVP and PEO polymers via hydrogen bonds. Also, FTIR studies showed a coordination interaction between MoO_3 nanoplates and the C=O group of PVP and/or the C-O-C group of PEO of the PVP/PEO blend. The optical band gap values of PNC films of $PVP/PEO/MoO_3$ decreased with increasing of MoO_3 content. These observations illustrate the applicability and potential uses of these PNC films as a nan dielectric material in ceramic capacitors and electrochemical applications such as devices of energy storage and separators in batteries.

1.6 Aim of the study

The principle aims of this work are:

1. Fabrication of new type for polymer nanocomposites.
2. Theoretical and experimental analysis of some physical properties such as optical, electrical and structural properties of nanocomposites.
3. Application of the nanocomposites as antibacterial effect.
4. Application of the nanocomposites as photocatalytic.

2.1 Introduction

The Schrödinger equation describes the movements of atomic and subatomic systems, electrons and nuclei, and even macroscopic systems. The time-dependent Schrödinger equation is written as follows [47-49]:

$\hat{H}\psi(\vec{r},t) = E\psi(\vec{r},t)$ ..... (2-1)

Where $\hat{H}$ the Hamiltonian operator, Ψ the total wave function of the molecular system, E the energy

The Hamiltonian operator in atomic units is expressed as follows:

$$\hat{H} = -\frac{1}{2}\sum_{i=1}^{N}\nabla_i^2 - \sum_{A=1}^{M}\frac{1}{2m_A}\nabla_A^2 - \sum_{i=1}^{N}\sum_{A=1}^{M}\frac{Z_A}{r_{iA}} + \sum_{i=1}^{N}\sum_{j>i}^{N}\frac{1}{r_{ij}} + \sum_{A=1}^{M}\sum_{B>A}^{M}\frac{Z_A Z_B}{r_{AB}} \quad \text{.....(2-2)}$$

$$\hat{H}_{\text{total}} = \hat{T}_{\text{elec.}} + \hat{T}_{\text{nucl.}} + \hat{V}_{\text{nucl. elec.}} + \hat{V}_{\text{elec. elec.}} + \hat{V}_{\text{nucl. nucl.}} \quad \text{.....} \quad (2\text{-}3)$$

Where $\hat{T}_e$ and $\hat{T}_n$ are the electrons' and nuclei's kinetic energy operators, respectively. ($\hat{V}_{ne}$) the Coulomb attraction between nuclei and electrons, $\hat{V}_{ee}$ the Coulomb repulsion between electrons, and ($\hat{V}_{nn}$) the Coulomb repulsion between nuclei. The kinetic energy operators are denoted by the symbols:

$$\hat{T}_e = -\frac{\hbar^2}{2m_e}\sum_i \nabla_i^2 \quad \text{.....} \quad (2\text{-}4)$$

$$\hat{T}_n = -\frac{\hbar^2}{2M_A}\sum_A \nabla_A^2 \quad \text{.....} \quad (2\text{-}5)$$

∇_i^2 is The Laplacian operator of i electrons, where m_e and M_A are the electron and nuclear mass, respectively, has the following form in Cartesian coordinates:

$$\nabla_i^2 = \frac{\partial^2}{\partial x_i^2} + \frac{\partial^2}{\partial y_i^2} + \frac{\partial^2}{\partial z_i^2} \quad \text{..... (2-6)}$$

The potential energy operators are represented as:

$$\hat{V}_{nn} = \sum_{A<B} Z_A Z_B \frac{e^2}{R_{AB}} \quad \text{.....(2-7)}$$

$$\hat{V}_{ne} = -\sum_A \sum_i Z_A \frac{e^2}{r_{Ai}} \quad \text{.....(2-8)}$$

$$\hat{V}_{ee} = \sum_{i<j} \frac{e^2}{r_{ij}} \quad \text{.....(2-9)}$$

Where $r_{ij} = |\vec{r_i} - \vec{r_j}|$ and Z_A is the charge of nuclei A, r_{Ai} is the distance between the nucleus and the electron, $r_{ij}$is the distance between the i electron and the j electron, and R_{AB} is the distance between A nucleus and B nucleus. Except for single-electron systems like hydrogen, the Schrodinger equation is known as an equation that cannot be solved. As a result, certain mathematical approximations are required to solve this equation, starting with the simplest of these approximations, the Hartree-Fock approximation, which is based on the central field principle. By integrating the repulsion component, the Coulombic electron-electron repulsion is taken into consideration. This offers the repulsion's average impact, but not the explicit repulsion interaction[50]. This is a variation of calculation, which means that all of the estimated approximate energies are equal to or larger than the exact energy. Hartrees (1 Hartree = 27.2116 eV) are used to determine the energies. This approach has the benefit of breaking the multi-electron Schrödinger equation down into many smaller one-electron equations. Each one-electron equation is solved to produce a single-electron wave function, which is the difference between an orbital and an energy, known as an orbital energy. The orbital defines how one electron behaves in the presence of all other electrons in the net field. The wave function must be represented by some mathematical function, which is known accurately for only

a few one-electron systems, which leads to the second approximation in HF calculations. The n-particle issue is reduced to a series of one-particle eigenvalue problems, known as the Hartree – Fock equations, using this method:

$$\hat{f}_i \Psi_i = \varepsilon_i \Psi_i \quad \text{(2-10)}$$

Where Ψ_i is the appropriate energy and is an aigen function of the operator, commonly known as the Fock operator. For each electron, the Fock operator can be written as:

$$\hat{f}_i = -\frac{1}{2} - \sum_A^M \frac{Z_A}{r_{iA}} + V_{HF}(i) \quad \text{(2-11)}$$

Where $V_{HF}(i)$ is the Hartree–Fock potential, which has two components, the Coulomb operator $\widehat{J}_1(j)$ and the exchange operator $\widehat{K}_1(j)r$, and describes the average repulsive potential experienced by each electron due to the other n-1 electrons:

$$V_{HF}(i) = \sum_j^N \left(\hat{J}_1(j) - \hat{K}_1(j)\right) \quad \text{(2-12)}$$

The primary drawback of this technique is that it ignores the electron-electron effect, thus a variety of theories and methods have been created that start with the Hartree–Fock method and then include the correlation of these ways, resulting in the self-consistent field (SCF) method. When electronic bonding (the influence of electrons among them) is added, the accuracy of calculations improves, whether it's in the energy calculation or the calculation of the spatial form. This technique is also considerably slower than molecular mechanics methods, but it's significantly more precise [51].

2.2 Density Functional Theory (DFT)

The computation of structural characteristics of condensed matter systems and electronic properties of basic metals has shown to be quite successful using DFT [52]. It has a number of advantages, including less computational effort, less computer time, and, in some circumstances, greater agreement with experimental results than other methods. DFT is based on the idea that the energy of a molecule may be calculated using the electron density rather than a wave function. The original theorem only applied to determining a molecule's ground-state electrical energy [53]. DFT concentrates on the much less complicated electron density. For a particular condition, the electron density is defined as the number of electrons N per unit volume. It is only reliant on three coordinates and is thus independent of the amount of electrons in the system[54].

$$N = \int \rho(\vec{r}) d\vec{r} \quad \text{.....(2-13)}$$

The difference between the methods of density function theory is the method of choosing the shape of function to calculate the energy of bonding and exchange.

2.3 The Hybrid Functional

The hybrid exchange-correlation functionals are another class of functionals that are extensively employed. Density function theory (DFT) and Hartree–Fock theory are combined in (HF). B3LYP (Becke's three-parameter exchange correlation functional with three parameters) and LYP are two of the most common hybrid functionals (The Lee, Yang and Parr correlation functional)[55].

2.4 Basis Sets

A basis set is a collection of functions that characterize the geometry of an atom's orbitals. Linear combinations of basis functions are used to construct molecule orbitals and complete wave functions. A predetermined basis set is used in most semi empirical techniques. A basis set must be supplied when performing ab initio or density functional theory computations. Although a basis set may be created from scratch, most computations are performed using pre-existing basis sets. The type of computation used and the basis set used are the two most important variables in influencing the precision of the findings. The foundation set functions must be chosen in order to have a chemically usable form. That is, the functions should have big amplitudes in areas where the electron probability density (wave function) is likewise large, and small amplitudes in areas where the probability density is small [56]. Several approaches, such as the use of hydrogen similarity functions, which are based on the Schrodinger equation for the hydrogen atom, or polynomial functions with customizable coefficients, can be used to discover electron dispersion around the nucleus. Additionally, we have Slater and Gauss functions (or Gaussian functions).

2.4.1 Slater Type Orbitals (STOs*)*

Have a variety of appealing characteristics, the most of which are related to how closely they mimic hydrogenic atomic orbitals. When the basis set functions are STOs, there is no analytical solution for the generic four-index integral. A typical (STO) is written as follows [51]:

$$\chi^{STO} = Nr^{n-1}e^{-\xi r}Y_{lm}(\theta,\varphi) \quad \text{.....(2-13)}$$

Here n, is a principal quantum number and *N* is the normalization constant. ξ is a constant related to the effective charge of the nucleus, i.e. the nuclear charge being partly shielded by electrons. $Y_{lm}$is a spherical harmonic which describes the angular part of the wave function. Slater type functions show a correct behavior nears the nuclei at r → 0 with a discontinuous behavior. The exact solution to the Schrödinger equation for the hydrogen atom is a Slater type orbital, or STO, of the form exp(-ξr) [57].

2.4.2 Gaussian Type Orbitals (GTOs)

In terms of Cartesian coordinates, GTOs may be expressed as [58]:

$$X^{GTO} = Nx^{l_x}y^{l_y}z^{l_z}e^{-\xi r^2} \quad \text{..... (2-14)}$$

The total $l_x, l_y and\ l_Z$ defines the kind of orbitals and represents the orbital exponent, which indicates how compact the orbitals are. The exponential dependency is due to a (GTO) deficit with regard to Slater-Type Orbitals (STO). GTOs have two major issues. The first issue is that GTO behaves incorrectly near the nuclei at r →0; the second issue is that GTO falls off too quickly distant from the nuclei when compared to STO. As a result, the tail of the wave function in the GTO is poorly represented. According to a preliminary calculation, three times as many GTOs as STOs are necessary to achieve the same degree of precision. Many-center integrals like as Coulomb and HF-exchange terms are difficult to compute using STOs, which is one of its drawbacks. As a result, it isn't used in contemporary quantum codes that are based on wave functions. The fact that the sum of two Gaussian functions is another Gaussian function is one of the advantages of the Gaussian basis set. As a result, for the time being, Coulomb and HF-exchange terms computations for Gaussian functions, an

analytical solution is provided. Because of extremely efficient techniques exist for analytically computing the many-center integrals, the GTO basis function in HF and related approaches is popular. A contracted GTO basis set, in which numerous basic Gaussian functions are combined to create a contracted Gaussian function (CGF), is commonly used to enhance GTO basis sets [59].

$$\chi_j^{CGF} = \sum_i^M C_{ij}\chi_a^{GTO} \quad \text{(2-15)}$$

The orbital expansion coefficients and M are the number of Gaussian primitives utilized in a linear combination. Minimal basis sets, split valence sets, polarization and diffuse functions, and other basis sets are utilized in Gaussian [57-,59].

2.4.3 Minimal Basis Sets

The minimal basis set is the minimum number of basis functions χ needed to describe the ground states of the component atoms in a molecule. A common name of minimal basis sets is STO-nG, the n (n=2 to 6) represents the number of Gaussian primitive functions that comprise a single basis function. In these basis sets, the same number of Gaussian primitives comprises core and valence orbitals. Minimal basis sets typically give rough results that are insufficient for research-quality publication, but are much cheaper than their larger counterparts. The following are examples of commonly used minimal basis sets: STO-2G, STO-3G, STO-6G [58,59].

2.4.4 Split-Valence Basis Sets

In terms of a split-valence basis set, the inner-shell atomic orbitals are represented by one basis function, while the valence orbitals are represented by two or more basis functions. Increasing the amount of basis set functions utilized

per orbital is an easy way to enlarge the basis set. For each valence orbital, split-valence basis sets use several basis functions with varying orbital exponents, but only one for each core orbital. The valence double-zeta (VDZ) basis set, for example, employs two basis set functions per valence orbital, whereas the valence triple-zeta (VTZ) basis set uses three, and so on. While split valence basis sets allow for changing atomic size, they cannot offer a balanced basis set on their own [60].

2.4.5 Polarization and Diffuse Functions

Polarization functions, such as d-type and f-type functions for heavy atoms and p-type and d-type functions for hydrogen and helium atoms, are functions with greater angular momentum[50]. By enabling the orbital form to alter, the flexibility of the basis set is increased (i.e., become polarized in one direction). In systems involving hydrogen, such as hydrogen-bonding and proton transfers, include polarization functions can be useful since they allow the s-orbital to deviate from its normal spherical form. Because of polarization functions generally result in more accurate calculated geometries and vibrational frequencies[58,61], they are frequently employed. After the contraction scheme, polarization functions are added in brackets, whereas diffuse functions are marked by a ‘+'. The 6-31++G(d, p) basis set, for example, provides d-type functions for all heavy atoms and p-type functions for hydrogen and helium. The first ‘+' denotes the inclusion of diffuse s-type and p-type functions on heavy atoms, whereas the second ‘+' denotes the inclusion of diffuse s-type functions on hydrogen. Dunning and coworkers' basis sets are another group that is frequently utilized. The polarized valence (double/triple/...etc) zeta basis sets, cc-pVXZ, are correlation-consistent polarized valence (double/triple/...etc) zeta

basis sets, where X specifies the degree of splitting. These were created particularly for use in electron correlation calculations [62,63].

2.5 Gaussian 09(G09) Program

One of the most well-known applications in computational physics of chemistry is available in 32-bit and 64-bit versions for Windows and Linux operating systems. The Gaussian 09 Revision- A.02 SMP suite of programs with GUI (Graphical User Interface) named Gauss view, version 5.0.8, was used to execute all of the computational computations (GV5 for short)[59]. Gaussian 03 Revision B.01 with Gauss view 3.07(GV3for short)[64]. The ‘09’ and ‘03’ refers to the year 2009 and 2003, respectively, in which the software was published. G09 is the most recent version.G09 contains about 500,000 lines (very approximate) of FORTRAN and C^{++} code. Initiated by sir John Pople (shared Nobel prize with Walter Kohn in 1998) in the late 1960, the first distributed Gaussian package was labeled Gaussian 70[65].

2.6 Structural Properties

The arrangement of atoms in the molecules and more specifically the electrons around the atom determine the energy level of that molecule. In fact, the energy of a molecular system varies even with small changes in its structure. This is why geometry is so important when performing calculations. The objective of a geometry optimization is to find the point at which the energy is at a minimum because this is where the molecule is most stable and most likely to be found in nature. All molecules possess geometry, characterized by [56]:

1. Number and types of atoms
2. Number and types of bonds

3. Relevant bond lengths $r: 0 \leq r \leq \infty$(in units of angstroms (A^0)
4. Relevant bond angles $\theta: 0 \leq \theta \leq 180°$ (in units of degrees)
5. Relevant dihedral angles: $-180° \leq \phi \leq 180°$(an angle between four atoms, which signifies the 3-dimensional shape of the molecule).

Geometry optimization is a chemistry-physical computation that determines a molecule's lowest energy or biggest relaxed conformation. The method is an iterative procedure in which the molecular shape is slightly altered at each stage and the molecule's energy is compared to the previous cycle. The computer moves the molecule a bit, calculates the energy, moves it a little more, and continues until the lowest energy is found. This is the molecule's lowest energy, as determined by the optimized shape[66,67].

2.7 Electronic Properties

The studied electronic features include:

2.7.1 Total Energy, Ionization Potential and Electron Affinity

The total energy for a system is the sum of total kinetic and potential energy, at the optimized structure that the total energy of the molecule must be at the lowest value because the molecule is at the equilibrium point this means that the resultant of the effective forces is zero. The ionization potential (IP) for a molecule is the amount of energy required to remove an electron from an isolated atom or molecule and expressed as the energy difference between the positive charged energy $E_{(+)}$ and the neutral $E_{(n)}$ according to the following relation:

$$IP = E_{(+)} - E_{(n)} \quad \text{(2-16)}$$

The electron affinity (EA) of a molecule or atom is the energy difference between the neutral energy and the negative charged energy when an electron is added to the neutral atom to form a negative ion, and is expressed as the energy difference between the neutral energy and the negative charged energy according to the following relationship:

$$EA = E_{(n)} - E_{(-)} \quad (2\text{-}17)$$

The orbital energies of the frontier orbitals are provided by: In molecular orbital (MO) theory, within the limitation of Koopmans theorem, the orbital energies of the frontier orbitals are given by [68]:

$$IP = -E_{HOMO} \quad (2\text{-}18)$$

$$EA = -E_{LUMO} \quad (2\text{-}19)$$

Where E_{HOMO} is the energy of highest occupied molecular orbital, and E_{LUMO} is the energy of lowest unoccupied molecular orbital.

2.7.2 HOMO, LUMO and Band Gap

These acronyms stand for the highest occupied molecular orbital (HOMO), and the lowest unoccupied molecular orbital (LUMO). The HOMO is the highest-energy molecular orbital inhabited by electrons. The LUMO is the lowest-energy molecular orbital that is not filled by electrons. The HOMO and LUMO play a significant role in regulating chemical reactivity and a molecule's capacity to absorb light [53]. According to the Koopmans theorem, the band gap is the energy difference between the highest occupied molecular orbital and the lowest unoccupied molecular orbital [69].

$$E_g = E_{LUMO} - E_{HOMO} \quad (2\text{-}20)$$

The energy gap between HOMO and LUMO (border orbital gap) not only determines how the molecule interacts with other species, but it also helps describe the chemical reactivity and kinetic stability of the molecule. A molecule with a small frontier orbital gap is highly polarizable and is often associated with strong chemical reactivity and low kinetic stability, and is referred to as a soft molecule

2.7.3 Dipole Moment

A molecule possesses a permanent electric dipole moment if its center of positive charge does not coincide with its center of negative charge. The permanent electric dipole moments are often present in neutral molecules for neutral systems, the dipole moment is calculated from the atomic charges and the lone-pairs as:

$$X_i = Ce \sum_A Q_A \, i_A + 2Cea^{\circ} \sum_A \rho(S - \rho_i)_A \; D(A) \quad \text{.....(2-21)}$$

Where $i = x, y, z$, C is speed of light, e is the electron charge, Q_A is total electron density, a^o is Bohr radius, ρ(S-ρi) is one-center S-ρi electron density matrix element, and D(A) is the one-center two-electron integral. The total dipole moment is [70]:

$$X = X_x + X_y + X_z \quad \text{..... (2-22)}$$

2.7.4 Chemical Potential (κ) and Electronegativity (χ)

The electronic chemical potential is a key variation principle in density functional theory, where the reactivity indicator is connected to how the electronic energy E of a molecule varies when the number of electrons N and the external potential vary. Parr *et.al*, demonstrated that there is an electronic chemical potential for every system of nuclei and electrons, denoted as [71]:

$$K = \left[\frac{\partial E}{\partial N}\right]_V \quad \text{(2-23)}$$

Where v is the potential due to nuclei.

The electronegativity (Pauling defines it as "the power of an atom in a molecule to attract electrons to itself") may thus be defined as the inverse of the electronic chemical potential [72]:

$$X = -K = -\left[\frac{\partial E}{\partial N}\right]_V \quad \text{(2-24)}$$

R. Mulliken defined electronegativity as the average of the ionization energy and electron affinity as follows [73]:

$$X = \frac{(IP+EA)}{2} \quad \text{(2-25)}$$

According to Koopmans' theorem, it can be defined as the negative value for average of the energy levels of the HOMO and LUMO[55,74]

$$X = -\frac{(E_{HOMO} + E_{LUMO})}{2} \quad \text{(2-26)}$$

2.7.5 Chemical Hardness (η) and Chemical Softness (S)

The chemical hardness (η) is a measurement of charge transfer resistance. The density functional theory provides a theoretical definition of chemical hardness as the second derivative of electronic energy with respect to the number of electrons N, assuming a constant external potential V (r) [75]:

$$\eta = \frac{1}{2}\left[\frac{\partial^2 E}{\partial N^2}\right]_V = \frac{1}{2}\left[\frac{\partial K}{\partial N}\right]_V = -\frac{1}{2}\left[\frac{\partial X}{\partial N}\right]_V \quad \text{(2-27)}$$

Finite difference approximation to chemical hardness gives,

$$\eta = \frac{IP-EA}{2} \quad \text{(2-28)}$$

The energy gap between the hard and soft molecules is high for the hard molecule and small for the soft molecule. Changes in the electron density of a system are caused by the mixing of appropriate excited state wave functions with the ground state wave function in quantum theory. The manifold of excited states will have minimal excitation energies if the energy gap is small. Soft molecules with narrow energy gaps are the result. Soft molecules are more reactive than hard molecules because their electron density changes more easily than a hard molecule's [67].

The global chemical softness, S, is a property of molecules that measures the extent of chemical reactivity. It is the inverse of the chemical hardness (η)[76].

$$S = \frac{1}{2\eta} = \left[\frac{\partial^2 N}{\partial E^2}\right]_V = \left[\frac{\partial N}{\partial K}\right]_V \quad \text{(2-29)}$$

2.7.6 Electrophilicity (ω)

Electrophilicity is defined as an index that evaluates the energy stability of a system after it receives an extra electronic charge from the environment [68]. On the other hand, it may be described as a measurement of energy loss as a result of maximum electron flow between the donor and acceptor [75].

$$\omega = \frac{\kappa^2}{2\eta} \quad \text{(2-30)}$$

Where κ chemical potential is associated with the negative of the electronegativity.

2.8 The Optical Properties

In recent years, the search for optical properties has increased because of their applications in integrated optics such as optical information, optical data storage, and optical modulation. The study of optical absorption useful for

clarification of the electronic structure and determine direct and indirect transitions [77]. The addition of nanoparticles in polymer improves the optical, electrical and mechanical properties of the materials. Metal oxides nanoparticles with polymers studied as alternative materials for optical applications such as micro optical elements and planar waveguide devices. The developments of polymer nanocomposite structures due to their ease of processing and production, light weight, good adhesion with reinforcing elements, resistance to corrosive environment and in some cases ductile mechanical performance [78,79].

2.8.1 Absorbance (A_0) and Transmittance (T_0)

Polymer optical characteristics research has a wide range of applications in optical and electrical devices such as solar cells, fuel cells, solid state batteries, and medical technology[80]. The absorption coefficient provides useful information such as the optical energy band gap and the electrical band structure. The following equation used to calculate the absorption coefficient (v) from the optical absorption spectrum [81,82]:

$$\alpha = 2.303\frac{A_0}{t} \quad \text{..... (2-31)}$$

Where, t is the sample thickness and A_0 is defined by log (I_0/I_T) where I_0 and I_T are the incident intensity and transmitted intensity beams, respectively[80,81]

The direct and indirect transitions can be defined in view of the models proposed by [83]:

$$\alpha h\nu = B_0(h\nu - E_g^{opt})^r \quad \text{.....(2-32)}$$

As shown in Figure (2.1)[84], ν is the frequency, B_0 is a constant, h is Planck's constant, E_g^{opt} is the energy band gap between the valence and

conduction bands, and r can take the values 2, 3, 1/2, or 3/2 for transitions designated as indirect allowed, indirect forbidden, direct allowed, and direct forbidden, respectively. The charting of $(\alpha h\nu)^{1/r}$ against $h\nu$ is used to calculate optical energy band gap values.

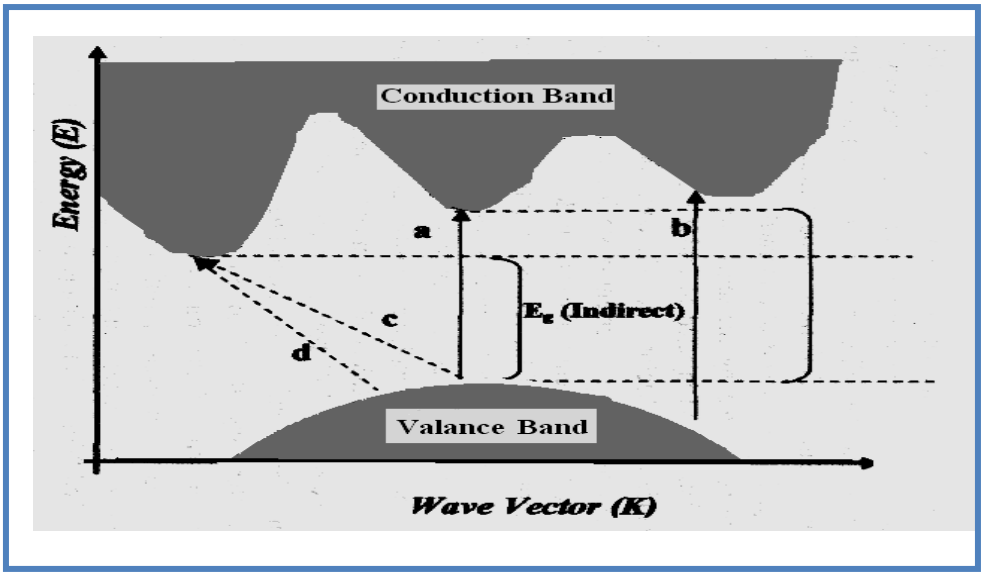

Figure.(2.1) :The transition process[85].

(a) allowed direct transition. **(c) allowed indirect transition.**

(b) forbidden direct transition. **(d) forbidden indirect transition.**

The reflectance (R_0) has been determined from values of transmission (T_0), and absorbance (A_0), using the relationship [86]:

$$A_0 + R_0 + T_0 = 1 \quad \text{.....(2-33)}$$

2.8.2 Absorption Regions

The absorption regions can be classified into three regions[87]:

A) High absorption region : the magnitude of absorption coefficient (α) is larger or equal to (10^4 cm^{-1}).

B) Exponential region: the value of absorption coefficient (α) is equal to ($1\ cm^{-1} < \alpha < 10^4\ cm^{-1}$).

C) Low absorption region: the absorption coefficient (α) is very small, it is about ($\alpha < 1 cm^{-1}$) as shown in Figure (2.4) which shows the absorption regions.

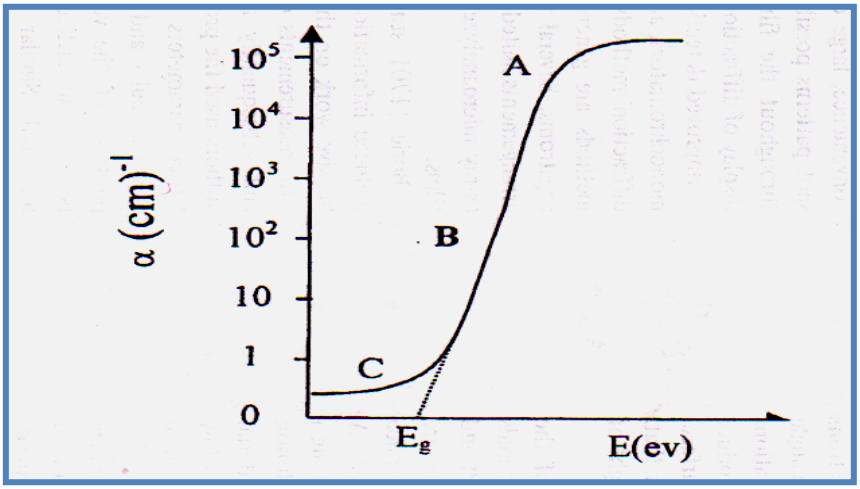

Figure: (2.2). The absorption regions [87].

2.8.3 Refractive Index and Extinction Coefficient

The index of refraction of a material is the ratio of the velocity of the light in vacuum to that in the specimen [88] :

$$n = \frac{c}{v} \quad \text{.....(2-34)}$$

where (c) is the velocity of the light in vacuum and (v) is the velocity of the light in specimen.

$$n^* = n - ik \quad \text{.....(2-35)}$$

Where n* is complex refractive index, n is real part of refractive index and k is imaginary part of refractive index (extinction coefficient).The energy loss of

electromagnetic radiation through that medium is measured by the extinction coefficient of a particular substance [84].

$$k = \frac{\alpha\lambda}{4\pi} \quad \text{.....(2-36)}$$

λ: wavelength of photon.

real part of refractive index(n) can be determined by [89]:

$$n = \frac{1+\sqrt{R_0}}{1-\sqrt{R_0}} \quad \text{.....(2-37)}$$

Where R_0 is the reflectance.

2.8.4 Dielectric Constant and Optical Conductivity

The real part of the dielectric constant shows how much it will slow down the speed of light in the sample and the imaginary part of the dielectric constant shows how a dielectric absorbs energy from an electric field due to dipole motion. The real part and imaginary part of the dielectric constant have been determined by[90]:

$$\varepsilon=(\varepsilon_1-i\varepsilon_2) \quad \text{.....(2-38)}$$

$$\varepsilon_1 = (n^2 - k^2) \quad \text{.....(2-39)}$$

$$\varepsilon_2=(2nk) \quad \text{.....(2-40)}$$

The optical conductivity was calculated using the following relation [91]:

$$\sigma = \frac{\alpha nc}{4\pi} \quad \text{.....(2-41)}$$

2.9 Fourier Transform Infrared Radiation

Fourier Transform Infrared Radiation (FTIR) is a technique used to obtain an infrared spectrum of absorption or emission of a solid, liquid or gas. An FTIR spectrometer simultaneously collects high-spectral-resolution data over a wide spectral range. This confers a significant advantage over a dispersive spectrometer, which measures intensity over a narrow range of wavelengths at a time. The term Fourier-transform infrared radiation originates from the fact that a Fourier transform (a mathematical process) is required to convert the raw data into the actual spectrum [87].

2. 10 Scanning Electron Microscope

Scanning electron microscope (SEM) is a type of electron microscope that produces images of a sample by scanning the surface with a focused beam of electrons. The electrons interact with atoms in the sample that contain information about the sample's surface topography. The most common SEM mode is detection of secondary electrons emitted by atoms excited by the electron beam. The number of secondary electrons can be detected depending on specimen topography[92].

2.11. Methylene Orange Dye

Methylene orange is common dye that are often used in industries like textile, paper, rubber, plastics, leather, cosmetics, pharmaceutical and food industries[93]. Presence of very low concentrations of these dyes in effluent is important for the environmental toxicity. It can cause irritation to the gastrointestinal tract with symptoms of nausea, vomiting, diarrhea and also causes irritation to the skin when in contact with it. Methylene orange can be used as an indicator in the titration of weak bases with strong acids Methylene

orange can be used as an indicator in the titration of weak bases with strong acids [94] .

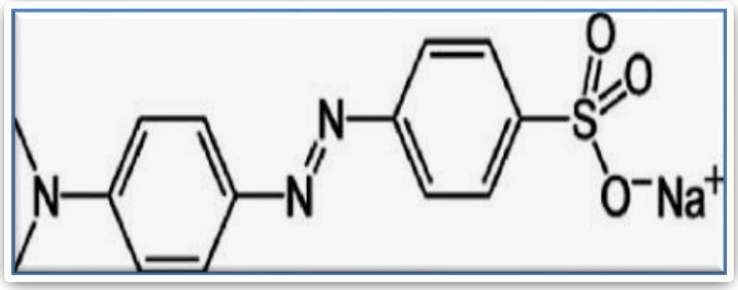

Figure (2.3):Molecular Structure of Methylene Orange Dye [94].

Table(2. 1): Properties and Molecular Structure of Methylene orange [94].

Properties	Methylene orange
Chemical Formula	$C_{14}H_{14}N_3NaO_3S$
Molecular Weight (g/mol)	327.33
Molecular diameter (A^o)	26,14 Å.
Maximum Absorbs ion Wavelength (nm)	640
Type of Dye	Anionic

2.17 Photocatalysis

Photocatalysis is described as the photoreaction acceleration process by the presence of a catalyst. A catalyst is a material that makes a chemical reaction more likely to happen by reducing the activation energy needed to start it. A catalyst speeds up a chemical reaction and does not vary in itself or being expended in the chemical reaction [95]. Chlorophyll in plants is a natural photocatalyst. The difference between chlorophyll and an industrial catalyst is that chlorophyll absorbs sunlight to convert water and carbon dioxide into oxygen and glucose, but the industrial catalyst gives a very strong oxidizing compound that breaks the bonds of toxic organic substances and bacteria when exposed to sunlight or ordinary light and turns them into carbon dioxide and

water. Most organic pollutants can be degraded by heterogeneous photocatalysis. Semiconductor nanoparticles meet the requirements for good photocatalysts because semiconductor materials have a small energy gap between the valence band and the conduction band[96].The addition of polymeric materials to the nanoparticles leads to the dispersion of the nanoparticles and preventing them from sedimentation, and this leads to a reduction in electron-hole recombination, thus increasing the photocatalytic efficiency of the nanoparticles [97]. For the photocatalysis process to take place, the semiconductor material absorbs a photon of energy from the direct sun's rays or from an ultraviolet source that is equal or greater than to its band gap ($h\nu \geq E_g$), the electrons move from the valence band to the conduction band, and the pairs of (electronsholes) are generated[98].The electrons contribute to the reduction reactions by the formation of superoxide radicals (O_2 •−), and the holes contribute to the oxidation of organic compounds by the formation of hydroxyl radicals (OH•). These radicals will be attacked by the organic molecule, which is finally oxidized to become H_2O, CO_2 and HCl. The processes of Photodegradation include the following [99]:

1- Formation of excitons by absorption of photons by photocatalyst nanocomposites.

$$\text{nanocomposites} + h\nu \rightarrow h^{+} + e^{-} \quad \text{..... (2-42)}$$

Where the electrons (e^-) are generated in the conduction band and holes (h^+) are generated in the valence band.

2. Formation of superoxide anion (O_2 •−).

$$O_2 + e^- \rightarrow O_2^{\bullet -} \quad \text{..... (2-43)}$$

3. Formation of hydroxyl radicals (OH•).

$H_2O + h+ \rightarrow H^+ + OH^\bullet$ ..... (2-44)

4. Neutralization of superoxide anion by protons and formation of Hyper oxide radical ($HO_2^\bullet$).

$O_2^{\bullet-} + H+ \rightarrow HO_2^\bullet$ ..... (2-45)

5. Formation of hydrogen peroxide (H_2O_2) and dismutation of oxygen.

$2HO_2^\bullet \rightarrow H_2O_2 + O_2$ ..... (2-46)

$H_2O_2 + e^- \rightarrow OH^- + OH^\bullet$ ..... (2-47)

6. Formation of degradation products.

R (Organic pollutant) + $H_2O_2 + OH^\bullet + O_2^{\bullet-} \rightarrow CO_2 + H_2O$ ..... (2-48)

The photo catalytic activity was evaluated by decomposition of methylene orange dye (MO) because of the dye of methylene orange has less absorption and proved to be a relatively strong and stable molecule under UV irradiation.

The degradation percentage (DP) of nanocomposites can be calculated by the following equation [100]:

$DP = [(A_0 - A_1)/A_0] \times 100\%$ ..... (2-49)

Where A_0 and A_1 are absorption before and after irradiation, respectively.

3.1 Introduction

This chapter includes the stages of samples preparation for (PEO-CuO-In_2O_3) and (PEO-NiO-In_2O_3) nanocomposites. The tests of the Samples and measurement stages are: optical microscopic, FTIR, scanning electron microscope (SEM), optical measurements, , antibacterial activity application measurements and Photodegradation activity of films under UV irradiation (135 W) application measurements.

3.2 The Materials Used in This Work

3.2.1 Polymer

The polymer is used in this work:

Poly(ethylene oxide) (PEO): it was obtained as powder form and could be obtained from local markets with high purity (99.8%) and average molecular weight (600000 g/ mol).

3.2.2 Metals Oxides Nanoparticles

1. **Copper oxide nanoparticles (CuO):** used as powder from US Research Nanomaterials, Inc
2. **Nickel oxide nanoparticles (NiO):** used as powder from US Research Nanomaterials, Inc
3. **Indium Oxide (In_2O_3):** it was obtained as powder from US Research Nanomaterials, Inc

3.3 Preparation of (PEO-CuO-In_2O_3) and (PEO-NiO-In_2O_3) Nano-composites

The nanocomposites of (PEO-CuO-In_2O_3) and (PEO-NiO-In_2O_3) are prepared by dissolving (0.982 gm) of PEO with (0.018gm) of CuO for (PEO-CuO) nanocomposites and (0.018gm) of NiO for (PEO-NiO) nanocomposites in 40 ml of distilled water, by using magnetic stirrer to mix the polymer and nanoparticles for 1 hour to obtain more homogeneous solution.

The In_2O_3 nanoparticles that are added to (PEO-CuO) and (PEO-NiO) nanocomposites with different concentrations are (1.8, 3.6 and 5.4) wt.% . The casting method is used to prepare the samples of (PEO-CuO-In_2O_3) and (PEO-NiO-In_2O_3) nanocomposites in the template (petri dish has diameter 10 cm). The samples were prepared with thickness range (140) μm, Table (3.1) and Figure (3.1) shows experimental work.

Table (3.1): Weight percentages for nanocomposites (PEO-CuO-In_2O_3) and (PEO-NiO-In_2O_3).

PEO (gm)	CuO (gm)	NiO (gm)	In_2O_3 wt %	Weight of Sample
0. 982	0.018	0.018	0	1 gm
0.964	0.0176	0.0176	1.8	
0.946	0.0173	0.0173	3.6	
0.928	0.017	0.017	5.4	

3.4 Measurements of Structural Properties for Nanocomposites

Measured structural properties include:

3.4.1 Microscopic Examination

The (PEO-CuO-In_2O_3) and (PEO-NiO-In_2O_3) nanocomposites samples are examined by using the optical microscope (supplied from Olympus name (Toup View) type (Nikon- 73346)) with magnification (x10) and (x40).

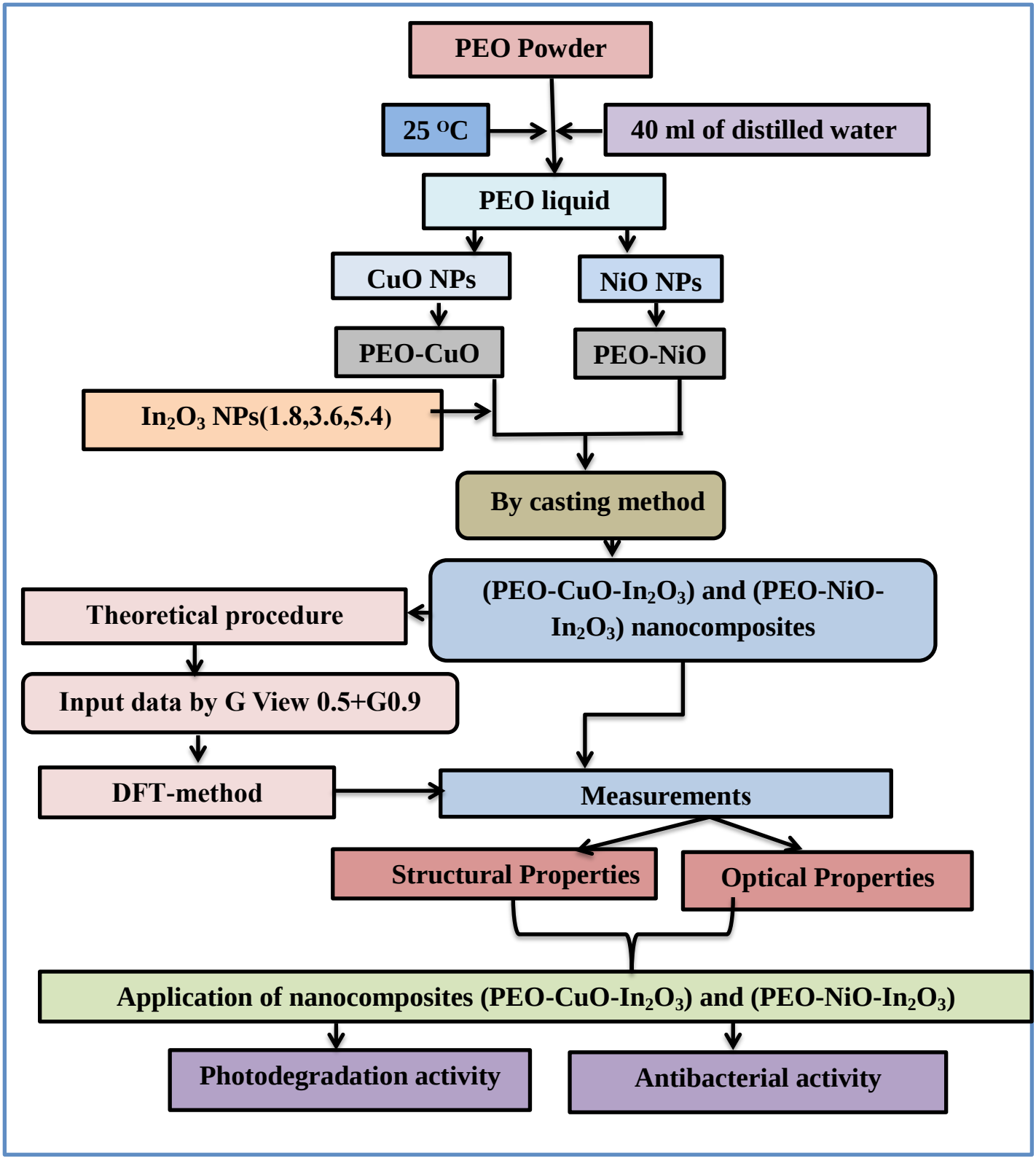

Figure (3.1): Schematic of experimental work.

3.4.2 Scanning Electron Microscope

The surface morphology of (PEO-CuO-In_2O_3) and (PEO-NiO-In_2O_3) nanocomposites for pure , concentration (1.8wt.%) , (3.6wt.%) and (5.4wt.%) are tested by using scanning electron microscope (Ziss, Sigma, German origin) in Shahrood university of technology, Iran.

3.4.3 FTIR Spectrometer

FTIR spectra for (PEO-CuO-In_2O_3) and (PEO-NiO-In_2O_3) nanocomposites are recorded by FTIR (Bruker company, German origin, type vertex-70) Fourier transform infrared spectrometer in wavenumber range (500–4000) cm^{-1}.

3.5 Optical Properties Measurements for Nanocomposites

The optical properties of (PEO-CuO-In_2O_3) and (PEO-NiO-In_2O_3) nanocomposites are measured by using the double beam spectrophotometer (shimadzu, UV-1800^{0}A) in wavelength (200-800) nm.

3.6 Photocatalytic Activity Application Measurements

In order to examine the photocatalytic activity of pure (PEO), (PEO-CuO), (PEO-CuO-In_2O_3), (PEO-NiO) and (PEO-NiO-In_2O_3) nanocomposites, an amount of (100 mL) aqueous solution of methylene orange dye with concentration (20 ppm) was placed in Pyrex glass. Different prepared samples were placed in this solution with magnetic stirring. Then, the samples were placed in an ultraviolet light exposure cabinet containing a magnetic stirrer to confirm the homogeneity of the mixture in which they were illuminated with (135W). The solution was kept in the dark under stirring for (90 min) to reach the adsorption/desorption equilibrium. Samples of solution (10 mL) were taken from the methylene orange solution every 15 min for (1.5 hours) and centrifuged at (5000 rpm). MO dye solution has a maximum absorption at about 460 nm. The absorbance was measured using the double beam spectrophotometer (Shimadzu, UV-1800Å), in wavelength (400-520) nm.

3.7 Antibacterial Activity Application Measurements of Nanocomposites

Antimicrobial activity of the (PEO-CuO-In_2O_3) and (PEO-NiO-In_2O_3) nanocomposites tested samples are determined using a disc diffusion method. The antibacterial activities are done by using gram positive organisms (Bacillus cereus) and gram negative organisms (Salmonella). Bacteria (Bacillus cereus and Salmonella coli) were cultured in Muller-Hinton Medium. The disks of the (PEO-CuO-In_2O_3)and(PEO-NiO-In_2O_3) nanocomposites were placed over the media and incubated at 37°C for 24 hours. The inhibition zone diameter was measured.

4.1 Introduction

This chapter presents the results and discusses of the structural, electrical, and optical properties of (PEO-CuO-In_2O_3) and (PEO-NiO-In_2O_3) nanocomposites. The Beckes, three parameter exchange with Lee, Yang and Parr correlation functional (B3LYP) density functional theory Stuttgart Dresden triple zeta (SDD) basis sets is used to calculate the ground state theoretically. The calculations for the excited states are done using the time-dependent DFT(TD-SCF) techniques with the (B3LYP) functional and (SDD) basis sets.

The implications and discussion of structural and optical measurements for the recommended pure PEO and its nanocomposites are part of the experimental phase. The effect of adding Indium Oxide nanoparticles (In_2O_3 NPS) to (PEO-CuO) and (PEO-NiO) nanocomposites on optical characteristics is explored in this chapter, with a comparison of theoretical and experimental results. Applications of antibacterial activity for polymers and nanocomposites are also considered and photo-degradation of dyes pollutants.

4.2 The Structural Properties of Pure PEO and Nanocomposites

Measured structural properties include:

4.2.1 Geometrical Properties

Number of physical and chemical characteristics are limited by the geometry of a molecule under investigation. It is required to identify the molecule's optimization, in which the relaxed structure of the molecules has the least amount of energy. The recommended nanocomposites are first developed using the Gauss View 5.0.8 software, and then relaxed using the Gaussian 09 package of programs' three-parameter hybrid functional of Becke (B3LYP) using density functional theory (DFT) and SDD basis set. The relaxed structures of the pure (PEO), (PEO-CuO), (PEO-NiO), (PEO-CuO-

In_2O_3) and (PEO-NiO-In_2O_3) nanocomposites in the gas state, are shown in Figures (4.1- 4.5).

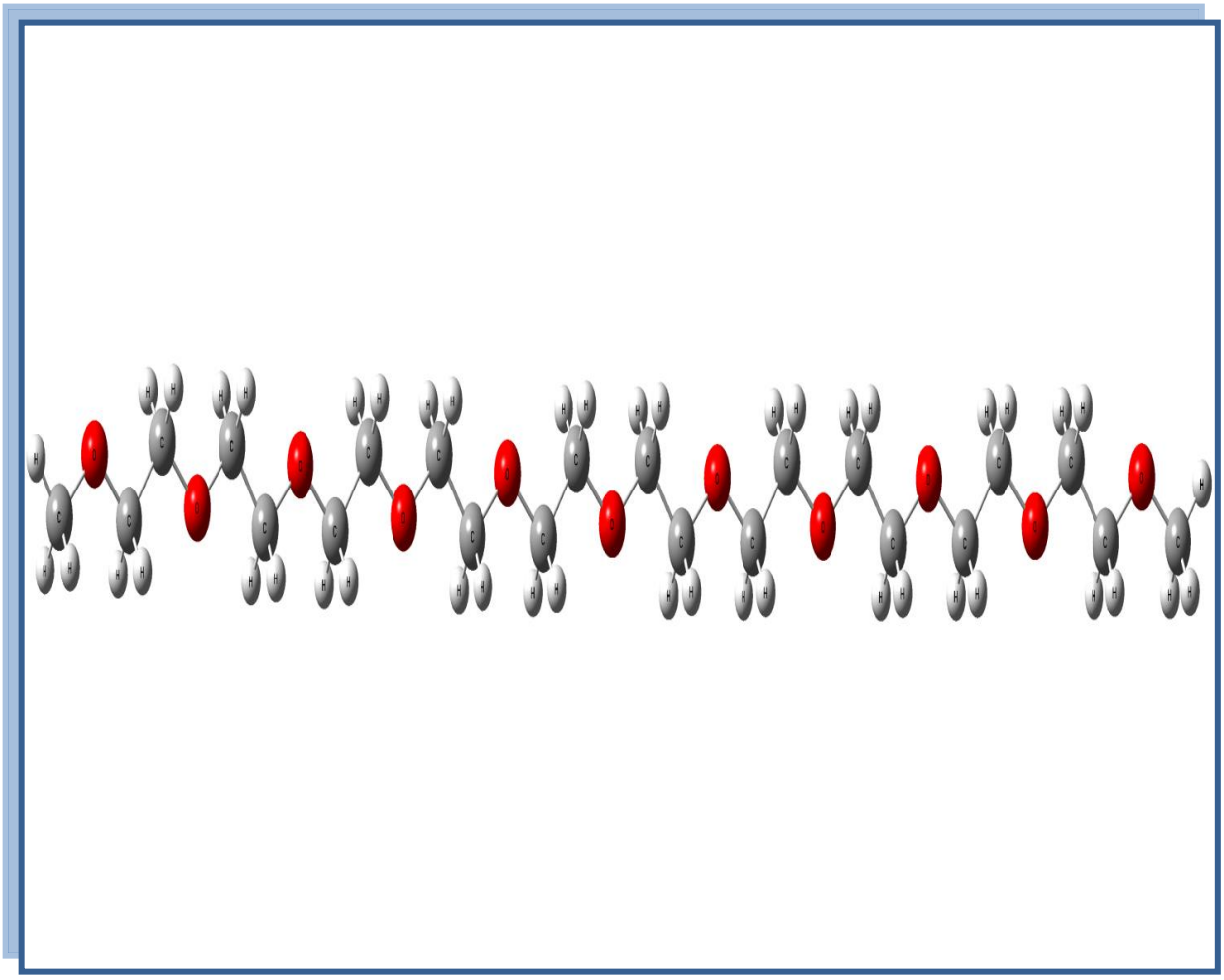

Figure (4.1): The relax structures of the pure (PEO) using DFT- B3LYP/ 6-31G basis set.

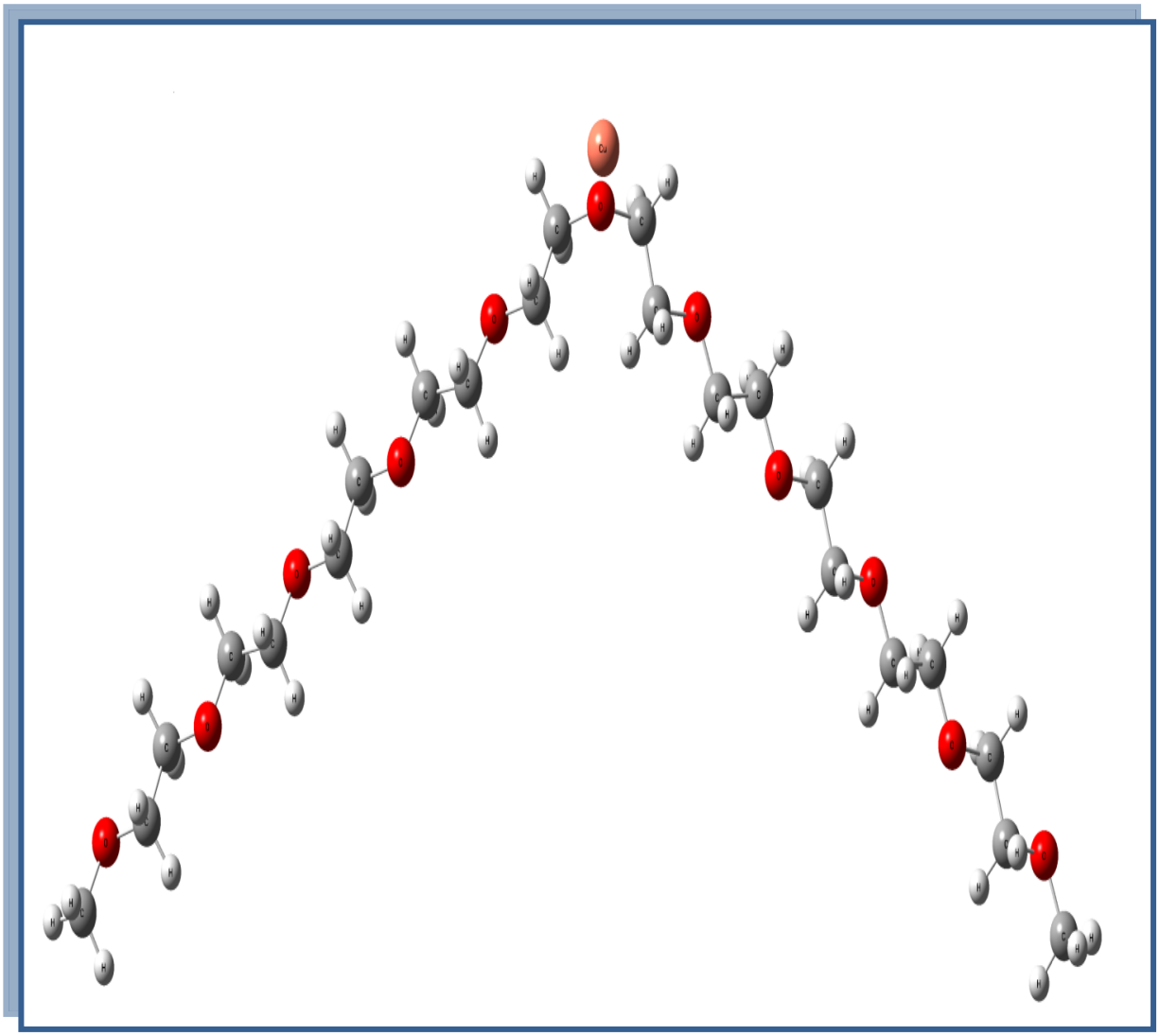

Figure (4.2): The relax structures of (PEO-CuO) nanocomposites using DFT B3LYP/ SDD basis set.

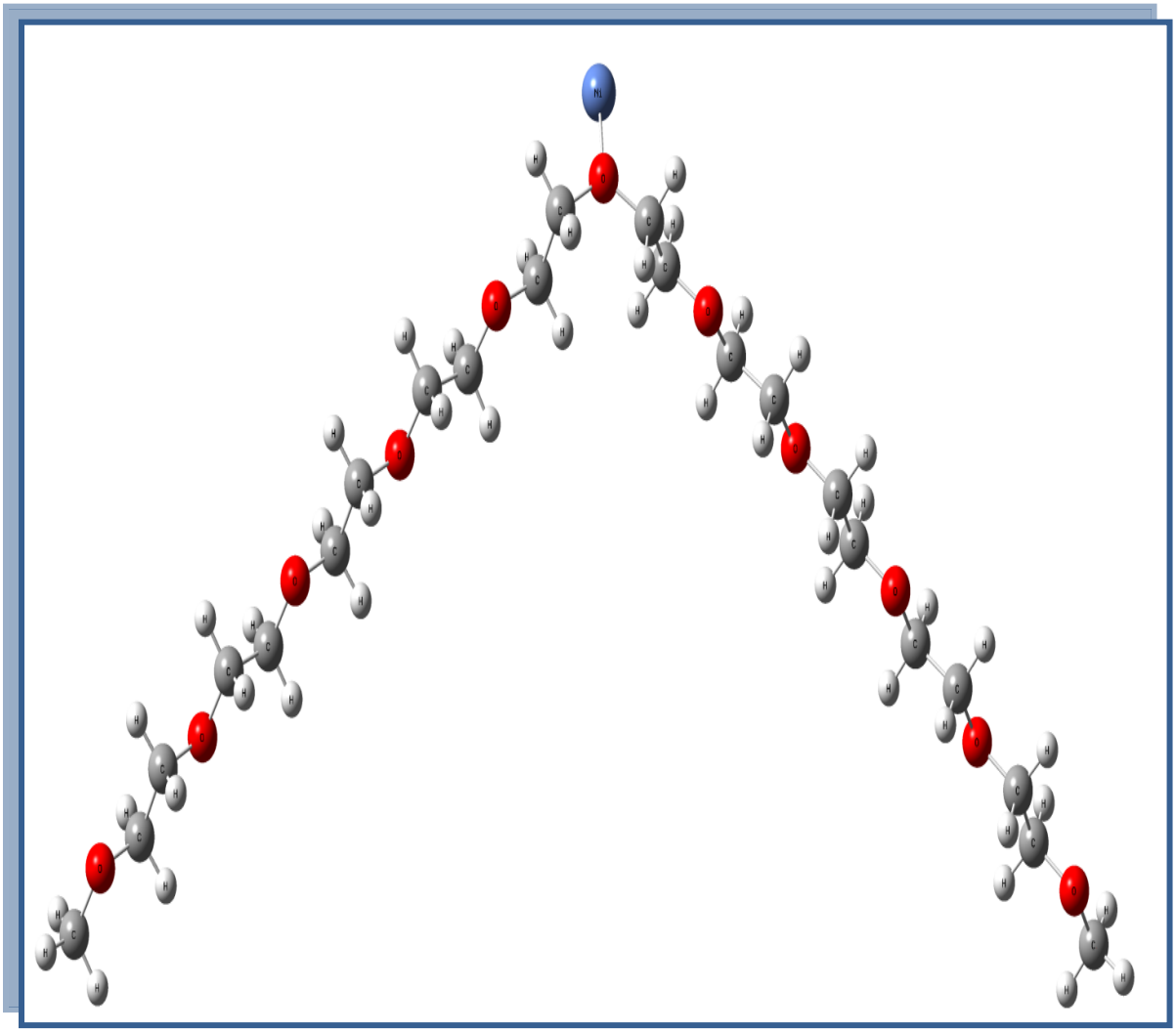

Figure (4.3): The relax structures of (PEO-NiO) nanocomposites using DFT-B3LYP/ SDD basis set.

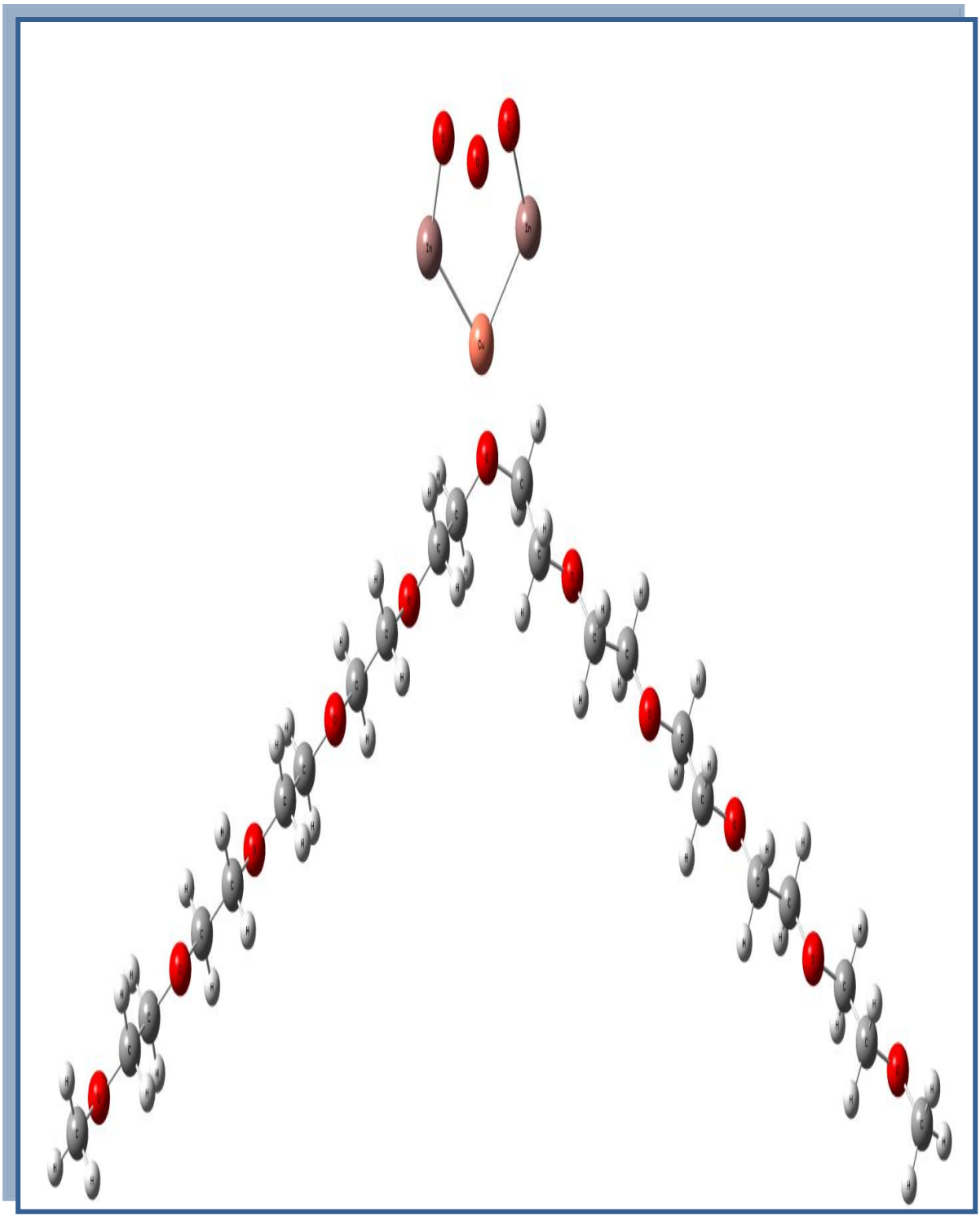

Figure (4.4): The relax structures of (PEO-CuO-In_2O_3) nanocomposites using DFT B3LYP/ SDD basis set.

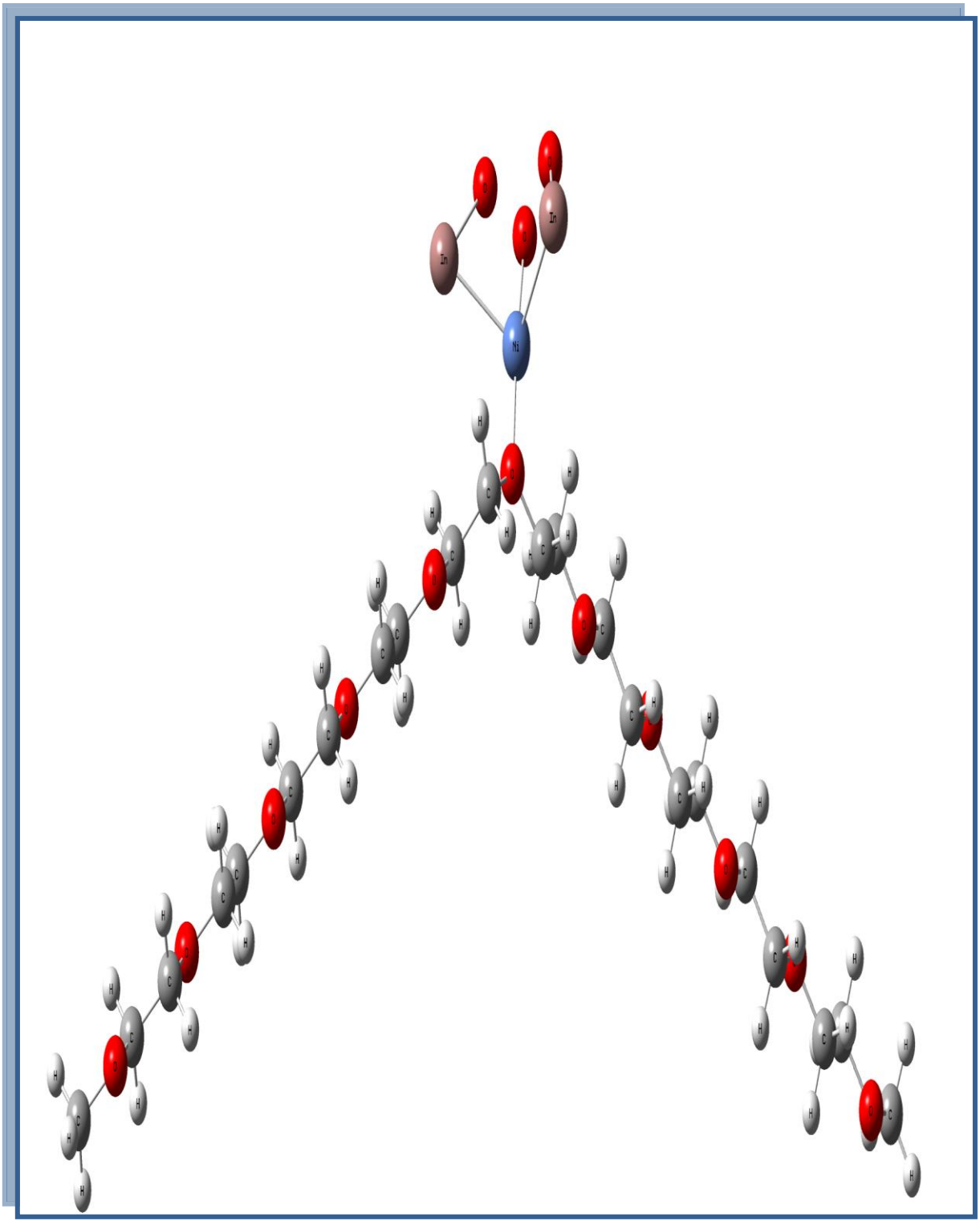

Figure (4.5): The relax structures of (PEO-NiO-In_2O_3) nanocomposites using DFT-B3LYP/ SDD basis set.

Table (4.1) shows the geometric parameters of the (PEO-CuO-In_2O_3) and (PEO-NiO-In_2O_3) nanocomposites which included the bond length in Angstrom and the bond angle in degrees It can be concluded that the DFT method is effective for estimating the optimal structure of the studied molecule, due to the DFT method which is characterized by its accuracy in estimating the molecular properties of any compound. The calculated values of the bonds in the present work are in good agreement with previous theoretical studies

Table (4.1): B3LYP/ SDD-DFT calculations of bond length in Angstroms (A^0) and bond angle in degree of pure PEO and nanocomposites.

Measurements	The optimization parameters	Present work	The previous studies
Bonds Å	(C−C)	1.537	1.49-1.501[101, 102]
	(C−O)	1.455	1.374-1.478[90,103]
	(C−H)	1.098	1.095-1.1[104,105]
	(In-O)	2.054	…….
	(In–Cu)	2.609	…….
	(O–Cu)	2.046	…….
	(Ni–O)	1.90727	…….
	(Ni–In)	2.72686	…….
Angles deg.	(H-C-H)	108.83735	
	(H-C-C)	110.168	…….
	(H–C–O)	110.573	…….
	(O-O-O)	110.444	…….
	(O-Cu-In)	130.62648	…….
	(In-Cu-In)	91.76066	…….
	(O-Ni-In)	109.85133	…….

4.2.2 Fourier Transform Infrared Radiation (FTIR) of Nanocomposites

The chemical structure of PEO molecules may be established by recognizing the linked bonds that appear in the FTIR transmission spectrum. The formula 3N-6 was used to calculate the number of vibrational modes in the spectrum, where N is the number of atoms in pure PEO and nanocomposites, and 6 is the number of vibrational modes in the spectrum. As the number of bonds in the molecule has grown, so has the number of vibrational modes.

Figures (4.6-4.12) and Tables (4.2-4.4) show the theoretical and experimental FTIR spectra of (PEO-CuO-In_2O_3) and (PEO-NiO-In_2O_3) nanocomposites. The left region, which lies between (1500-4000) cm^{-1}, is known as the diagnostic region, and the second region, which lies between (400-1500) cm^{-1}, is known as the fingerprint region, which points out to the functional group region. The left region, which is especially close to 4000cm^{-1} is for the high energy bonds.

The use of FTIR spectroscopy to determine vibrational groups of pure polymers and their interaction with produced nanoparticles has been proven experimentally [106]. Pure PEO has a significant peak in the FTIR spectrum about 2879.55 cm^{-1}, which is linked to asymmetric C-H stretching vibrations of CH_2 groups. The bands at 1341 cm^{-1} and 1278 cm^{-1} were assigned to CH_2 asymmetric bending and CH_2 symmetric twisting[107]. The peak about 1466.33 cm-1 was attributed to CH_2 scissoring mode of PEO. The strong band about 1098.35 cm-1 for all samples of nanocomposites attributed to the OH bending mode[108]. Stretching vibration of C-O at 960 cm^{-1} is due to PEO with CH_2 rocking asymmetric vibration [42], and C–O stretching is likewise assigned to the band at 841.23 cm^{-1} in PEO [109]. Because of incoming radiation is absorbed by free electrons in nanoparticles, the strength of the

peak increases as the concentration of nanoparticles increases. According to FTIR investigations, introducing (NPs) results in the displacement of certain bonds rather than the development of additional peaks [45]. Variations in the spectrum of (PEO-CuO) and (PEO-NiO) nanocomposites, including shifts in certain bonds and changes in intensities, generate In_2O_3NPS interactions with (PEO-CuO) and (PEO-NiO) nanocomposites were responsible for these modifications. According to FTIR investigations, adding In_2O_3 NPS causes the displacement of certain bonds rather than the creation of new peaks, which is the nanocomposites' basic concept. The transmittance in the figures reduces significantly as the amount of In_2O_3 NPS increases, indicating that the density of nanocomposites has increased. When the theoretical value was compared to the experimental value, there was more than an approximation value for all samples with the previously described experimental findings. This is a good lead. The spectra of pure polymers and the pure- Nanoparticle combination have no differences. This demonstrates that the polymer and the nanoparticles do not react chemically.

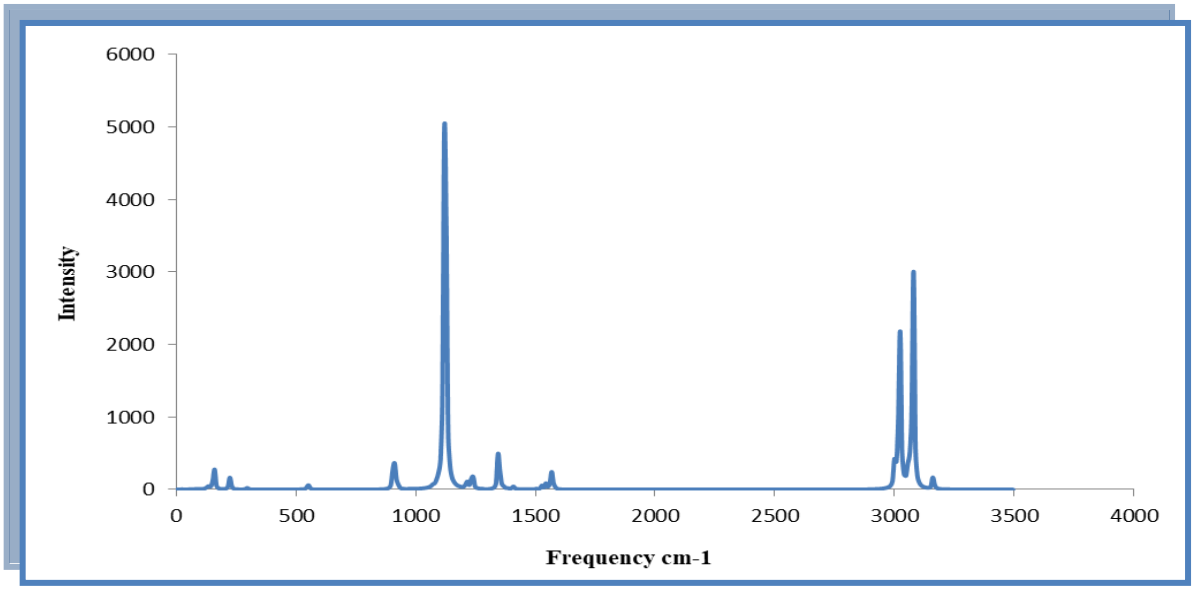

Figure (4.6): Theoretically IR-spectra for pure (PEO).

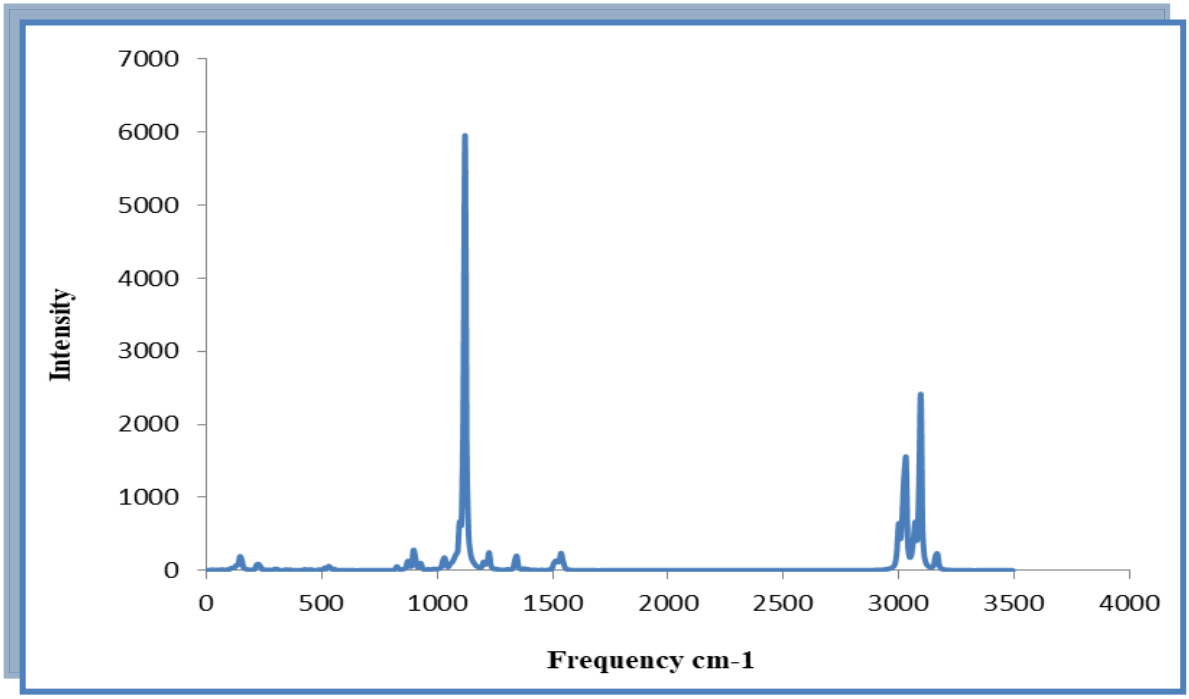

Figure (4.7): Theoretically IR-spectra for (PEO-CuO) nanocomposites .

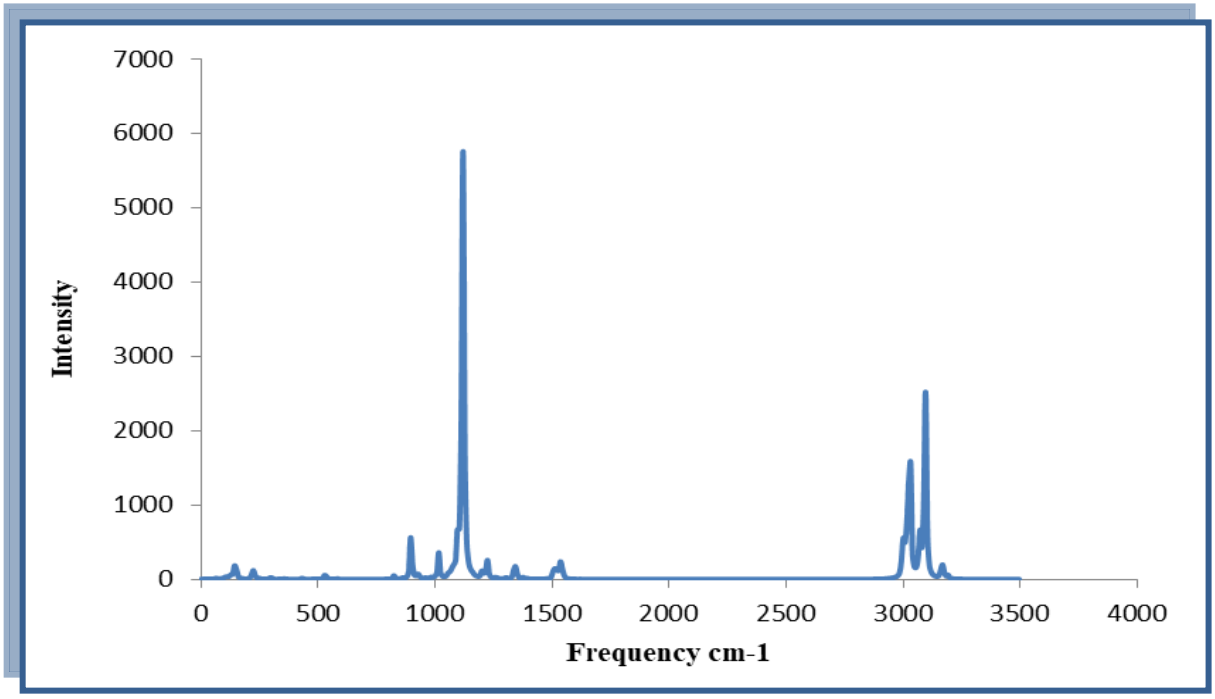

Figure (4.8): Theoretically IR-spectra for (PEO-NiO) nanocomposites .

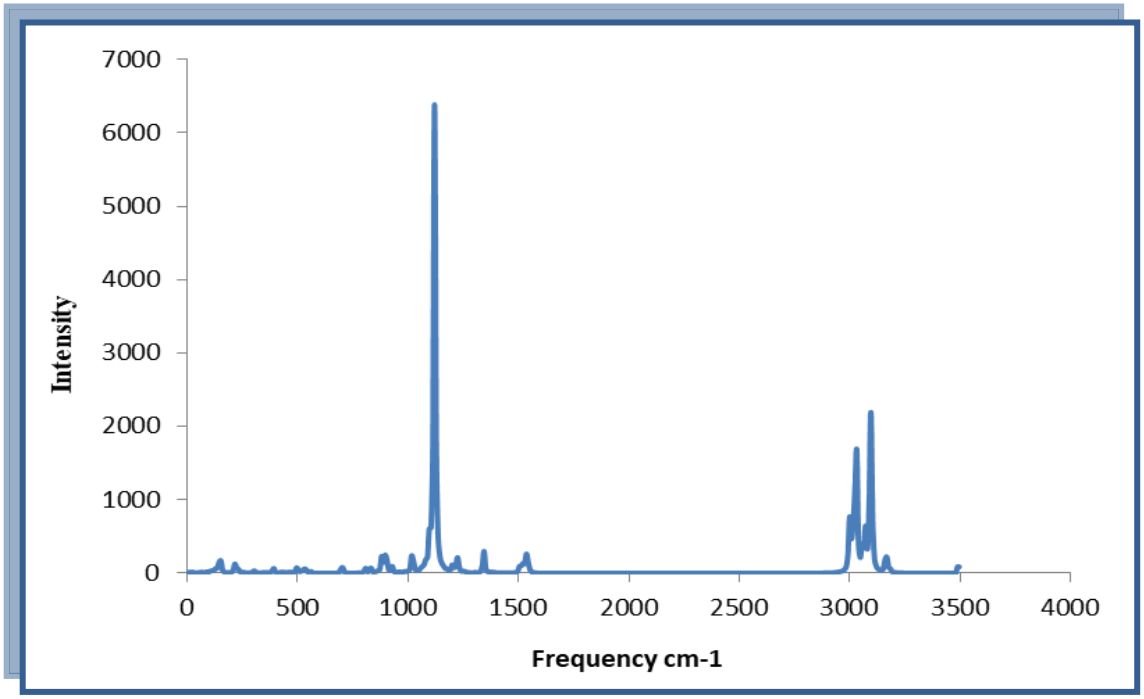

Figure(4.9): Theoretically IR-spectra for (PEO-CuO-In_2O_3) nanocomposites.

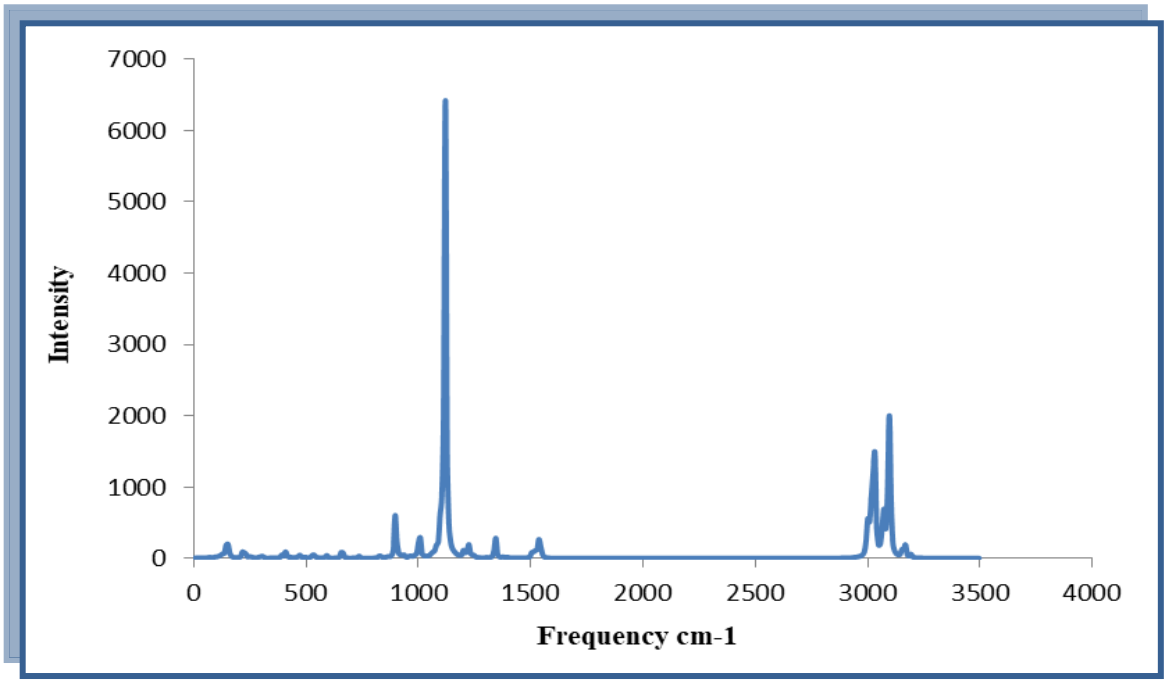

Figure(4.10): Theoretically IR-spectra for (PEO-NiO-In_2O_3) nanocomposites .

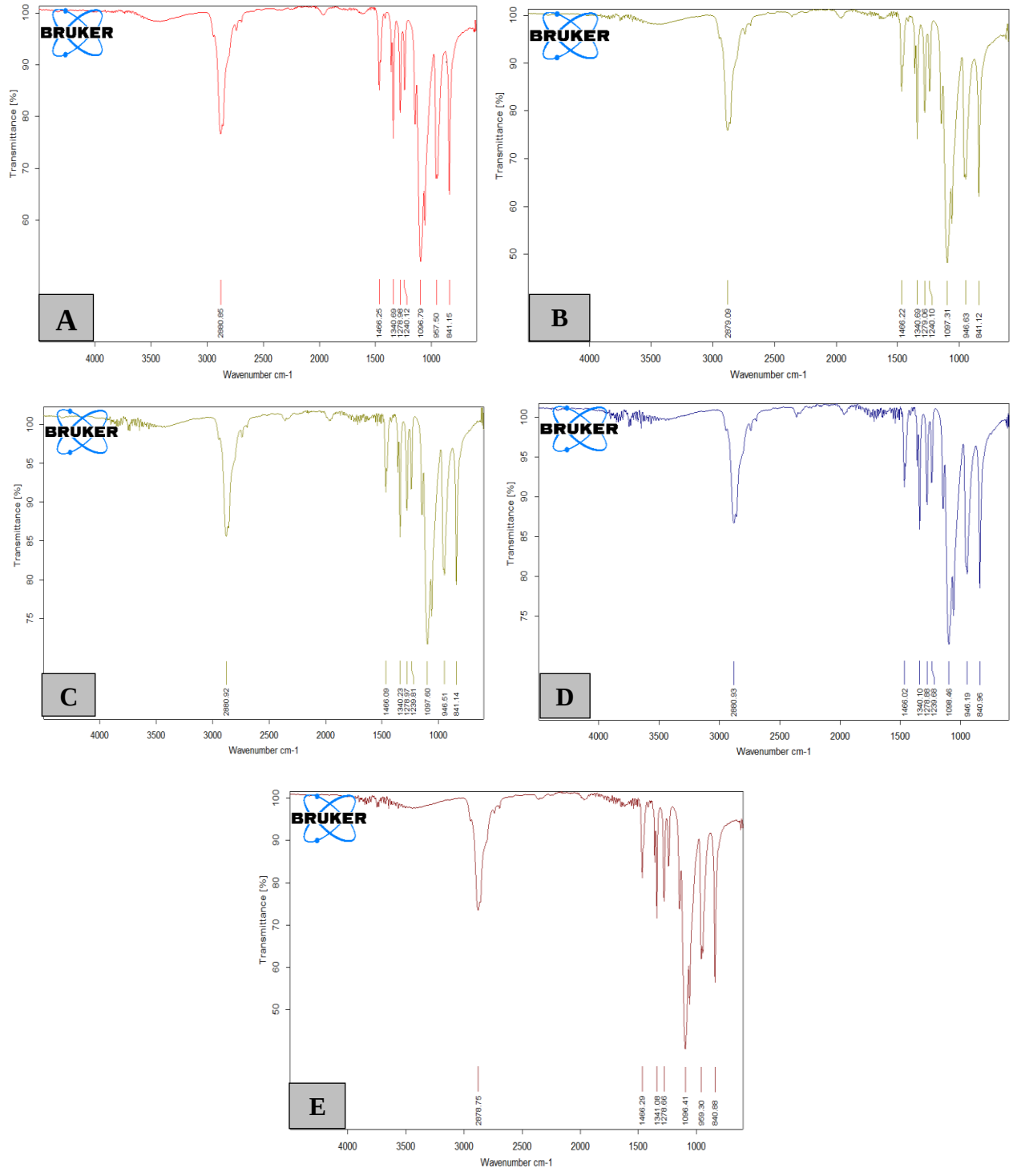

Figure(4.11): FTIR spectra for (PEO–CuO–In_2O_3) nanocomposites (experimentally) A. for pure, B. for (PEO- CuO) NPS, C. for 1.8 wt% In_2O_3 nanoparticles, D. for 3.6 wt%In_2O_3 nanoparticles and E. for 5.4 wt% In_2O_3 nanoparticles.

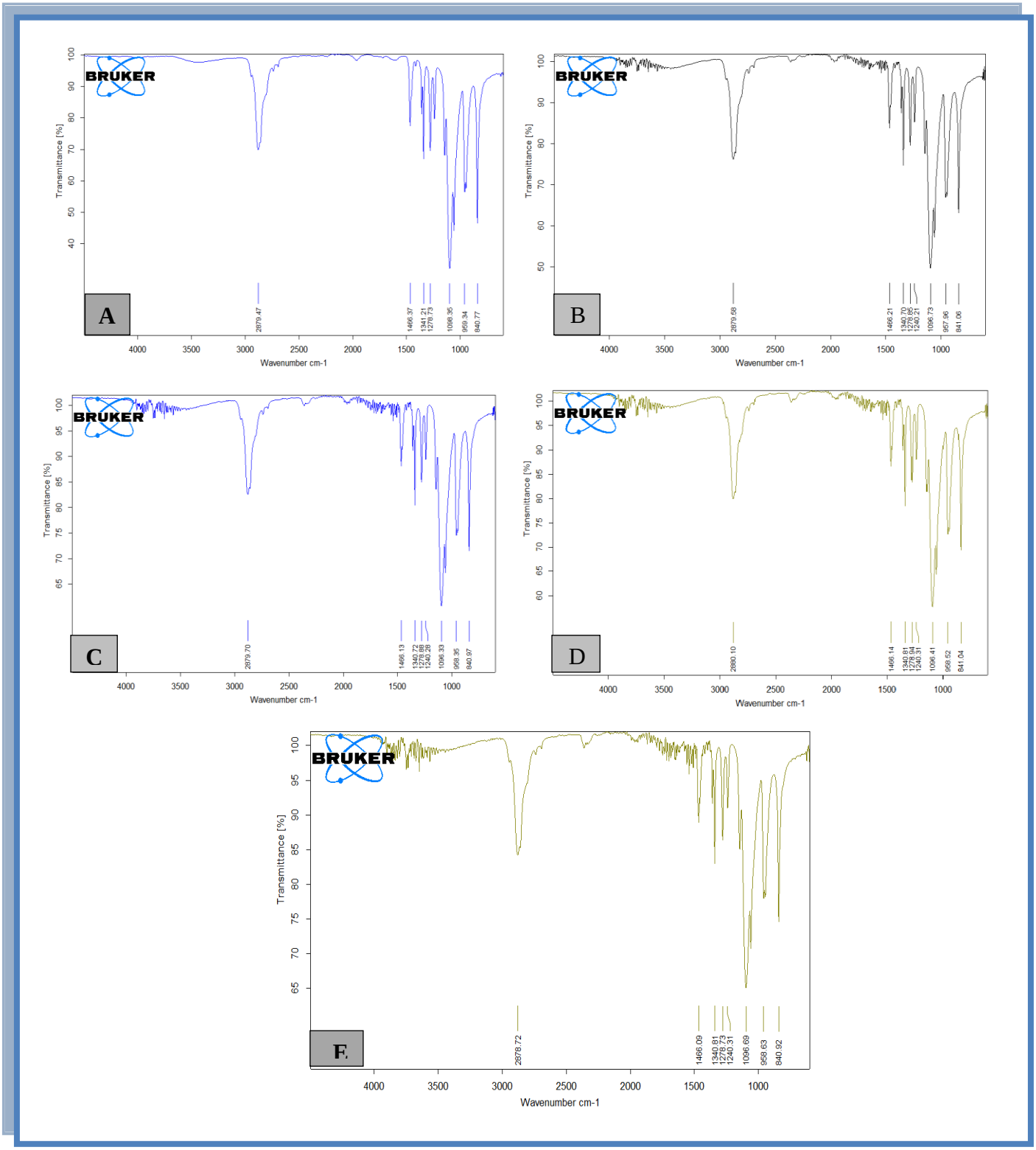

Figure (4.12): FTIR spectra for (PEO–NiO–In_2O_3) nanocomposites (experimentally) A. for pure, B. for (PEO- NiO) NPS, C. for 1.8 wt% In_2O_3 nanoparticles, D. for 3.6 wt%In_2O_3 nanoparticles and E. for 5.4 wt% In_2O_3 nanoparticles

.

Table (4. 2) : IR frequency with their assignment of (PEO-NiO-In_2O_3) nanocomposites obtained by DFT using B3LYP/SDD basis set.

Assignment	Vibrational mode Type	Frequency (cm^{-1})	Typical vibrational frequency (cm^{-1})
C-O	Stretching	1002.08	1000-1280 [41]
CH2	in–plane bending	1352.80	1340–1465 [41]
C- C	Stretching and bending	827.87	700–1600 [110]
C-O-C	Bending	1244.28	1238-1291 [41]
Ni-O	stretching	469.88	457-600 [111]
In-O	stretching	469.18	441 -583 [112]
CH3	Asymmetric stretching	2997.80	2900-3100[113]
O-O-O	Stretching and bending	389.73	……..

Table(4. 3) : IR frequency with their assignment of (PEO-CuO-In_2O_3) nanocomposites obtained by DFT using B3LYP/SDD basis set.

Assignment	Vibrational mode Type	Frequency (cm−1)	Typical vibrational frequency (cm^{-1})
C-O	Stretching	1078.79	1000-1280 [41]
CH_2	in–plane bending	1343.37	1340–1465 [41]
C- C	Stretching and bending	830 .10	700–1600 [112]
C-O-C	Bending	1165.38	1190-1150[114]
Cu-O	stretching	517.13	457-600 [111]
In-O	stretching	469.18	441 -583 [113]
CH_3	in–plane bending	1202.02	841-1420 [115]
O-O-O	Stretching and bending	659.81	……..

Table (4.4): Experimental values for the wavenumber of the absorption peaks and the corresponding bond[106- 109].

.

Wavenumbers (cm^{-1})	Assignments
2878	Asymmetry CH stretching of CH_2
1465	CH_2 scissoring mode of PEO
1341	CH_2 asymmetric bending
1278	CH_2 symmetric twisting
1097	OH bending
960	C-O stretching with some CH_2 rocking asymmetric vibration
841	C-O stretching in PEO

4.2.3 The Ultraviolet-Visible UV-Vis Spectra of Nanocomposites

The electrical structure of the molecule determines the Ultra Violet and Visible spectra. Figures (4.13) - (4.17) show the UV-Vis spectra that theoretically obtained by using Gaussian 09 program and Gaussian view 5.0.8 program and using density functional theory (DFT) at B3LYP level with 6-31G basis sets and SDD basis sets. When comparing the experimental and theoretical results, it can be seen that the spectrum in the experimental part is in the Ultra Violet (UV) region of the spectrum, whereas the spectrum in the theoretical part is within the Ultra Violet and Visible (UV-Vis) region of the spectrum, because of the spectrum in the experimental part is calculated as a function of concentration, whereas the spectrum in the theoretical part is calculated for each concentration. Which will compute the highest concentration at which the sample will be fully opaque and only visible in the visible spectrum, as well as the lowest concentration in the Ultra Violet spectrum. When the number of atoms that formation the nanocomposites

increases, it can be seen that the spectrum is far away from the visible area to approach an infrared area .This is illustrated by Figure (4.15). We find in Figures (4-14) and (4-15) that the absorbance of the nanocomposite (PEO-NiO) is higher than that of the nanocomposite (PEO-CuO), because the absorbance of NiO nanoparticles is greater than that of CuO nanoparticles

When adding In_2O_3 nanoparticles, we find clear differences in the absorption spectra due to the different absorption areas in which the nanoparticles operate.

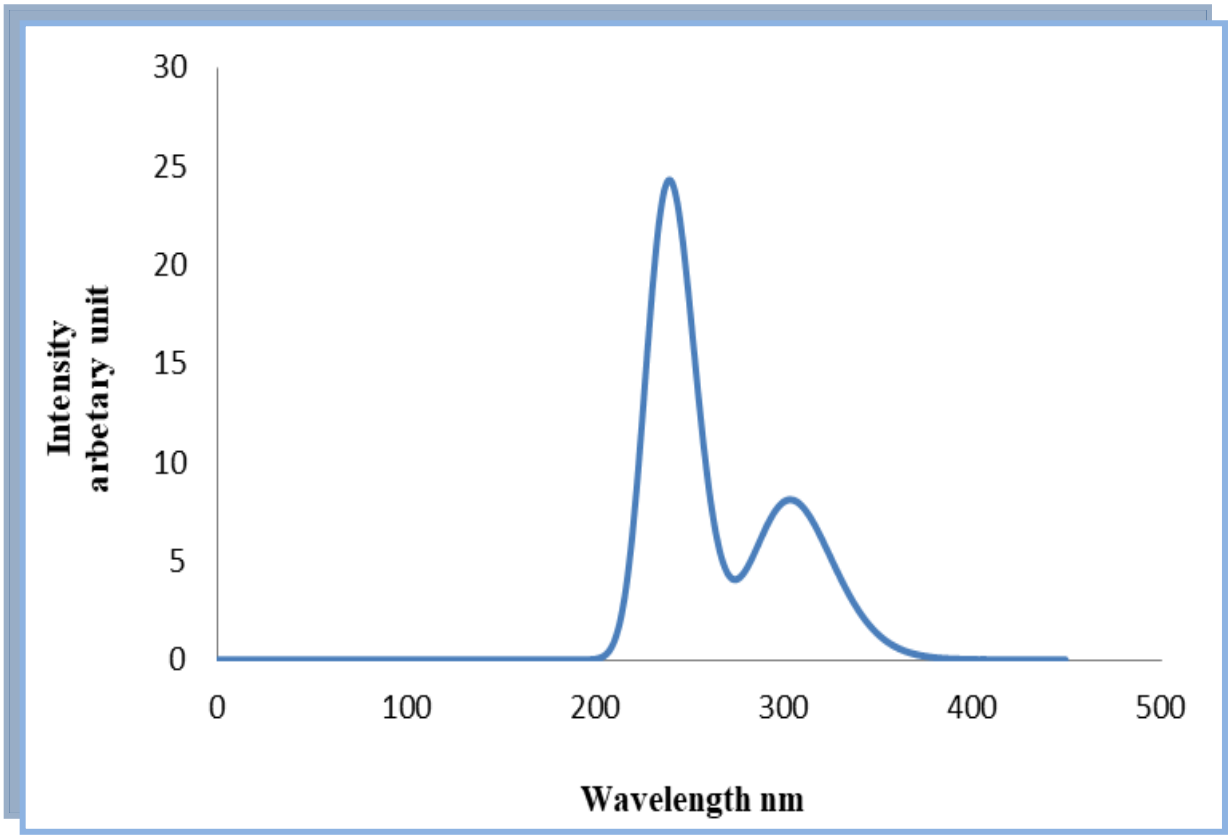

Figure (4.13): Ultraviolet-Visible spectrum for pure (PEO) using B3LYP/SDD.

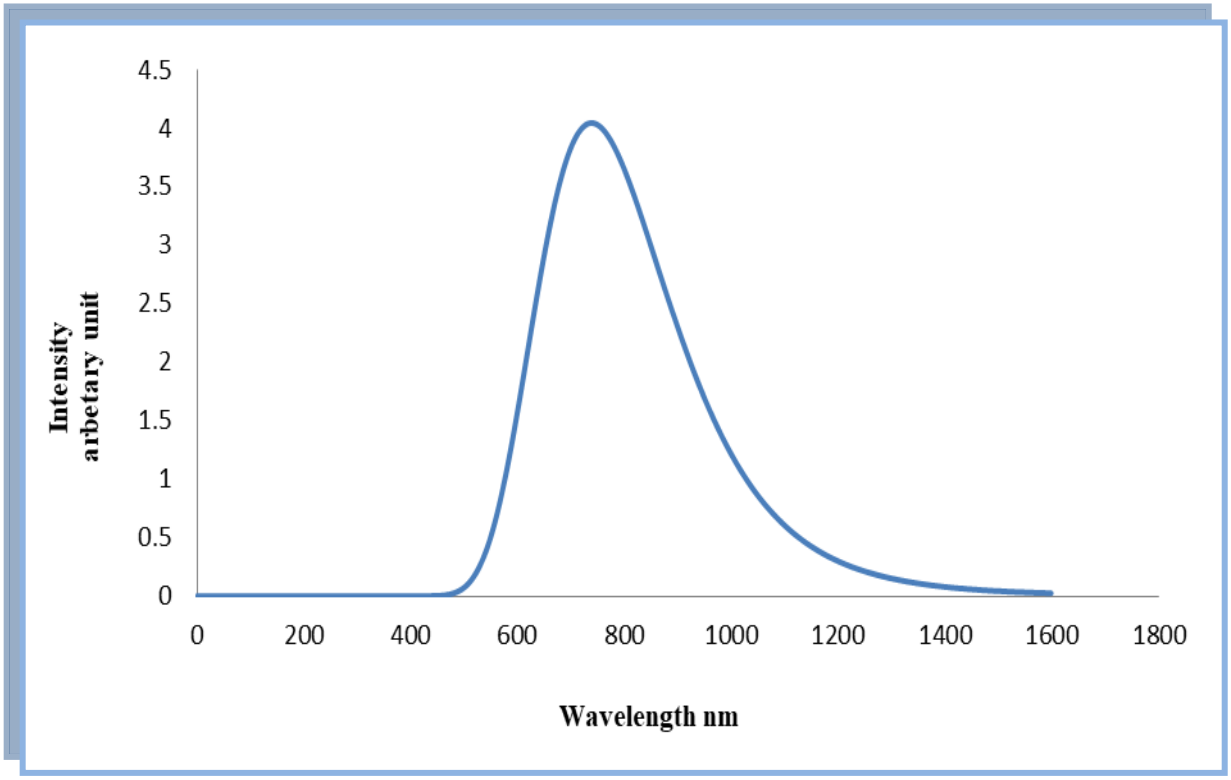

Figure (4.14): Ultraviolet-Visible spectrum for (PEO-CuO) nanocomposites using B3LYP/SDD.

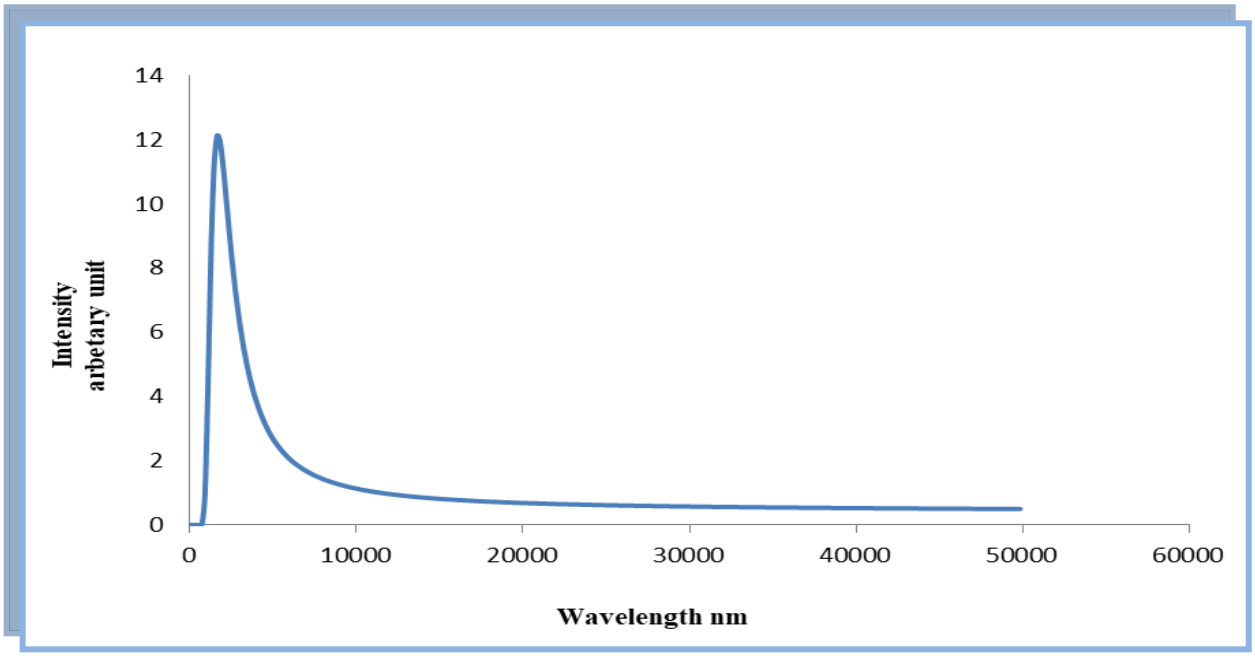

Figure (4.15): Ultraviolet-Visible spectrum for (PEO-NiO) nanocomposites using B3LYP/SDD.

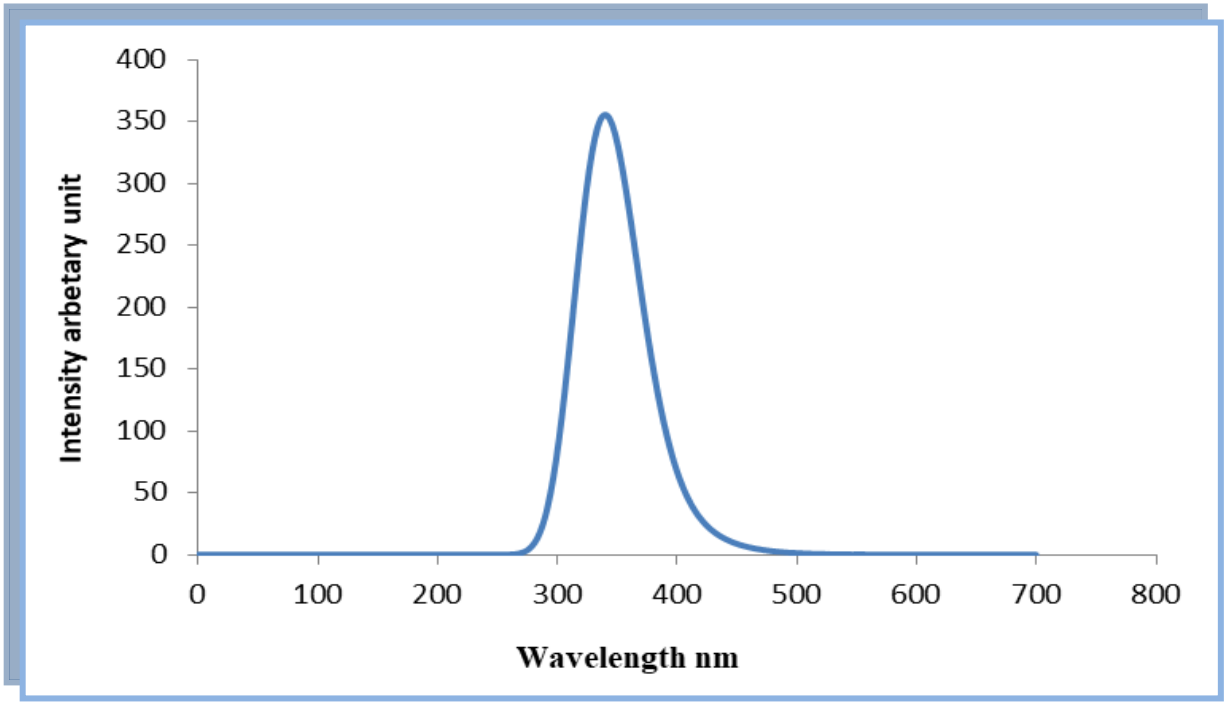

Figure (4.16): Ultraviolet-Visible spectrum for (PEO-In_2O_3) nanocomposites using B3LYP/SDD

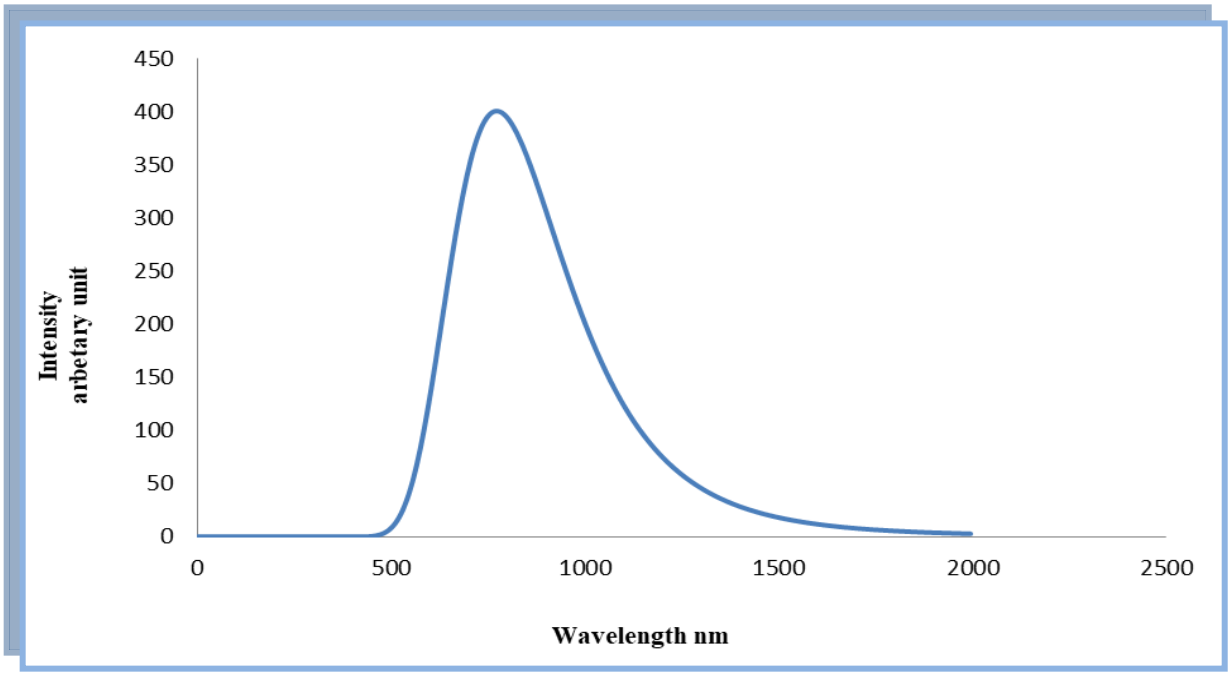

Figure(4.17): Ultraviolet-Visible spectrum for (PEO-CuO-In_2O_3) nanocomposites using B3LYP/SDD.

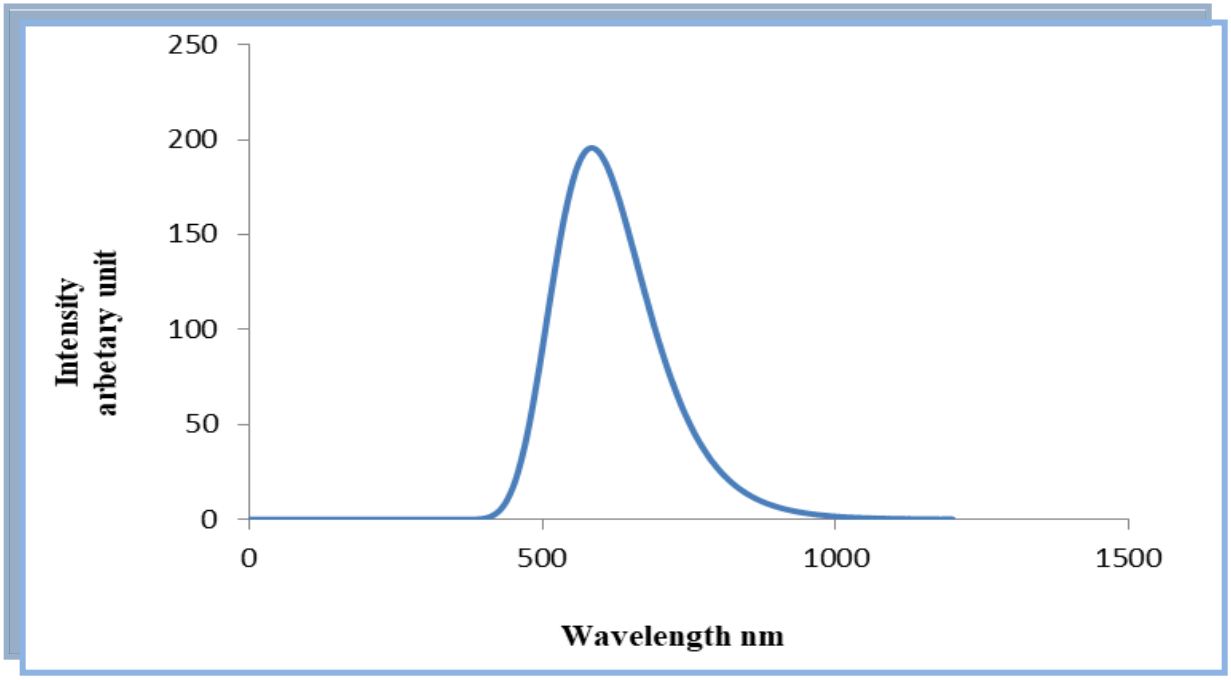

Figure (4.18): Ultraviolet-Visible spectrum for (PEO-NiO-In_2O_3) nanocomposites using B3LYP/SDD.

4.2.4 Optical Microscopic of (PEO-CuO-In_2O_3) and (PEO-NiO-In_2O_3) Nanocomposites

The spread of nanoparticles in a polymer mixture is examined using nanocomposites microscopy. At magnification power (10x), Figures (4.19) and (4.20) show the configurations of copper oxide, nickel oxide, respectively with indium oxide nanoparticles in (PEO) polymer. At lower concentrations, the nanoparticles consolidate in a cluster, as shown by the microscope photos. When the concentration of In_2O_3 nanoparticles in the (PEO) polymer is increased, the nanoparticles form a network of routes within the polymer, allowing charge carriers to move through. This is identical with the results of researcher[116].

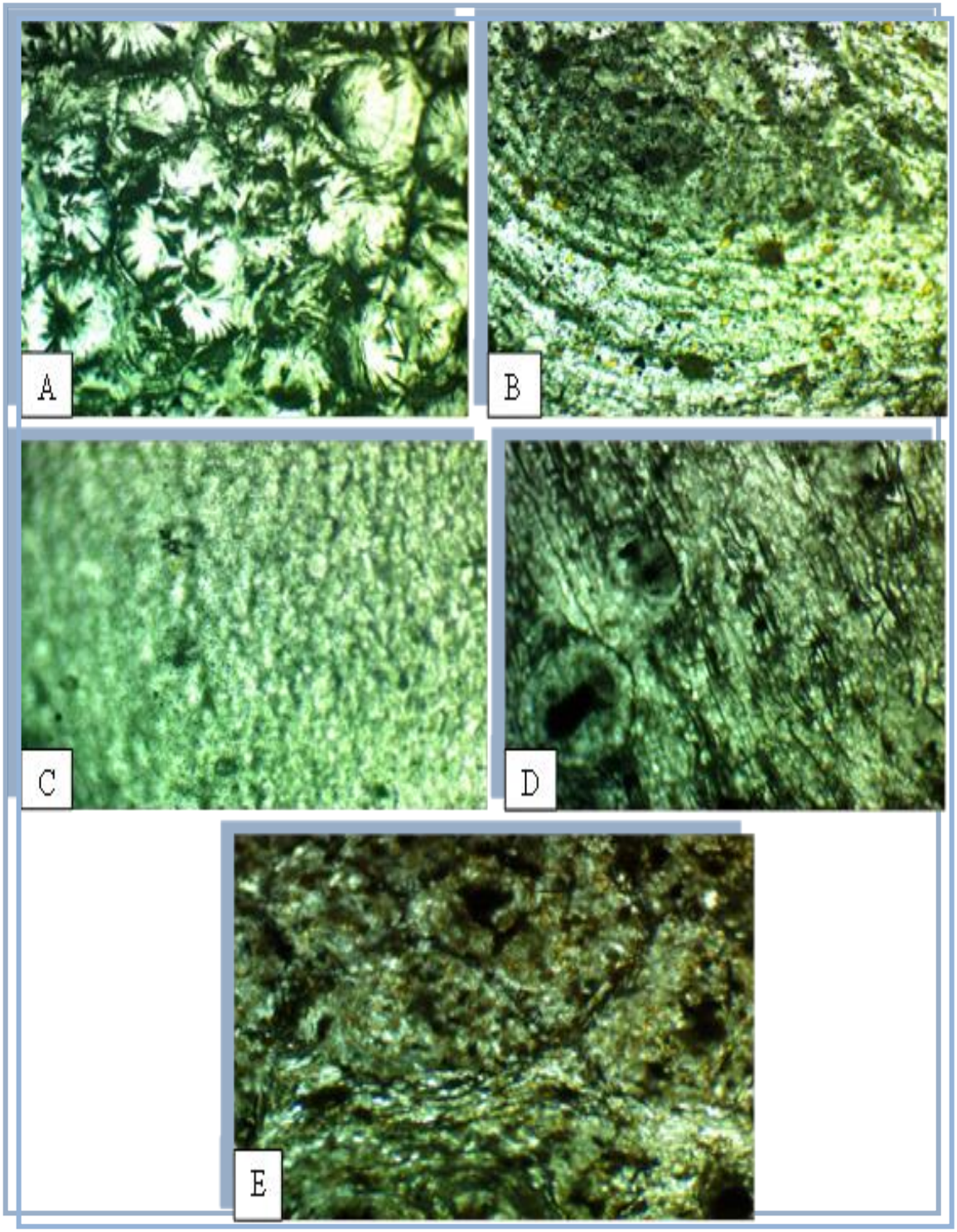

Figure (4.19): Photomicrographs (x10) for (PEO-CuO-In_2O_3) nanocomposites:(A) for pure (B) for 1.8 wt.% CuO nanoparticles (C) for 1.8 wt.% In_2O_3 nanoparticles (D) for 3.6 wt.% In_2O_3 nanoparticles (E) for 5.4 wt.% In_2O_3 nanoparticles.

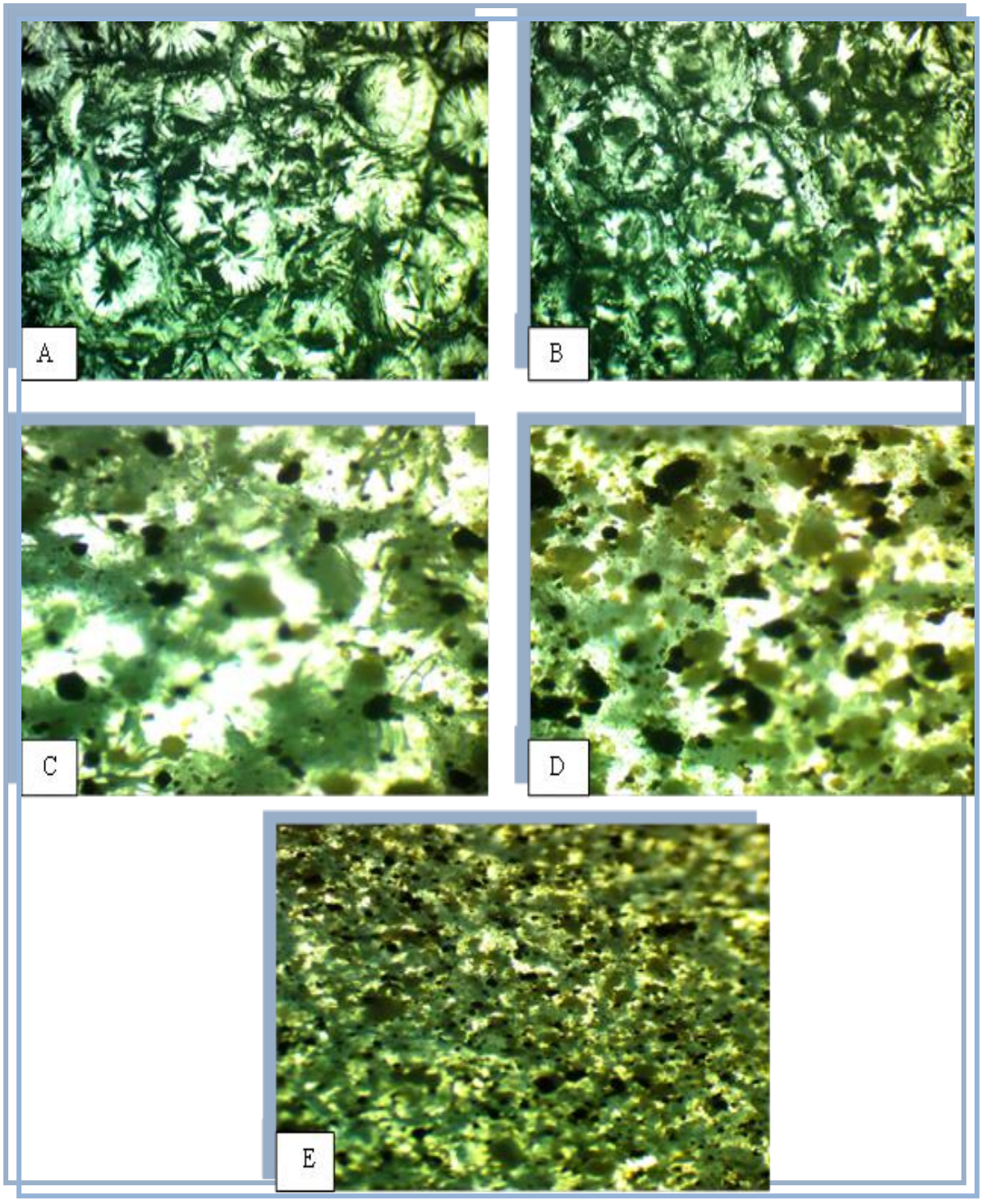

Figure (4.20): Photomicrographs (x10) for (PEO-NiO-In_2O_3) nanocomposites:(A) for pure (B) for 1.8 wt.% NiO nanoparticles (C) for 1.8 wt.% In_2O_3 nanoparticles (D) for 3.6 wt.% In_2O_3 nanoparticles (E) for 5.4 wt.% In_2O_3 nanoparticles.

4.2.5 Scanning Electron Microscope (SEM) of (PEO-CuO-In_2O_3) and (PEO-NiO-In_2O_3) nanocomposite

The SEM micrographs of the (PEO), (PEO-CuO), (PEO-CuO-In_2O_3), (PEO- NiO) and (PEO-NiO-In_2O_3) nanocomposites with In_2O_3 concentration (1.8,3.6,5.4) wt% at different magnification power are shown in Figures (4.21-4.22), respectively to study the morphology of the nanocomposites and arrangement of the nanoparticles at lower and higher concentrations of In_2O_3 nanoparticles. Figures below show that the SEM image of the polymer has pores. These Figures show uniform distribution of nanoparticles in the (PEO). Nanoparticles are aggregated as a clusters at lower concentrations. At high concentrations of In_2O_3 NPs, the nanoparticles form a network of pathways within (PEO) and thus, the pore size of the sample will decrease.

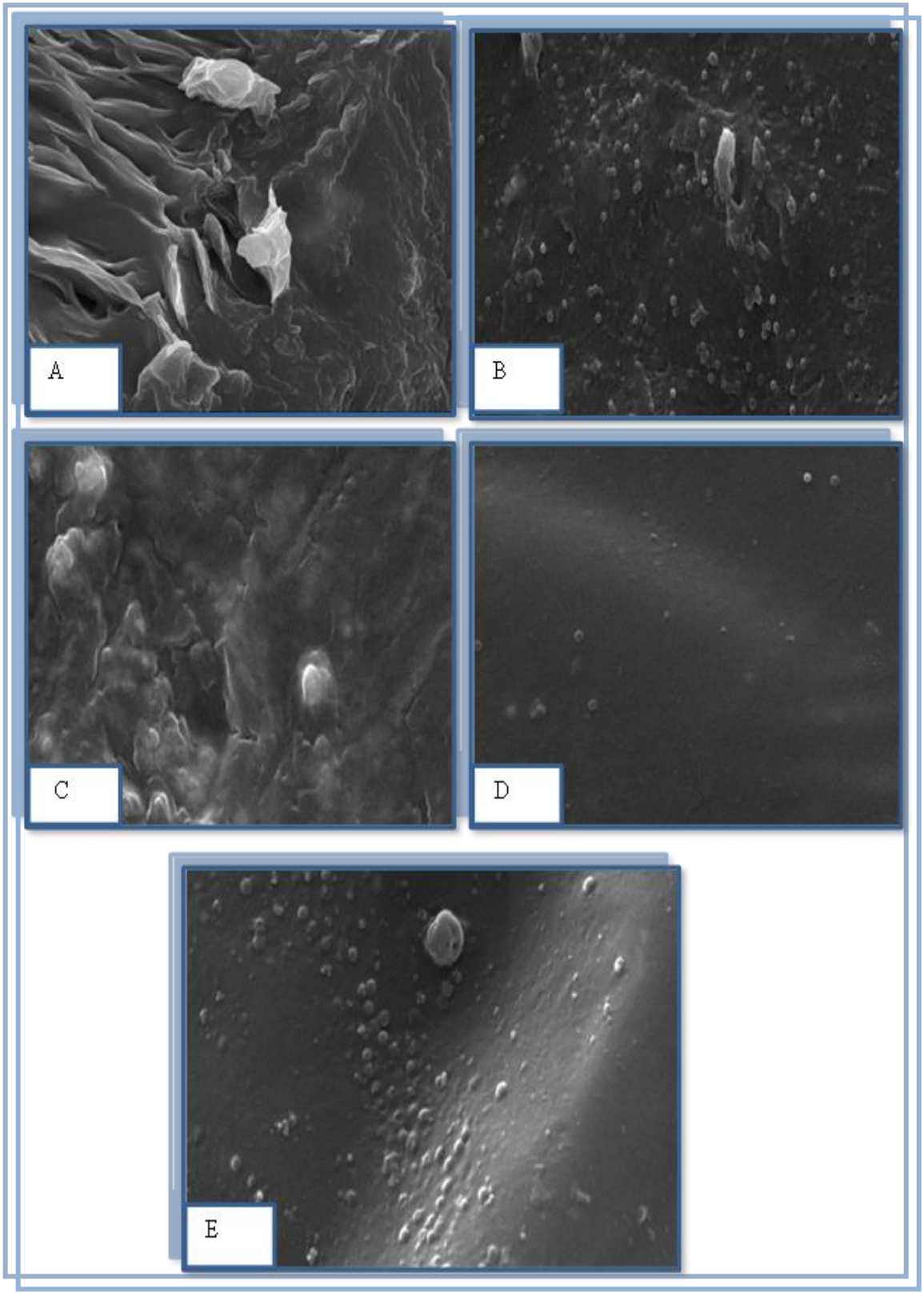

Figure (4.21): SEM images of (PEO-CuO- In_2O_3) nanocomposites:(A) for pure (B) for 1.8 wt.% CuO nanoparticles (C) for 1.8 wt.% In_2O_3 nanoparticles (D) for 3.6 wt.% In_2O_3 nanoparticles (E) for 5.4 wt.% In_2O_3 nanoparticles.

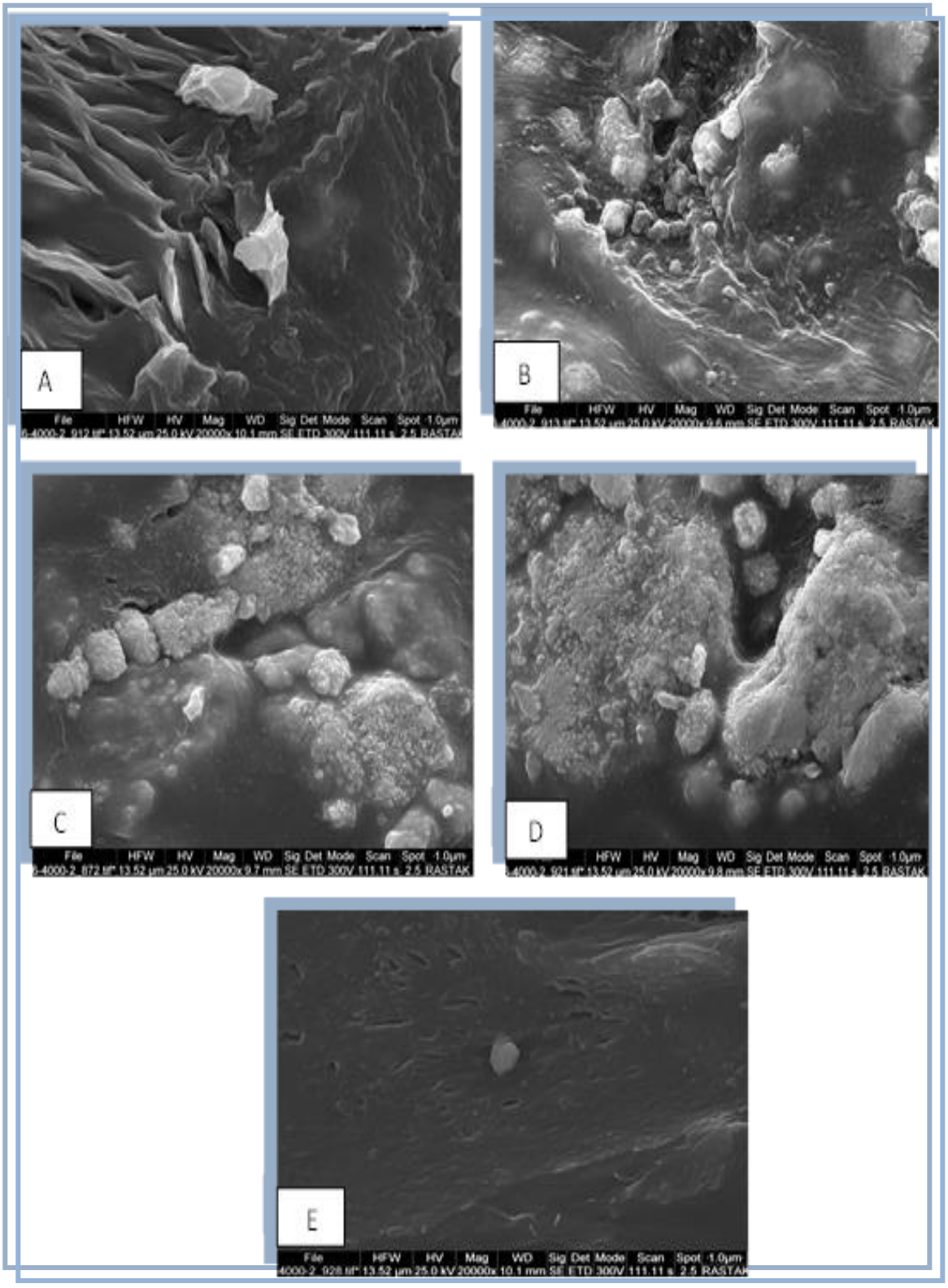

Figure (4.22) :SEM images of (PEO-NiO- In_2O_3) nanocomposites:(A) for pure (B) for 1.8 wt.% NiO nanoparticles (C) for 1.8 wt.% In_2O_3 nanoparticles (D) for 3.6 wt.% In_2O_3 nanoparticles (E) for 5.4 wt.% In_2O_3 nanoparticle

4.3 Computed Energies of (PEO-CuO-In_2O_3) and (PEO-NiO-In_2O_3) Nanocomposites

Energy band gap was calculated using the equation (2-20). Band gap is defined as the energy difference between the highest occupied molecular orbital and the lowest unoccupied molecular orbital, according to the Koopmans theorem. Table (4.5) shows the energy gap for (PEO-CuO-In_2O_3) and (PEO-NiO-In_2O_3) nanocomposites. Figures (4.23-4.25) depict the 3-D distribution of HOMOs and LUMOs in the investigated nanocomposites. As seen in this diagram, the shape of the nanocomposites has the same effect on both the HOMO and LUMO distributions. Changing the form of nanocomposites modifies the map of HOMO and LUMO distribution, according to the linear combination of atomic orbitals-molecular orbital LCAOs-MO.

Table (4.5): The values of energy gap in (eV) of the studied structures.

PEO (79) Atoms			PEO-CuO-In_2O_3 (85) Atoms			PEO-NiO-In_2O_3 (85) Atoms		
E_{HOMO} (eV)	E_{LUMO} (eV)	E_g (eV)	E_{HOMO} (eV)	E_{LUMO} (eV)	E_g (eV)	E_{HOMO} (eV)	E_{LUMO} (eV)	E_g (eV)
-6.7995	1.2679	8.0674	-4.4850	-2.1327	2.3523	-5.0972	-2.0641	3.0330

linked the metal oxides (CuO) and (NiO)led to reduce the energy gap from (8.0674eV) for (PEO) (79Atoms) to (2.3523 eV) for (PEO-CuO-In_2O_3) (85Atoms) and (3.0330 eV) for (PEO-NiO-In_2O_3) (85Atoms). From the results of the energy gap calculated decreases with increasing the number of atoms theoretically. The calculated values of energies gaps in present work are in a good agreement with previous theoretical studies[117-119].

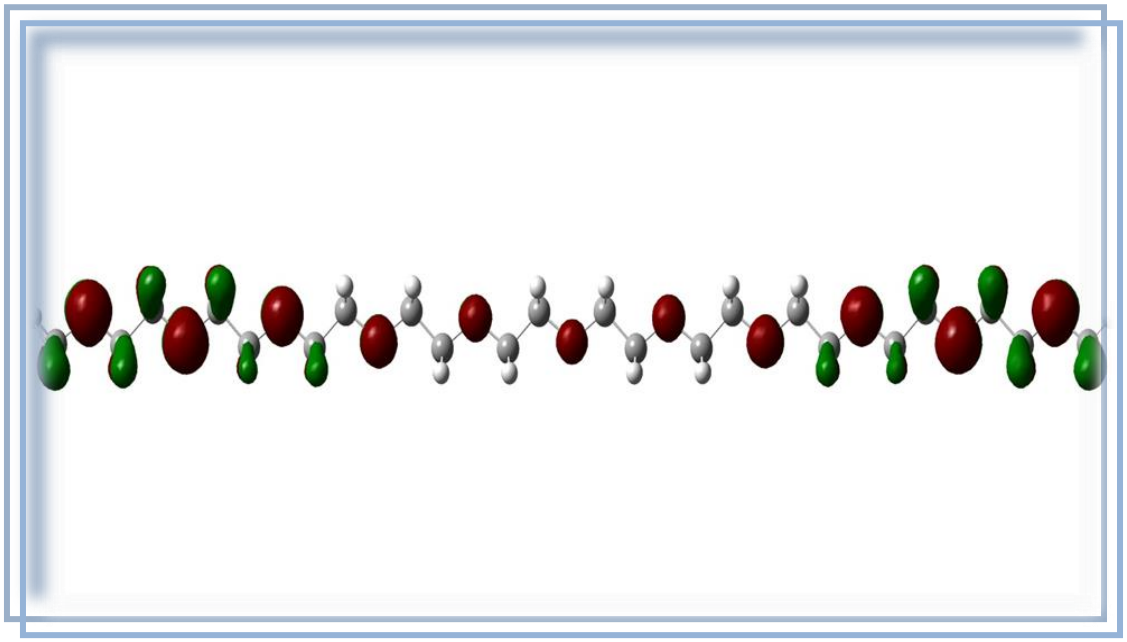

A

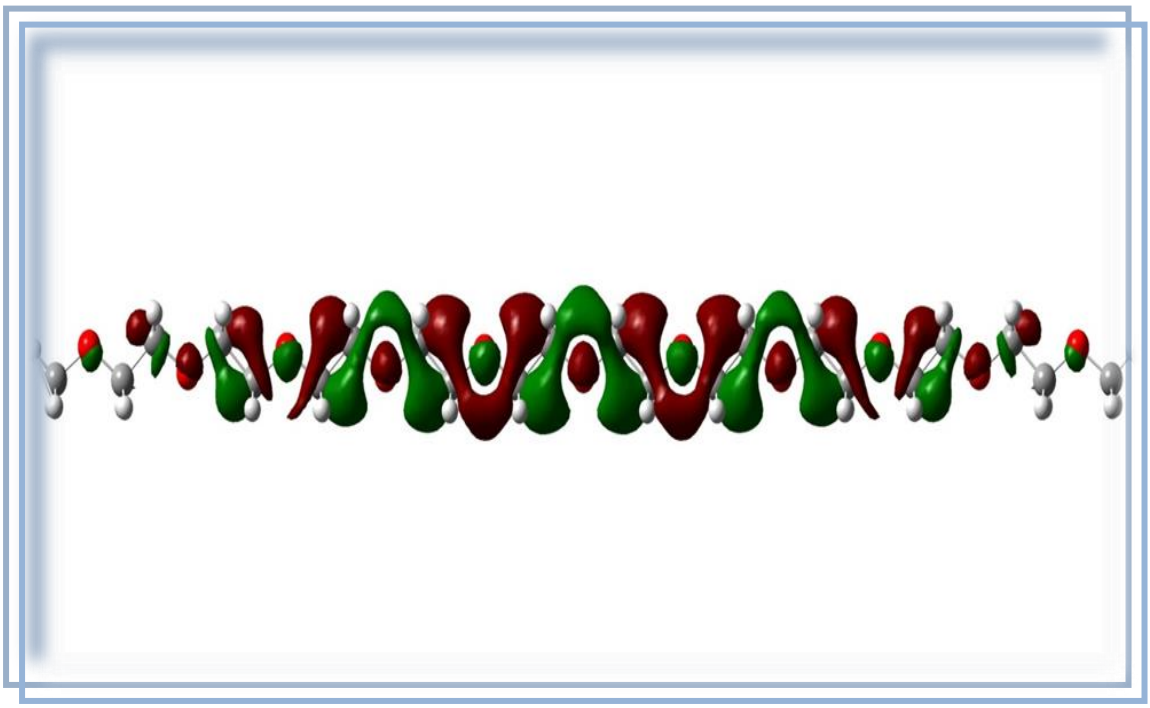

B

Figure (4.23):The distribution of HOMO (A) and LUMO (B) for (PEO).

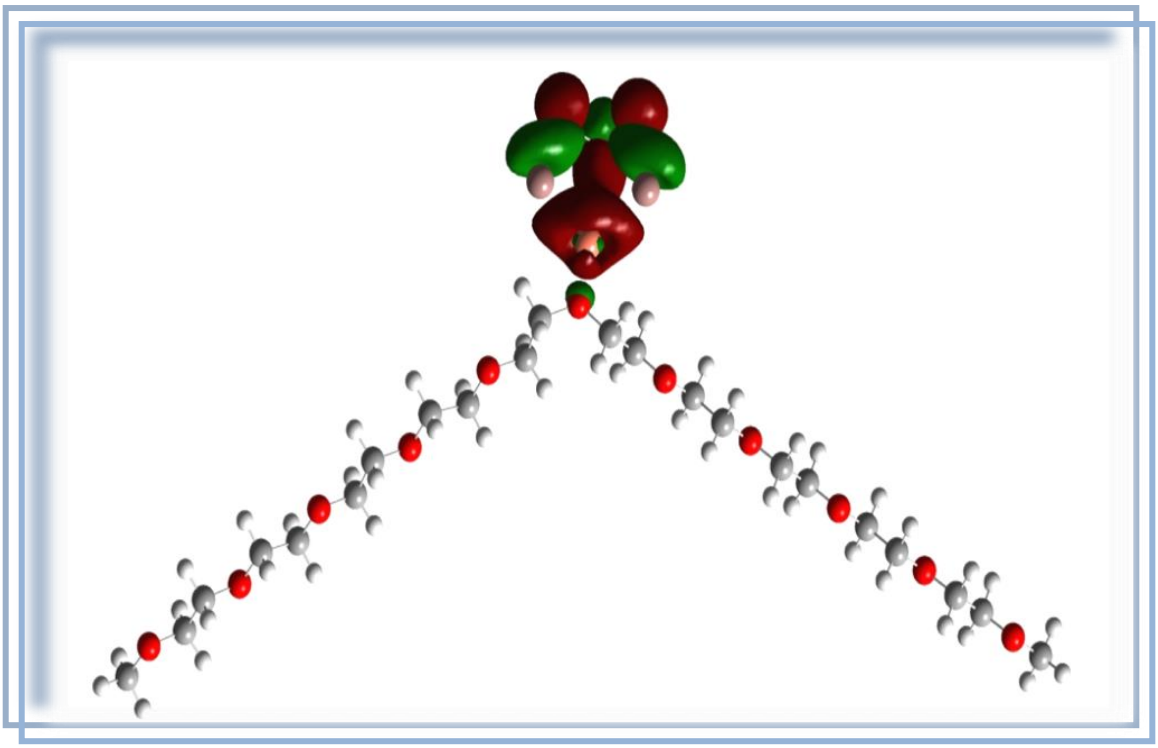

A

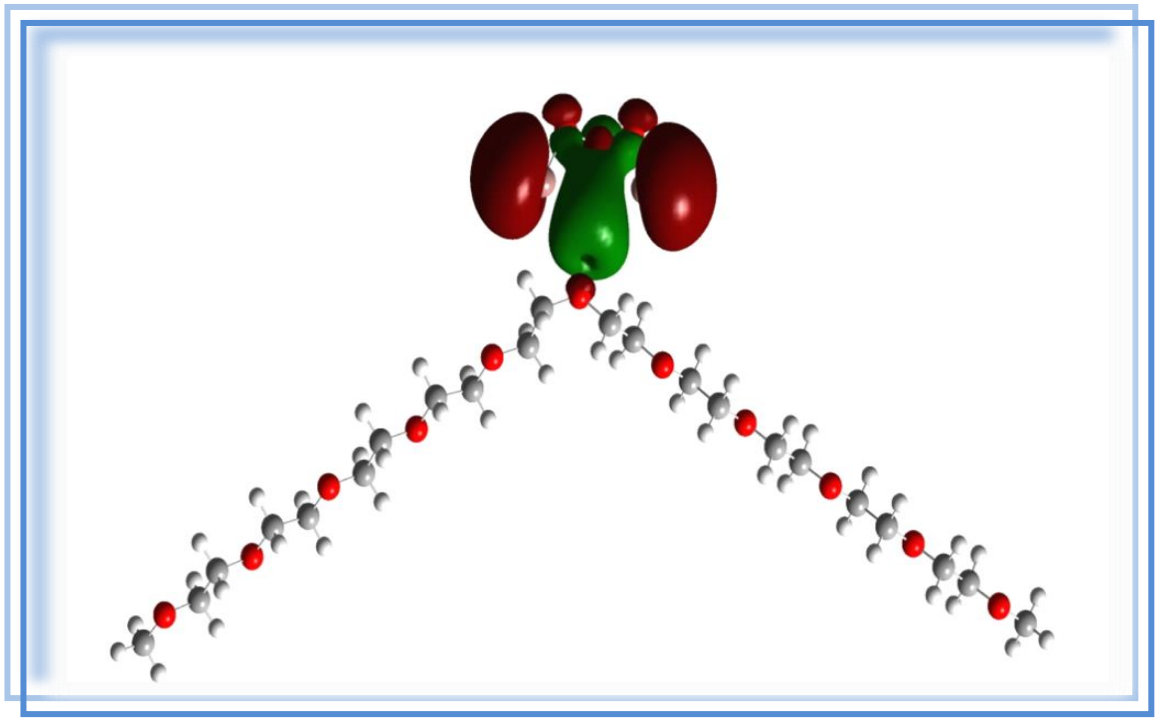

B

Figure (4-24): The distribution of HOMO (A) and LUMO (B) for (PEO-CuO-In_2O_3) contain (85 Atom) .

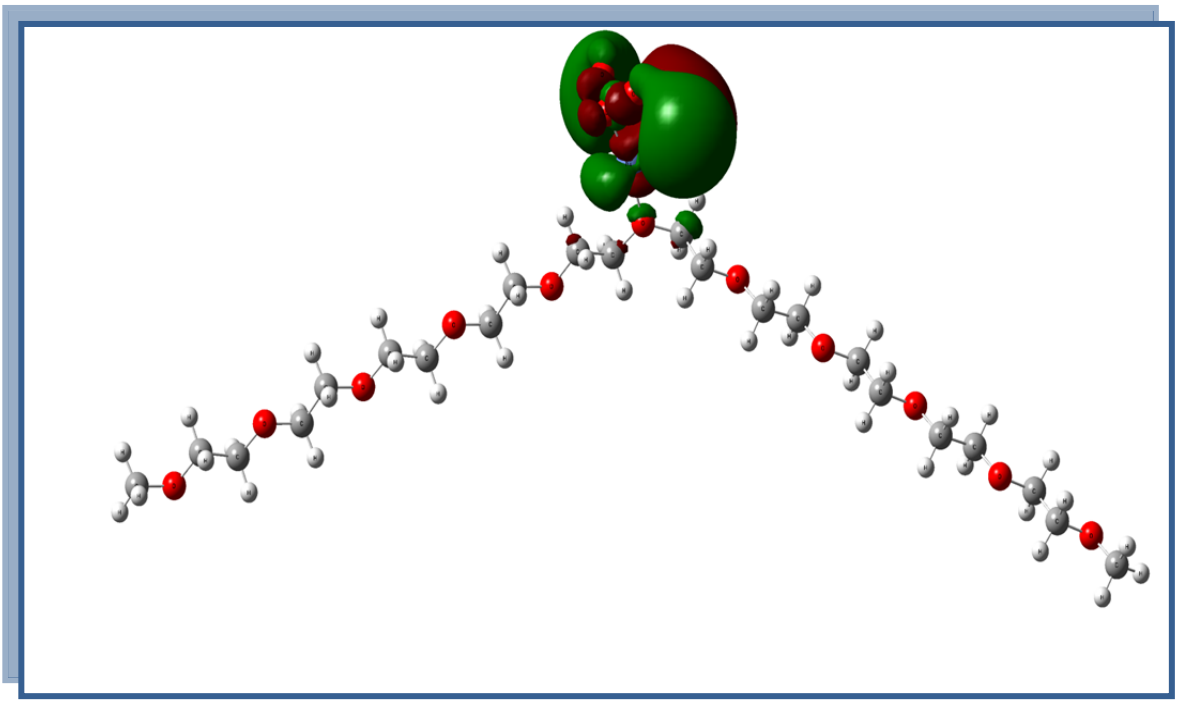

A

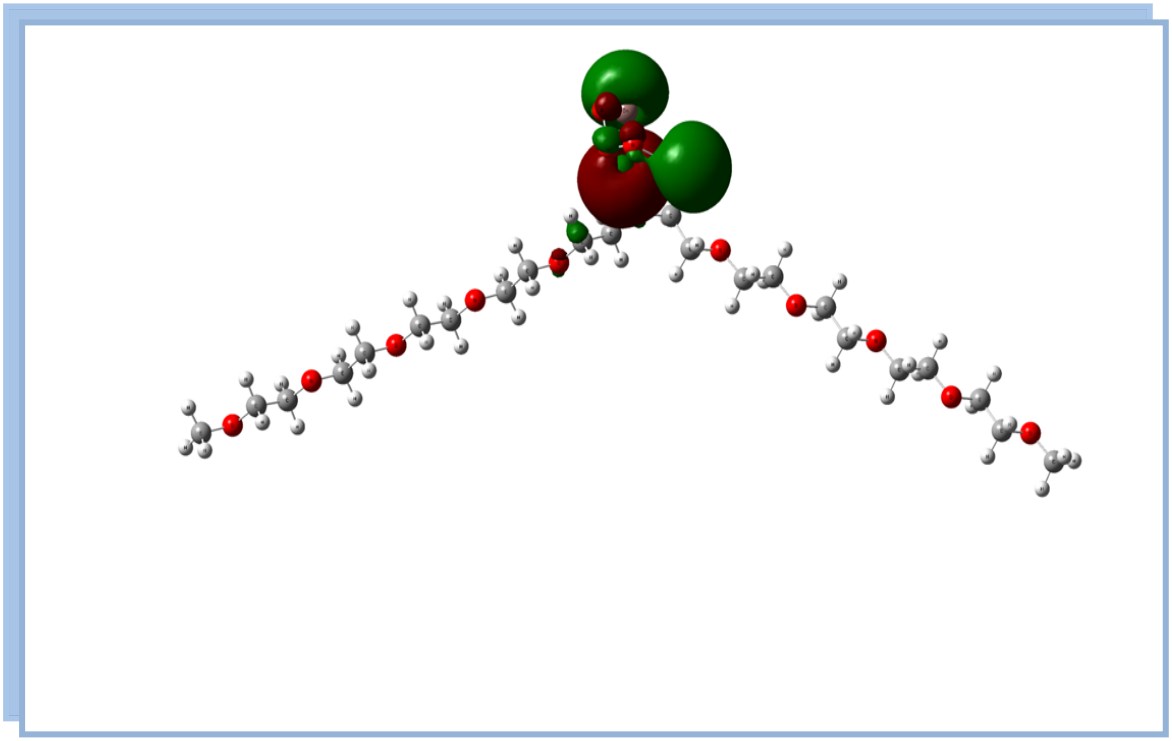

B

Figure(4-25): The distribution of HOMO (A) and LUMO (B) for (PEO-Ni-In_2O_3) contain (85 Atom)

The total ground state energy for each structures is approximately the summation of the ground state energy for all atoms in the structures. The calculated value of total energy depends on the number of electrons in the structures. The pure PEO has the largest value of total energy, E_T was decreased with addition of nanoparticles to polymer. Table (4.6) shows the decreasing of the total energy, this result is a reflection of the binding energy of each structures and indicates that these structures have good relaxation, this leads to be certain that the effect of adding (In_2O_3) NPS to pure PEO on the total energy of the molecule was effective.

Ionization energy (IE) and electron affinity (EA) can be expressed in terms of the HOMO and LUMO energies, according to Koopman's theorem. The amount of energy required to remove an electron from a molecule is known as the ionization potential (IE). These values were computed in electron Volts (eV). The ionization potential of pure PEO is greater than the ionization energy of other nanocomposites, as shown in Table (4.6). This means that pure PEO requires a lot of energy to form cation. This suggests that nanocomposites have a high ability to donate electrons based on their function order. With the addition of nanoparticles to pure PEO, the electron affinity was enhanced. These findings suggest that the nanocomposite (PEO-CuO-In_2O_3) and (PEO-NiO-In_2O_3) have a high ability to accepting an electron.

Table (4.6) also shows that the pure PEO has a high electrochemical hardness H and a low electronic softness S, but all nanocomposites have a low electrochemical hardness H and a high electronic softness S. The decreasing of hardness and increasing in softness is the main feature as a sign that the band gap will be softer because of these are small excitation states from the ground and lowering the resistance of the species to lose an electron. These results correspond to the result of energy gap that indicate to the high activity of the nanocomposites in reaction with interaction with the environment.

The results of the electrophilic index in Table (4.6) gave us an idea about the interest of the donor and acceptor to construct the molecular system. All nanocomposites are more chemically reactive to interact with other species in comparison with the original structure pure PEO, they have high values of electrophilicity W than PEO. This indicates that the presence of nanoparticles give the structure the ability to accept an electron from the surrounding species.

It is obvious from Table (4.6) that the nanocomposites have the highest value of electronegativity than the pure PEO, the reason goes back to the symmetrical distribution of the same type of atoms in the nanocomposites.

Table (4.6) shows the total dipole moment (in Debye) calculated using the DFT-B3LYP/SDD basis set for pure PEO and nanocomposites. The results demonstrated that adding the nanoparticles to pure PEO changed the symmetric charge distribution, resulting in changes in PEO's dipole moment. This influence is determined by the addition of nanoparticles to the PEO molecule and corresponds to each molecule symmetry point group.

The estimated average polarizability in Table (4.6) shows that all nanocomposites have high polarizability values when compare with the PEO molecule, implying that these molecules are more reactive in charge transfer with the surrounding media. This may a result of the presence of nanoparticles in the molecule [103]. We notice from the tables (4.5-4.6)the improvement and stability of the electronic properties of the nanocomposite (PEO-CuO-In_2O_3) more than the nanocomposite (PEO-NiO-In_2O_3).

Table (4.6) :The values of some electronic properties of the studied structure

Property	(PEO) Pure	(PEO-Cu-In_2O_3) composites	(PEO-NiO-In_2O_3) composites
Total energy (a.u)	-1692.8063	-2119.8614	-2093.4601
Ionization potential (eV)	6.7995	4.4850	5.0972493
Electron affinity (eV)	-1.2679	2.1327	2.0641
Electronegativity (eV)	2.7658	3.3088	3.5806
Chemical hardness (eV)	4.0337	1.1761	1.5165
Chemical softness (eV)	0.1239	0.4251	0.3297
Chemical potential (eV)	-2.7658	-3.3088	-3.5806
Electrophilicity (eV)	0.9482	4.6544	4.2269
Dipole moment (Debye)	1.6673	5.5244	8.3365
Polarizability (a.u)	289.470	473.49	432.914

4.4 Density of States

The strength of interactions may be investigated further by looking at orbital interactions between nanocomposite atoms in terms of density of states (DOS), as shown in Figures (4.26 - 4.28). Because of the DOS affects numerous physical properties and hence plays a significant role in solid state physics, being able to predict how the DOS will behave for various molecule structure geometries is critical. The nanocomposite (PEO-CuO-In_2O_3) has a doublet state, whereas the others have a singlet state, as illustrated. The degeneracies of vacant molecular orbitals are always greater than the degeneracies of occupied molecular orbitals. DOS of the relax structures in the figures indicating that (PEO-NiO-In_2O_3) nanocomposites is semiconductors with energy gap is (3.0330eV) but the energy gap for (PEO-CuO-In_2O_3) nanocomposites is (2.3523eV), it is therefore a fully connected nanocomposite. The highest number of degenerate states in the conduction and the valence bands is 8 for (PEO-CuO-In_2O_3) and (PEO-NiO-In_2O_3) nanocomposites. The high density of states at a specific energy levels refers to

that there are many states in the structure available for occupation. If there is no states can be occupied at that energy level that refers to zero density of states.

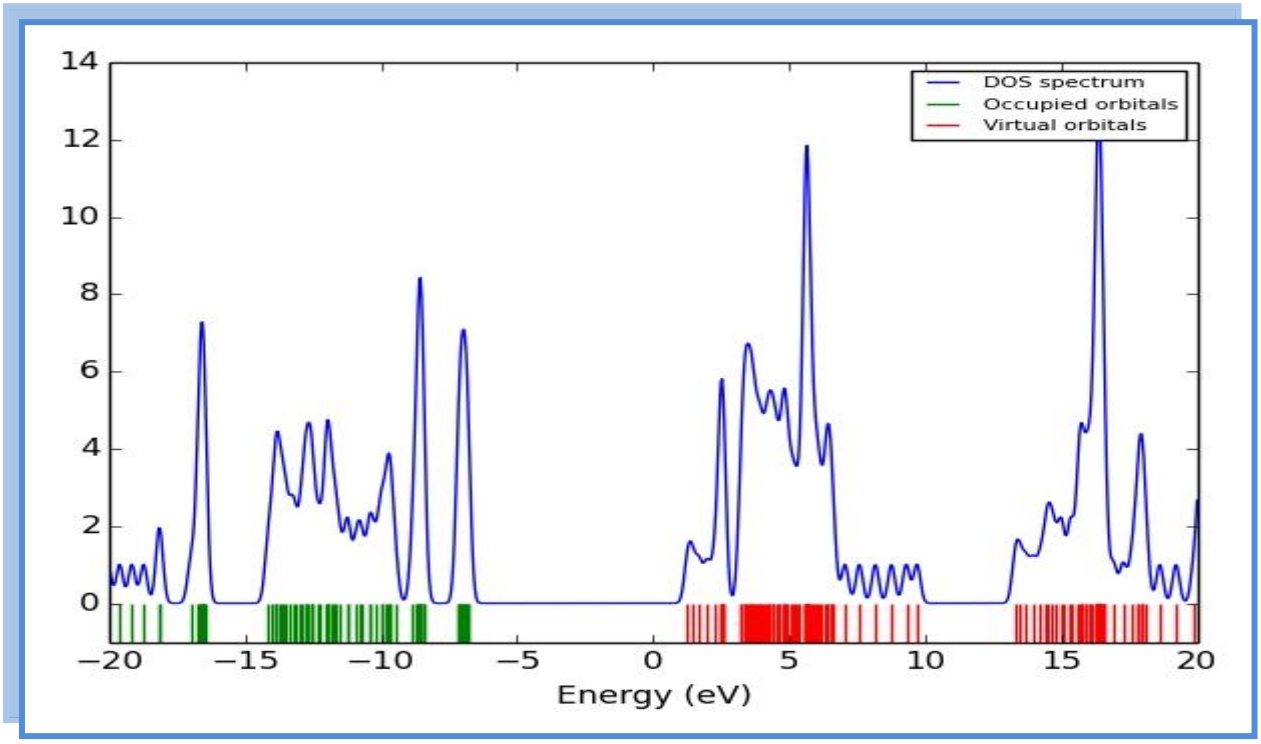

Figure (4.26): The density of states of pure PEO.

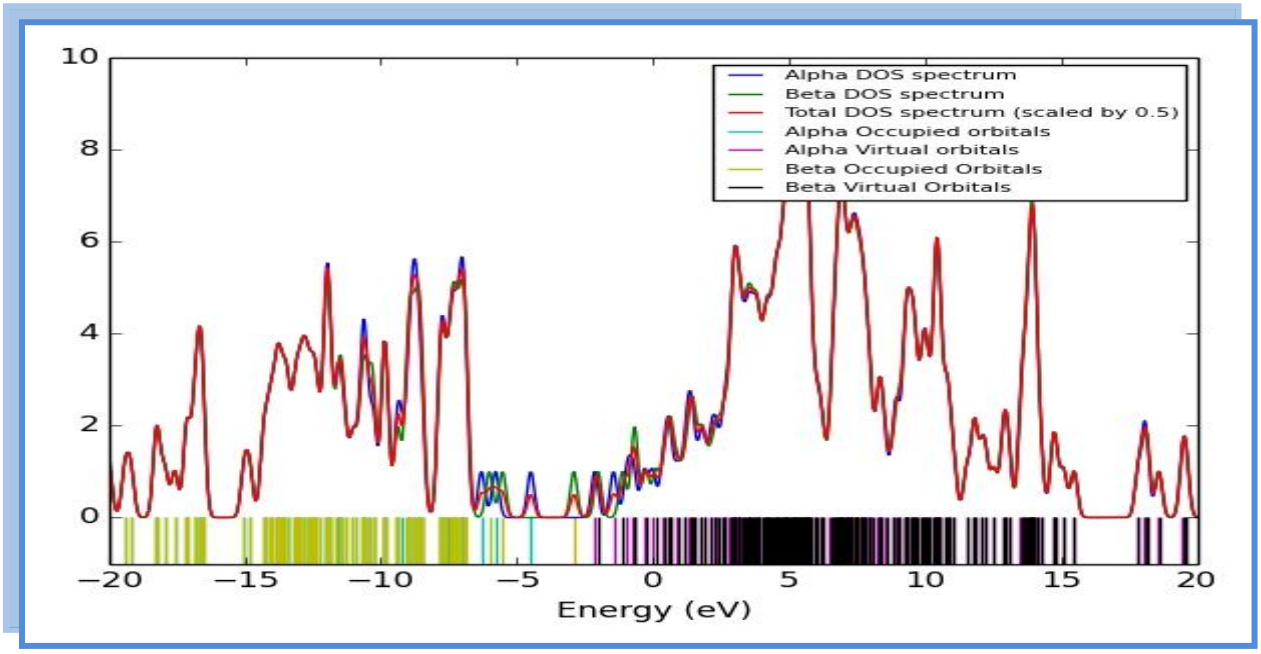

Figure (4.27): The density of states of (PEO-CuO-In_2O_3) nanocomposites

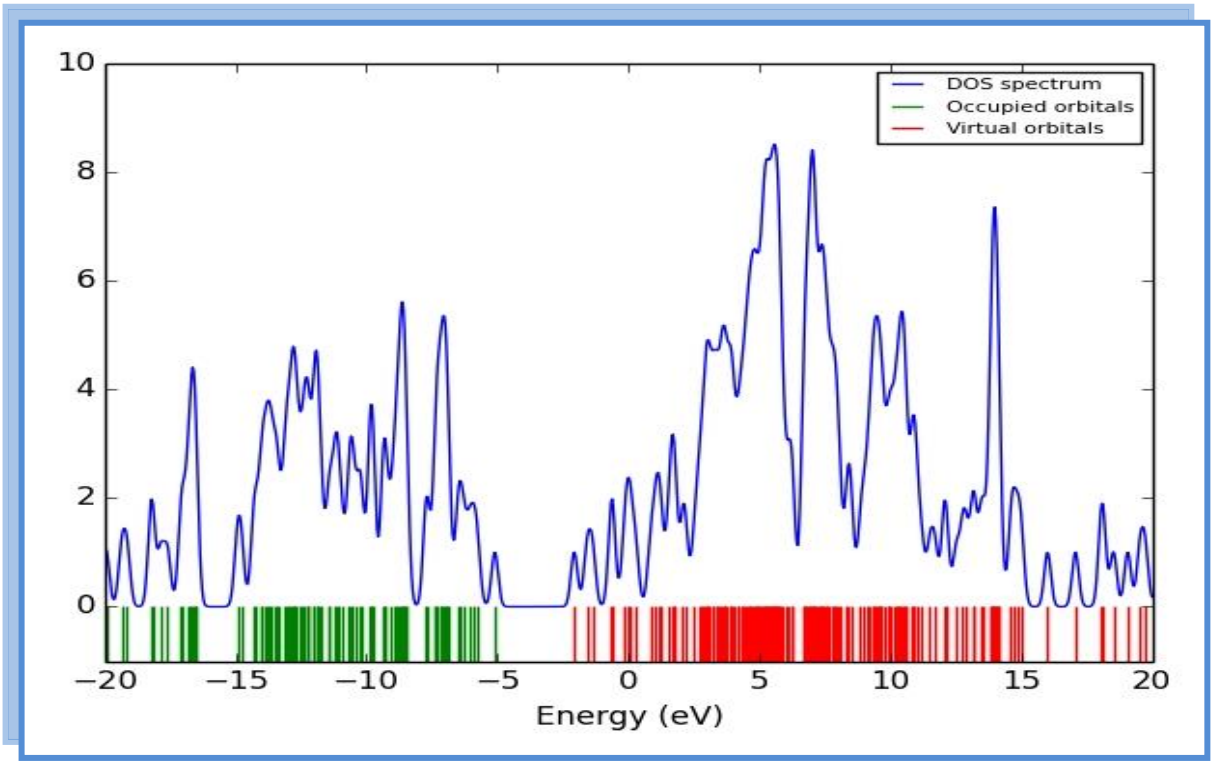

Figure (4.28): The density of states of (PEO- NiO-In_2O_3) nanocomposites.

4.5 The Optical Properties of (PEO-CuO-In_2O_3) and (PEO-NiO-In_2O_3) Nanocomposites

The optical properties of (PEO-CuO-In_2O_3) and (PEO-NiO-In_2O_3) nanocomposites are including: the absorbance, transmittance, the absorption coefficient, energy band gap, extinction coefficient, reflection index, dielectric constants and optical conductivity.

4.5.1 The Absorbance of (PEO-CuO-In_2O_3) and (PEO-NiO-In_2O_3) Nanocomposites

Figures (4.29-4.31) show the variation of absorbance for (PEO-CuO-In_2O_3) and (PEO-NiO-In_2O_3) nanocomposites with wavelength of the incident light experimental and theoretical, respectively. The figures show that the absorption of all nanocomposites samples rises in the UV area due to the excitation of electrons from the valance band to the conduction band. At these

energies, the photons have sufficient energy to interact with atoms. When a photon is absorbed, an electron transitions from a low to a high energy state. In general, it has been observed that the absorbance decreases with increasing wavelength for all nanocomposites samples . This physically means that an incident photon will not be able to excite the electron or even transport it from the valence band to the conduction band since the incident photon's energy is less than the semiconductor's energy gap value [120]. In the visible and near infrared regions, the absorbance of all samples of nanocomposites is generally lowered . As the wavelength of the photon decreases, more photons enter the substance because of increased absorption [121]. The absorbance of PEO rises about 28.5% at (λ= 200 nm) when the In_2O_3 NPs content reached (5.4 wt.%)for nanocomposite (PEO-CuO-In_2O_3). The absorbance of PEO increases with increase in the NPs contents and due to increase the charges carriers in the polymer matrix. This behavior is useful for optoelectronics, photocatalysis and solar cells.

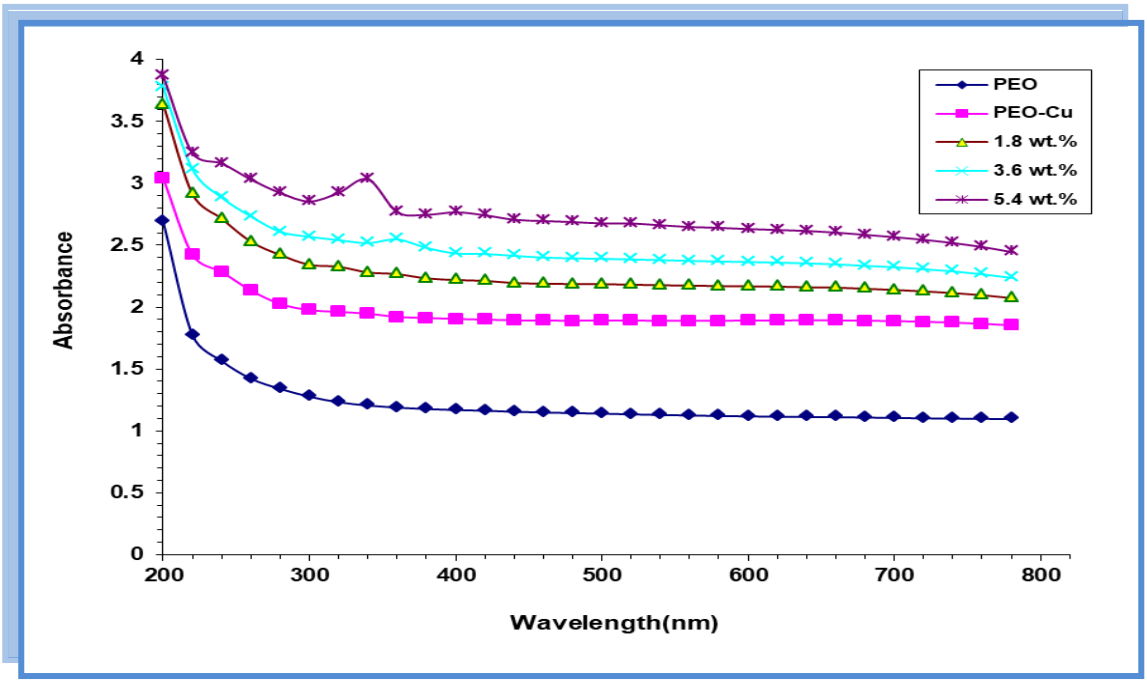

Figure (4.29): Variation of absorbance for (PEO-CuO-In_2O_3) nanocomposites with wavelength.

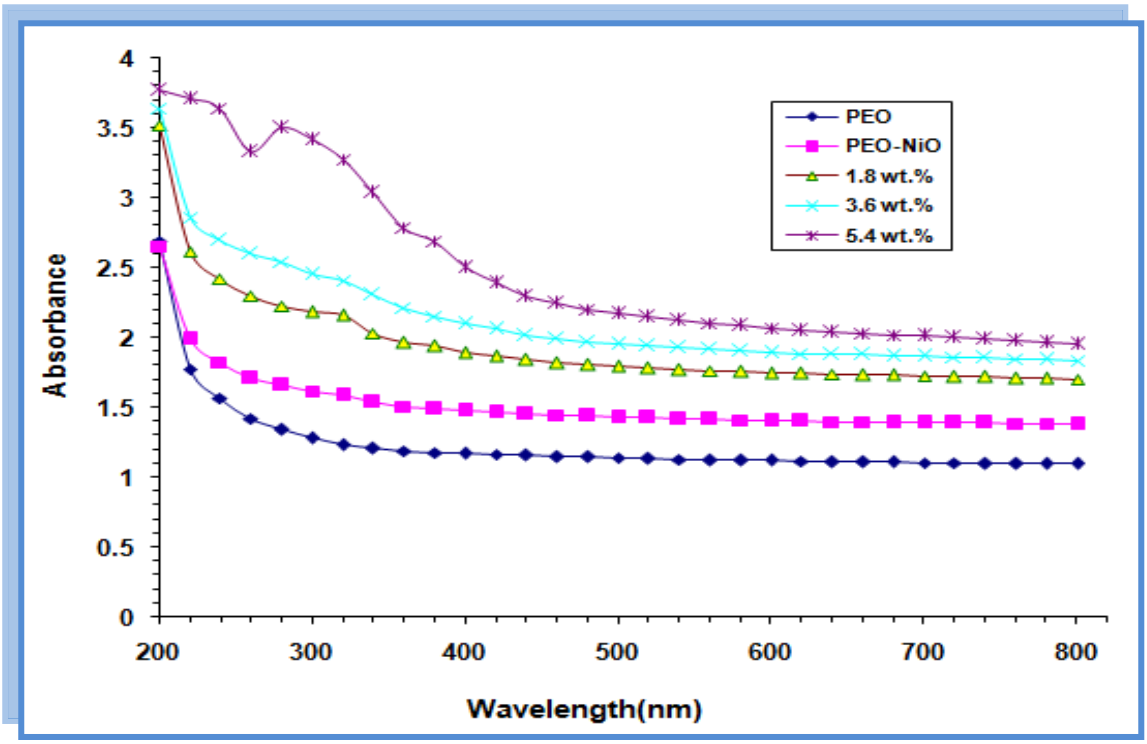

Figure (4.30): Variation of absorbance for (PEO-NiO-In_2O_3) nanocomposites with wavelength.

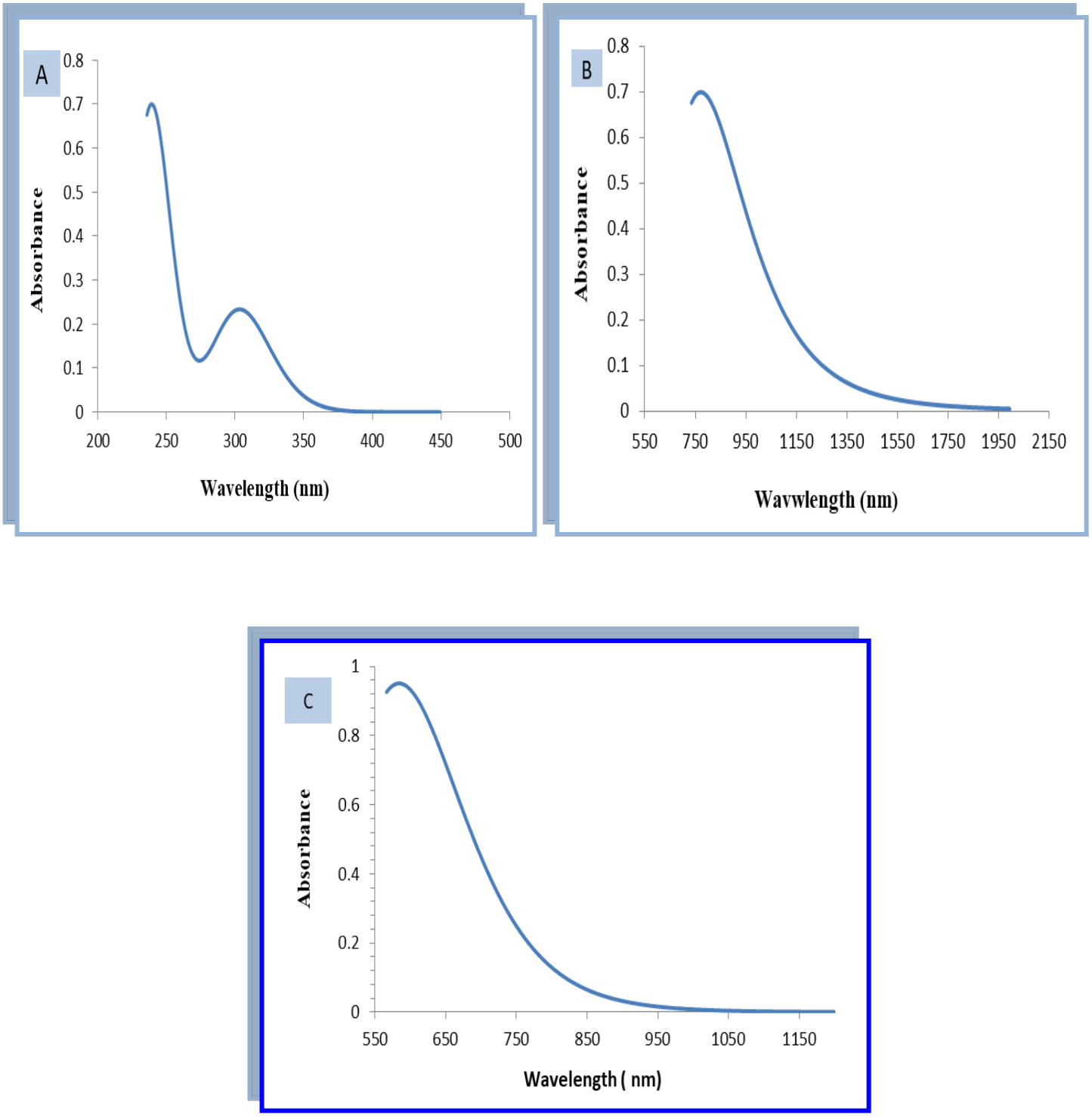

Figure (4.31): Absorbance as a function of wavelength (A). for PEO (B).for (PEO-CuO-In_2O_3 (C). for (PE-ONiO-In_2O_3)nanocomposites(Theoretically).

4.5.2 Transmittance of (PEO-CuO-In_2O_3) and (PEO-NiO-In_2O_3) Nanocomposites

Figures (4.32-4.34) display the variation of transmittance (T) for (PEO-CuO-In_2O_3) and (PEO-NiO-In_2O_3) nanocomposites with the wavelength of the incident light experimental and theoretical respectively. When the wavelength is increased, the transmittance of all nanocomposites rises. The transmittance decreases as the concentration of nanoparticles increases. This is related to the accumulation of nanoparticles lead to increase in the number of charge carriers[122]. The transmittance decreases about 58.7% at λ=500 (nm) for nanocomposite (PEO-CuO-In_2O_3), which may be useful for optical applications.

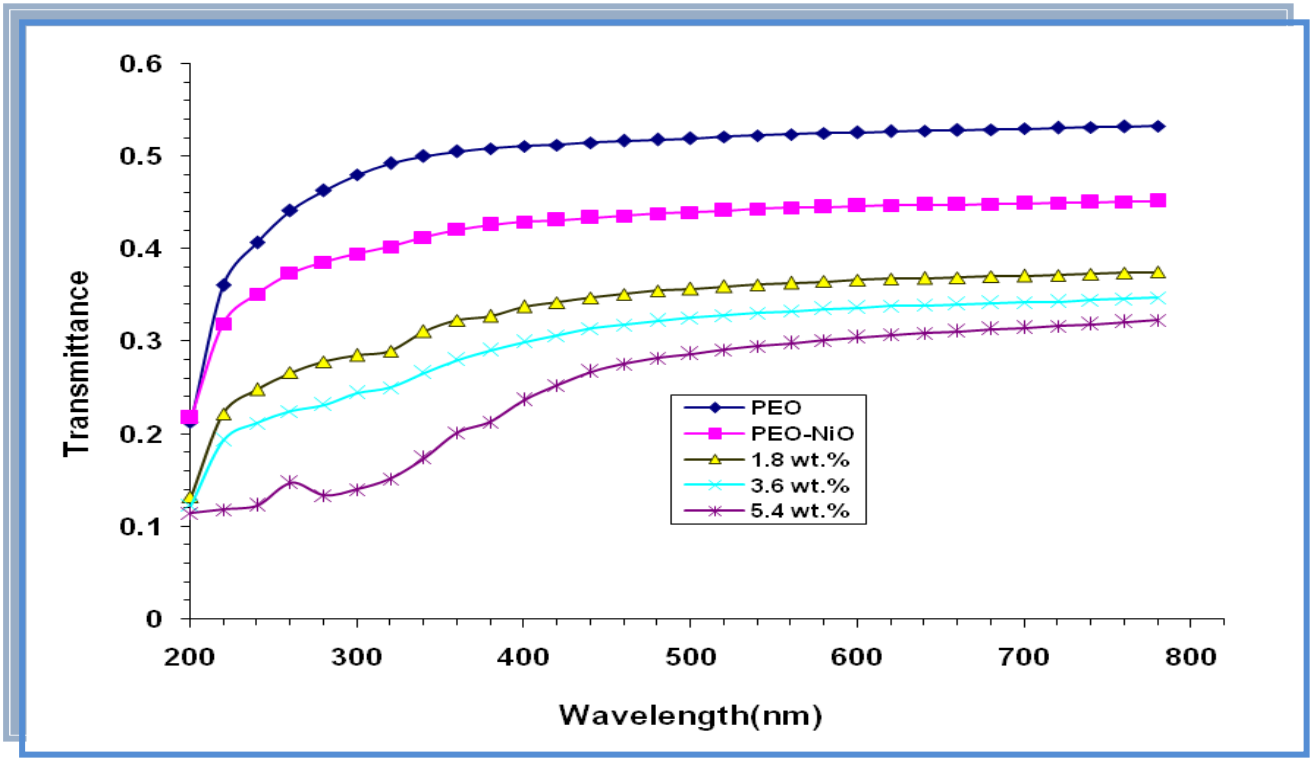

Figure (4.32): Transmittance spectra of (PEO-CuO-In_2O_3) nanocomposites with wavelength.

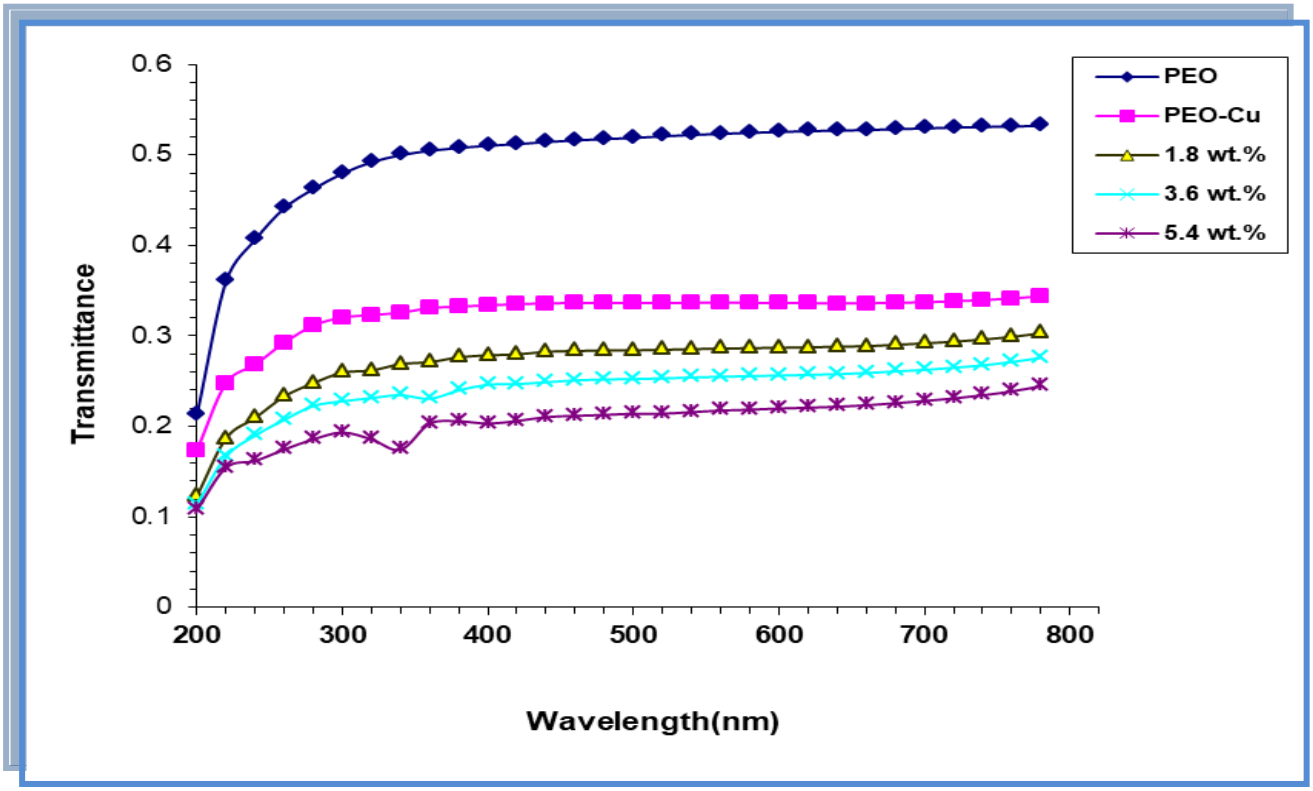

Figure (4.33): Transmittance spectra (PEO-NiO-In_2O_3) nanocomposites with wavelength.

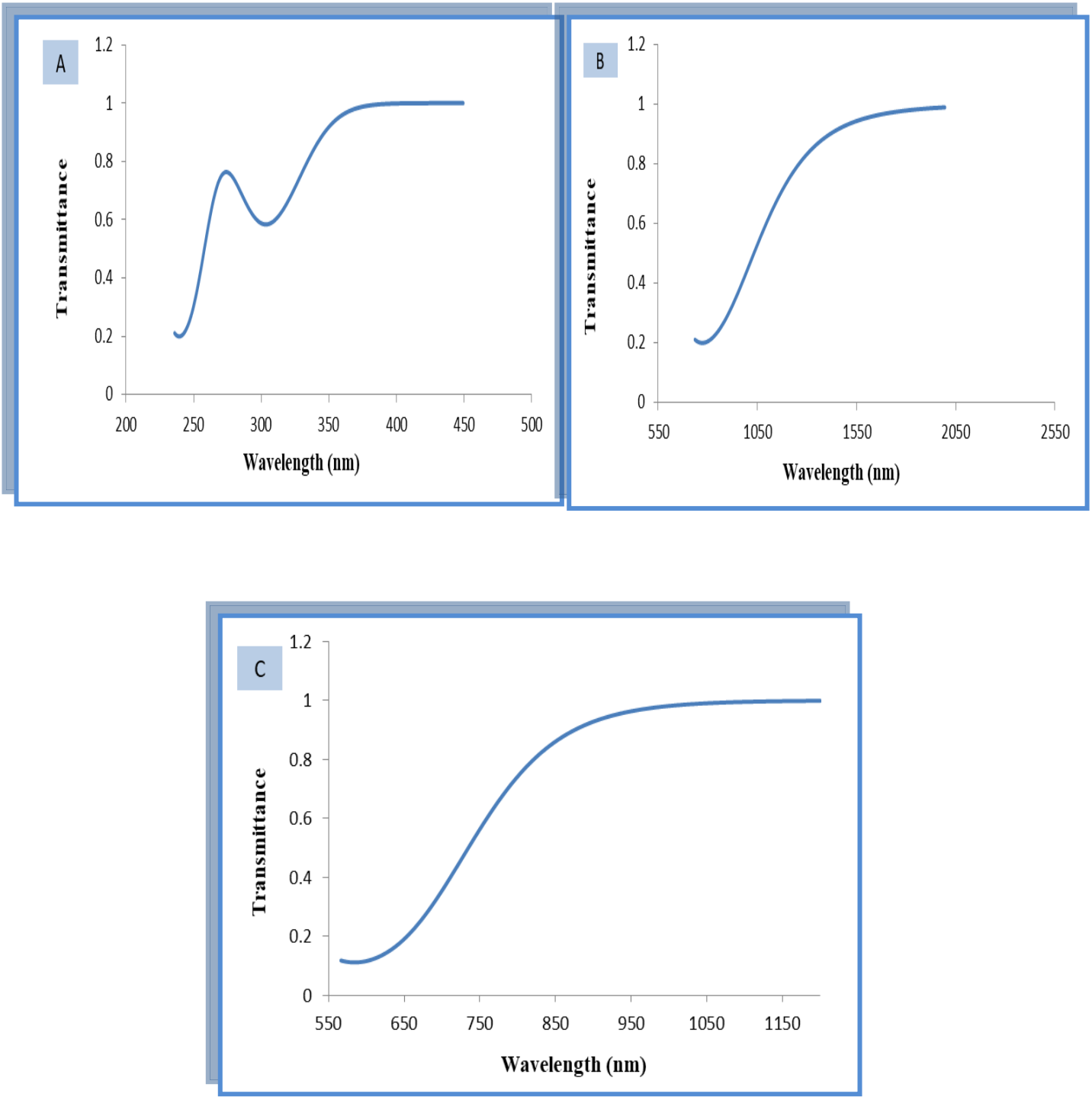

Figure (4.34): Transmittance as a function of wavelength (A). for PEO (B).for (PEO-CuO-In_2O_3) (C). for (PE-ONiO-In_2O_3)nanocomposites(Theoretically).

4.5.3 Absorption Coefficient and Energy Band Gap of (PEO-CuO-In_2O_3) and (PEO-NiO-In_2O_3) Nanocomposites

Absorption coefficient (α) of nanocomposites is measured by using equation (2.29). Figures (4.35-4.37) show the variation of the absorption coefficient as a function of the photon energy of the incident light for (PEO-CuO-In_2O_3) and (PEO-NiO-In_2O_3) nanocomposites experimentally and theoretically respectively. The absorption coefficient of produced nanocomposites increases as the concentration of nanoparticles increase, which is attributable to the increased number of charge carriers in nanocomposites, resulting in enhanced absorbance (A) and absorption coefficient (α) for nanocomposites increased. When the concentration of In_2O_3 nanoparticles reached 5.4 wt% at a wavelength of 500 nm, the absorption coefficient of (PEO-CuO-In_2O_3) and (PEO-NiO-In_2O_3) nanocomposites increased, making them beneficial for optoelectronics, photocatalysis, solar cells, and many other optical applications. The absorption coefficient of all prepared nanocomposites increases with increasing energy of the incident photon. This means that the electron transition has high probability; i.e. the energy of the incident photon is sufficient to interact with atoms. The absorption coefficient helps to know the electron transition nature [123,124]. When the values of the absorption coefficient of material are usually minimal ($\alpha<10^4$) cm^{-1} ; the transition of electron is indirect. From the results, it's found that the absorption coefficient of (PEO-CuO-In_2O_3) and (PEO-NiO-In_2O_3) nanocomposites have values that are less than (10^4) cm^{-1} which means the transition of electrons is indirect [16].

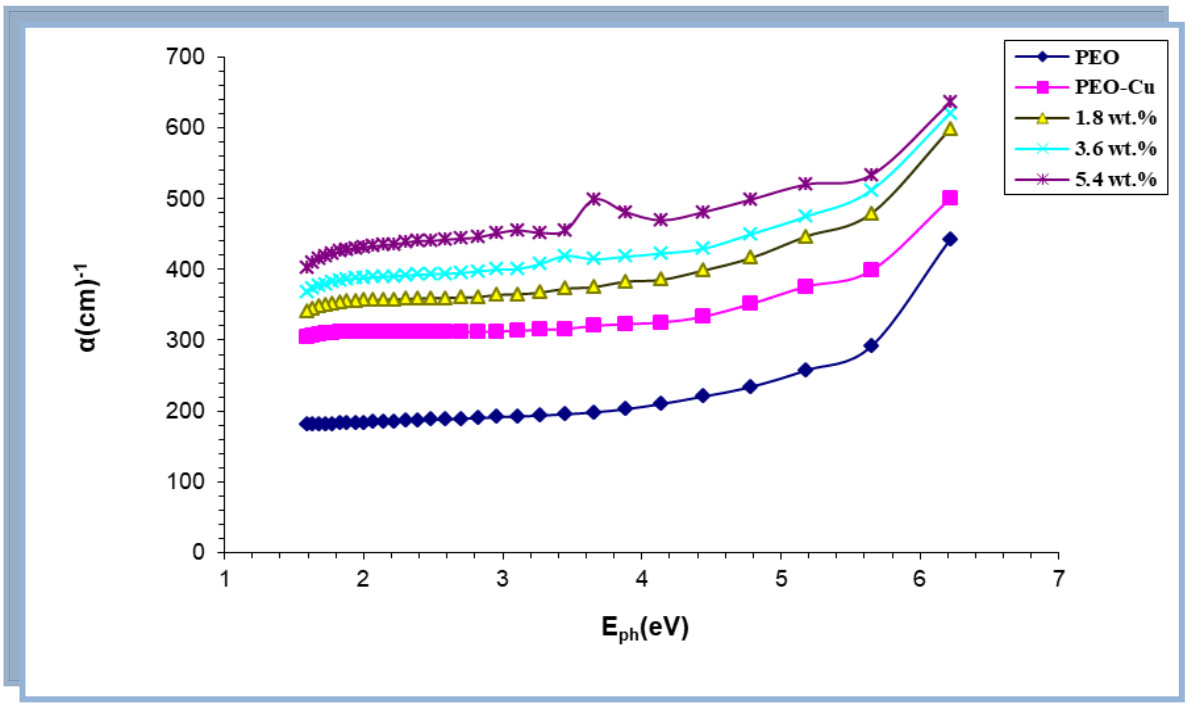

Figure (4-35): Variation of absorption coefficient of (PEO-CuO-In_2O_3) nanocomposites with photon energy.

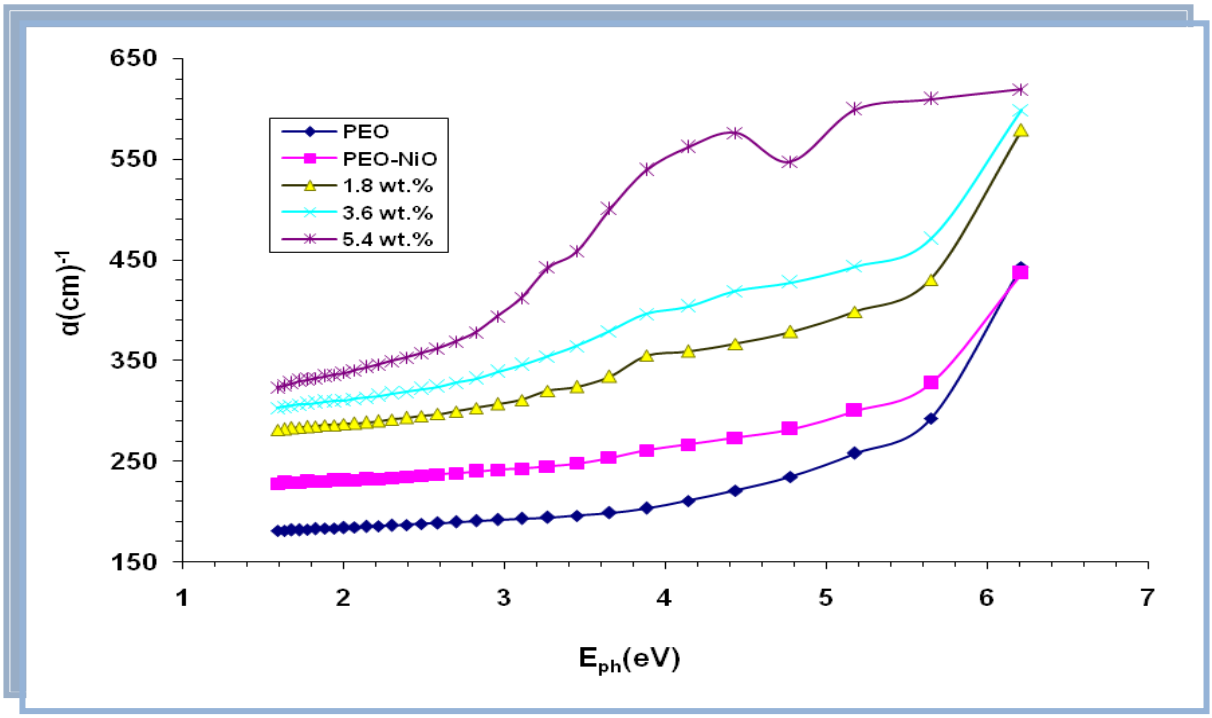

Figure (4-36): Variation of absorption coefficient of (PEO-NiO-In_2O_3) nanocomposites with photon energy.

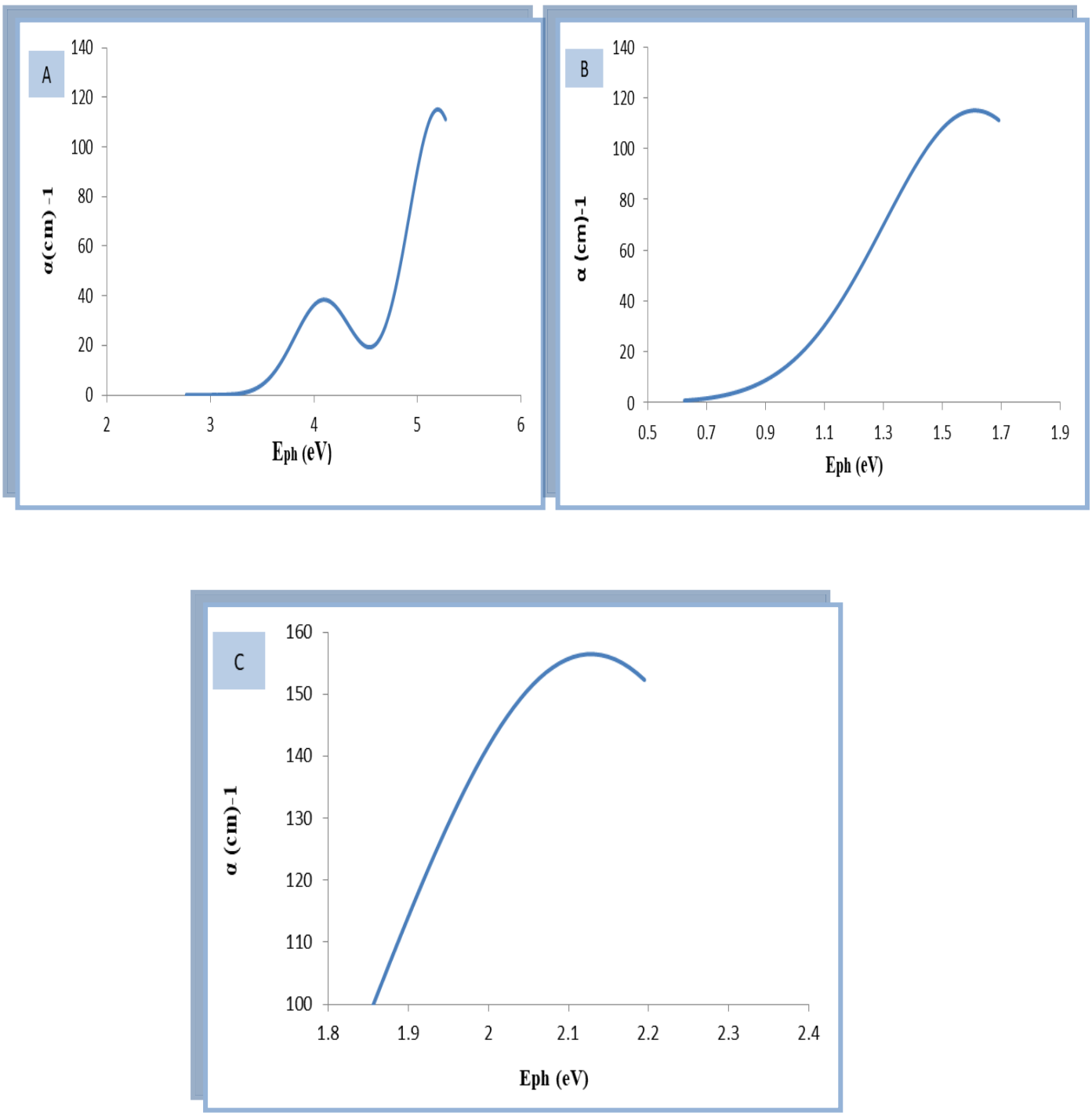

Figure (4.37): Variation of absorption coefficient (α) (A). for PEO (B).for (PEO-CuO-In_2O_3) (C). for (PE-ONiO-In_2O_3)nanocomposites (Theoretically).

The values of the optical energy band gap (E_g^{opt}) of nanocomposites are measured by using equation (2.30). E_g^{opt} is calculated for all created nanocomposites by drawing between $(hv)^{1/2}$ as a function of (E_{ph}), stretching a straight curve line, and intersecting it with the x-axis, which produces the energy gap value. Figures (4.38-4.40) illustrate the energy gaps for permissible indirect transitions in (PEO-CuO-In_2O_3) and (PEO-NiO-In_2O_3) nanocomposites experimental and theoretical, respectively. Figures (4.41-4.43) illustrate the energy gaps for forbidden indirect transitions in (PEO-CuO-In_2O_3) and (PEO-NiO-In_2O_3) nanocomposites experimental and theoretical, respectively. The values in Tables (4.7-4.10) show that as the concentrations of In_2O_3 nanoparticles increase, the values of permissible and forbidden indirect energy gap of all produced nanocomposites decrease. When the concentration of In_2O_3 nanoparticles reached to 5.4% at λ=500 nm, the energy gap of (PEO-CuO- In_2O_3) and (PEO-NiO- In_2O_3) nanocomposites decrease about 41.1% and 55.3% for allowed indirect transitions respectively this makes the samples useful for optical devices and low cost electronics. The creation of localized levels in the energy gap may explain the gradual decrease in the values of the energy gap as the concentration of nanoparticles increases [125]. The transition of electronics in this case occurs in two stages, with one transition from the valence band to the local levels in the energy gap and the second transition from the local levels to the conduction band when the concentrations of In_2O_3 nanoparticles rise.

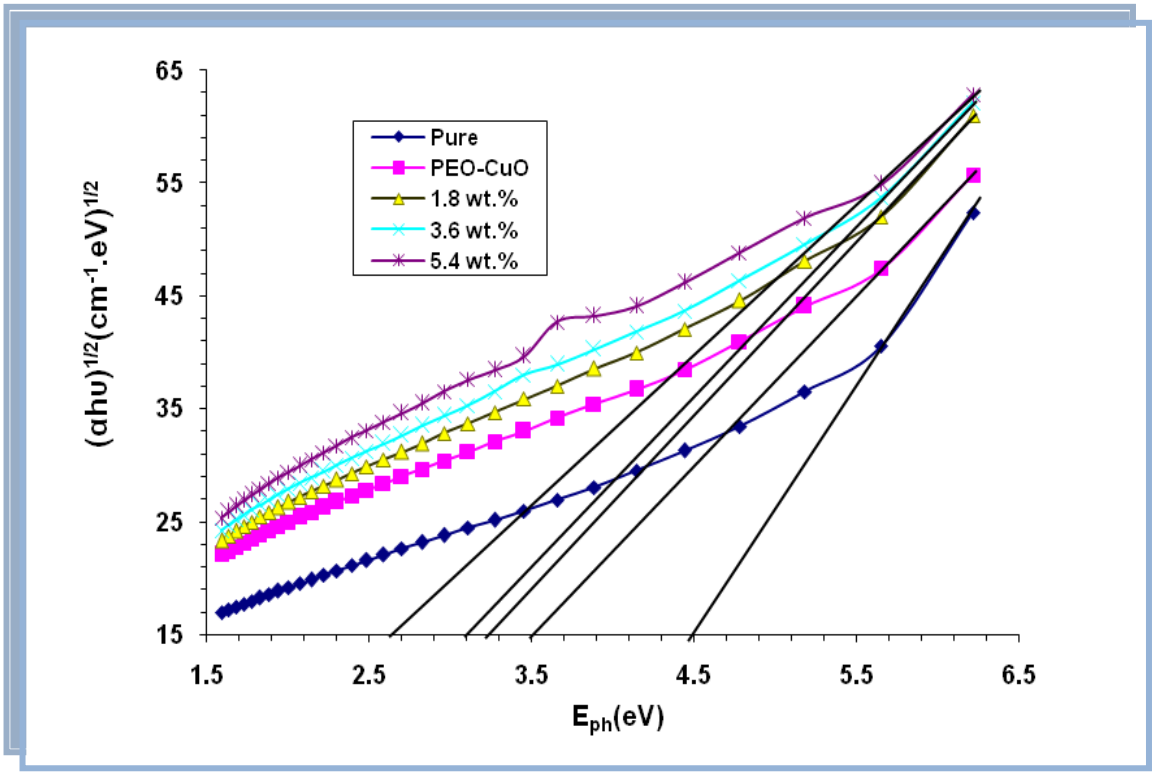

Figure (4.38): Variation of $(\alpha h\upsilon)^{1/2}$ for (PEO-CuO- In_2O_3) nanocomposites with photon energy.

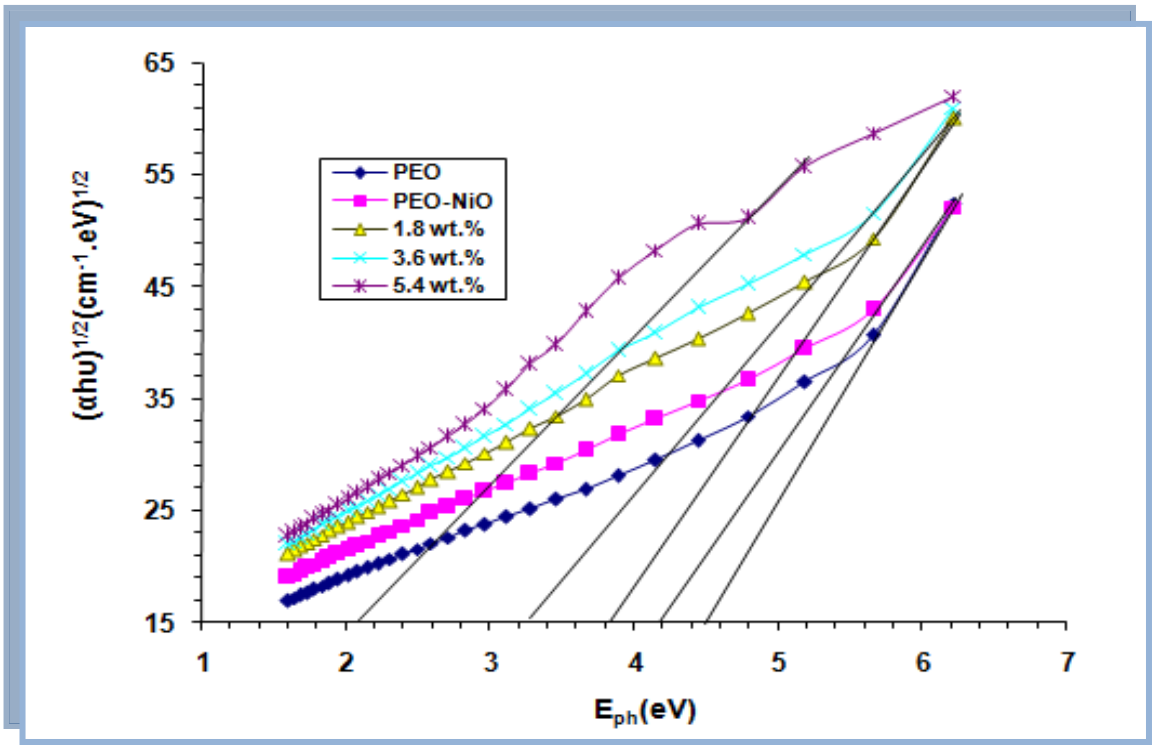

Figure (4.39): Variation of $(\alpha h\upsilon)^{1/2}$ for (PEO-NiO- In_2O_3) nanocomposites with photon energy.

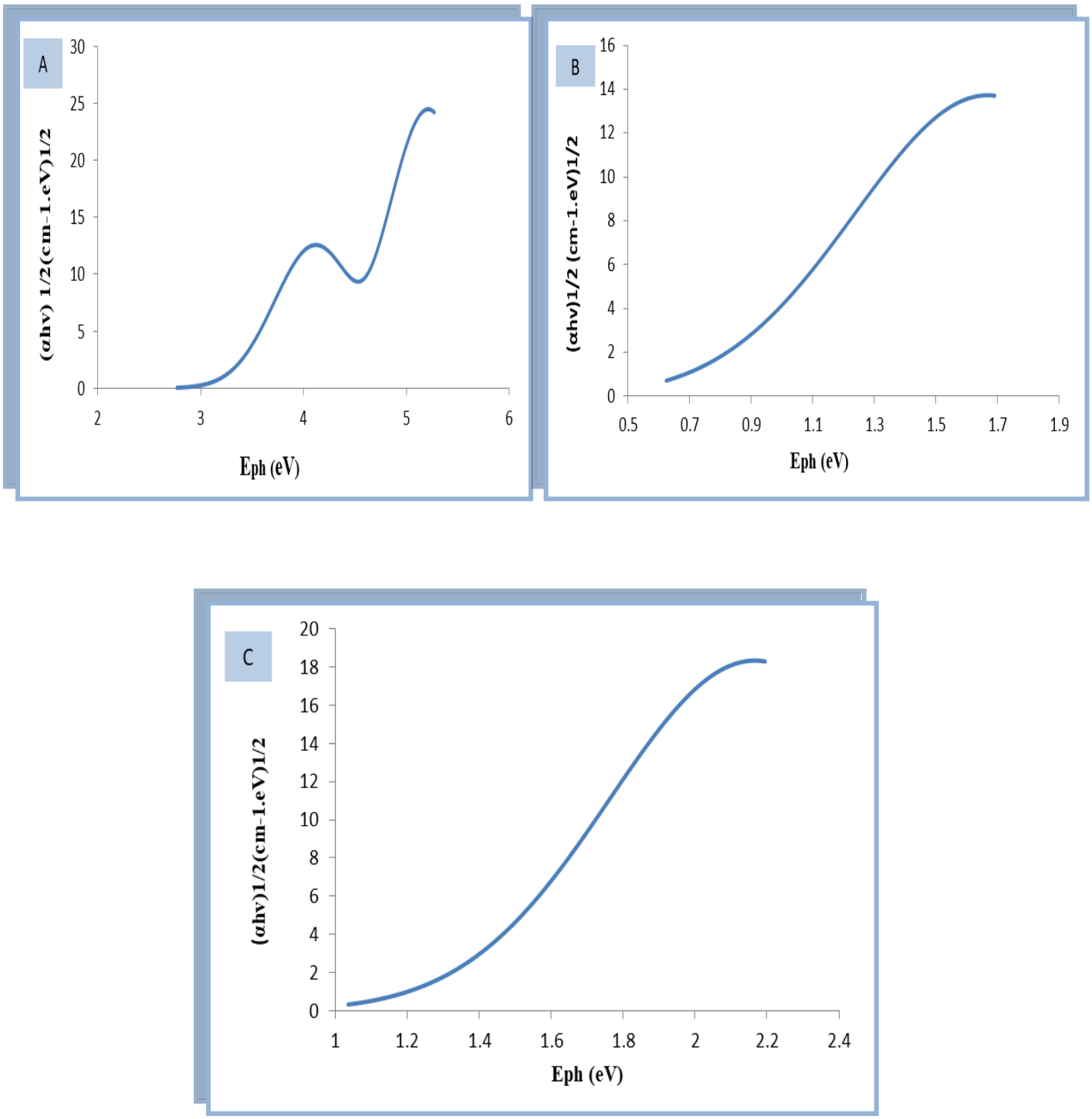

Figure (4.40): Variation of $(\alpha h\upsilon)^{1/2}$ (A). for PEO (B).for(PEO-CuO-In_2O_3) (C). for (PE-ONiO-In_2O_3) nanocomposites (Theoretically).

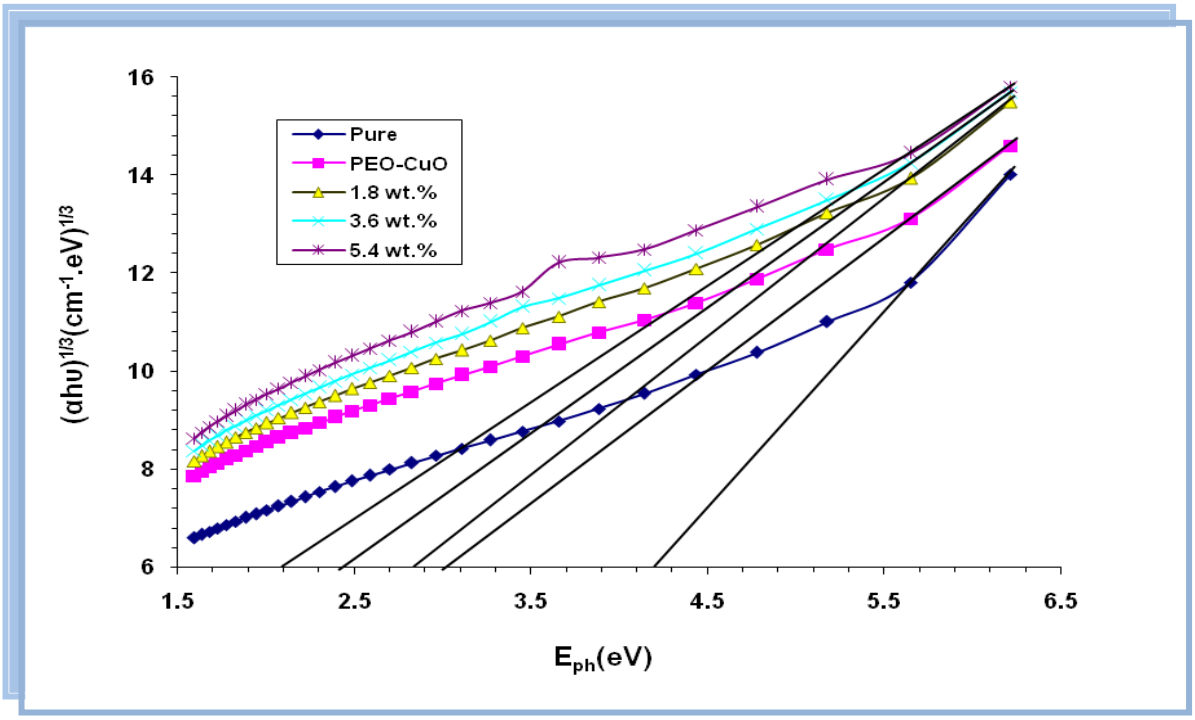

Figure (4.41): Variation of $(\alpha h\upsilon)^{1/3}$ for (PEO-CuO- In_2O_3) nanocomposites with photon energy.

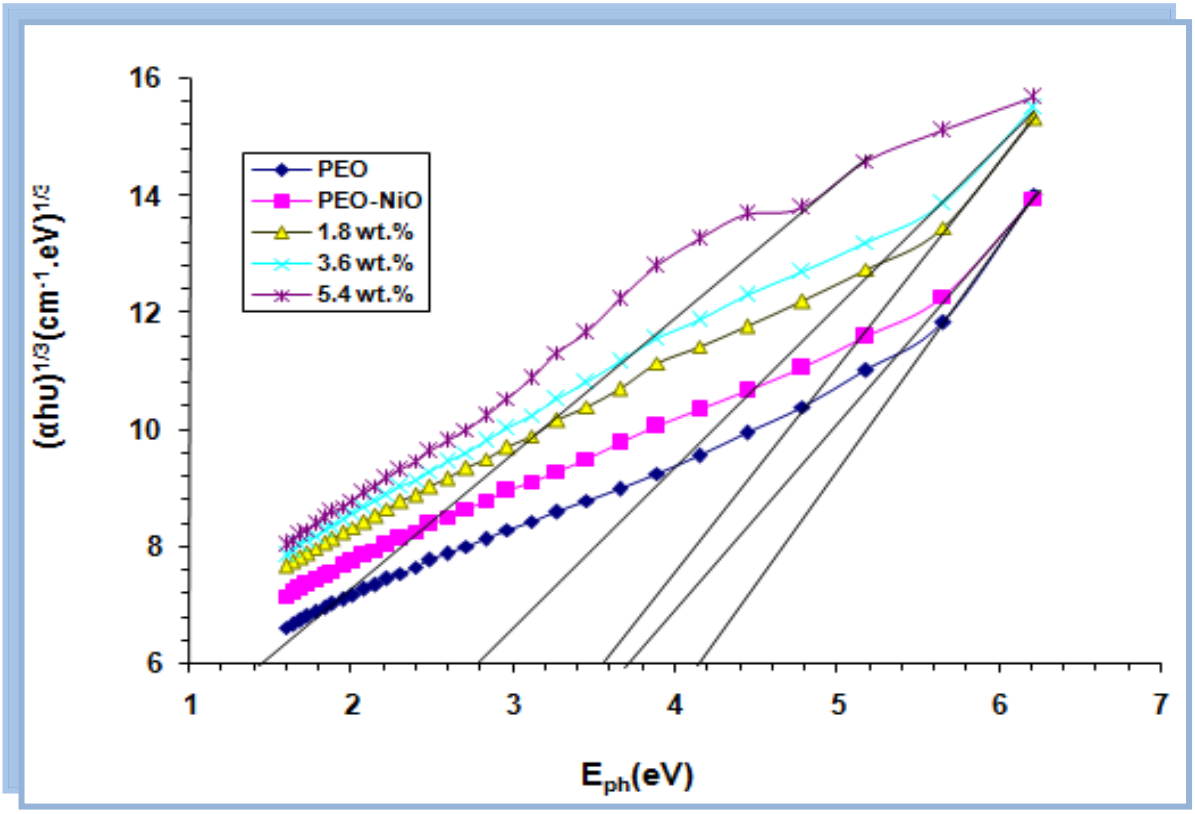

Figure (4.42): Variation of $(\alpha h\upsilon)^{1/3}$ for (PEO-NiO- In_2O_3) nanocomposites with photon energy.

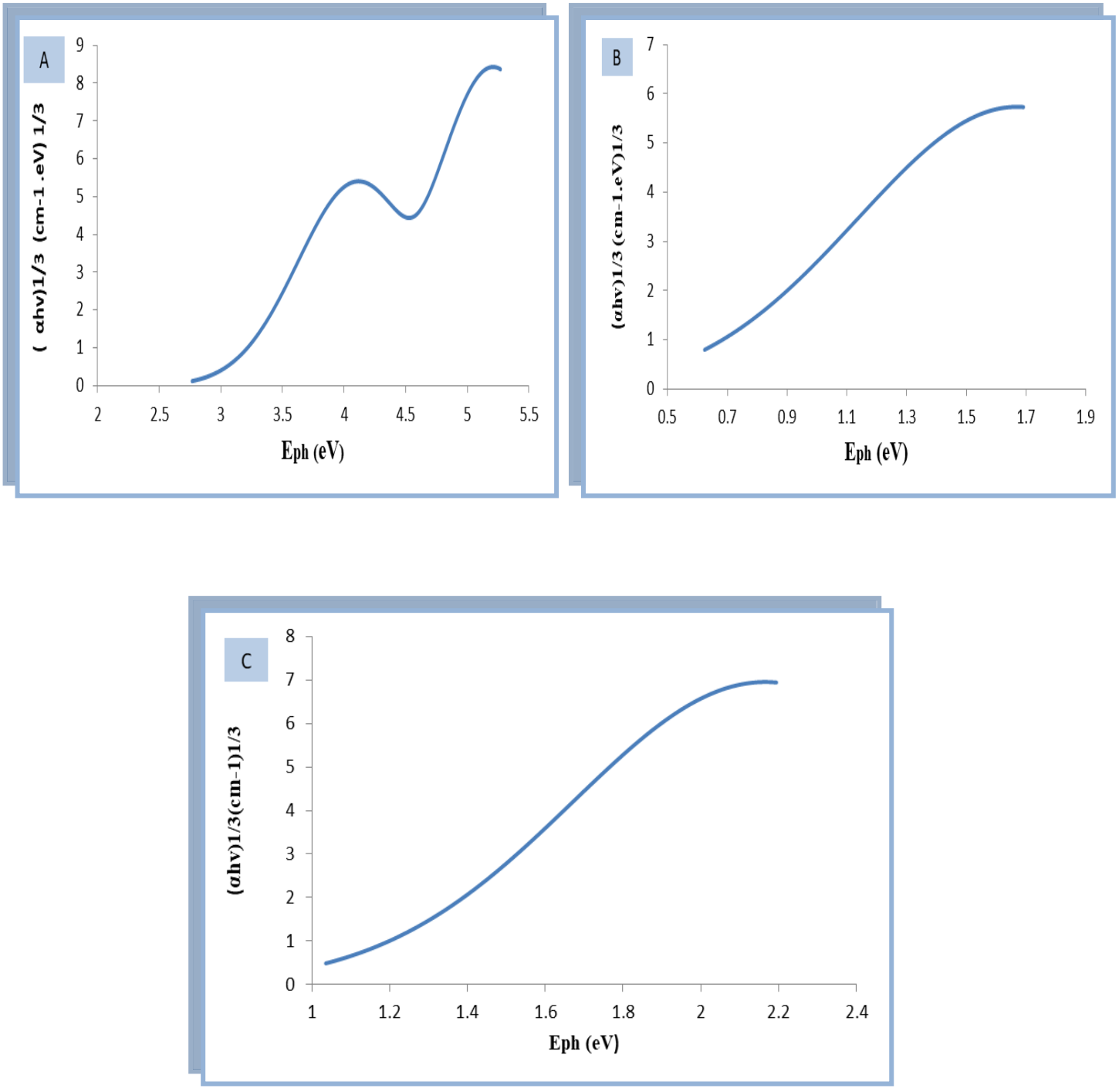

Figure(4.43): Variation of $(\alpha h\upsilon)^{1/3}$(A). for PEO (B).for(PEO-CuO-In_2O_3) (C). for (PE-ONiO-In_2O_3) nanocomposites(Theoretically).

Table (4.7):The energy gaps for allowed indirect transitions of (PEO-CuO-In_2O_3) Nanocomposites (experimentally).

Samples	Concentrations of In_2O_3 NPs wt.%	Values for allowed energy gap of the indirect transition (eV)
(PEO)	**0**	**4.5**
(PEO-CuO) Nanocomposites	**0**	**3.5**
(PEO-CuO-In_2O_3) Nanocomposites	**1.8**	**3.3**
(PEO-CuO-In_2O_3) Nanocomposites	**3.6**	**3.1**
(PEO-CuO-In_2O_3) Nanocomposites	**5.4**	**2.7**

Table (4.8):The energy gaps for allowed indirect transitions of (PEO-NiO-In_2O_3) Nanocomposites (experimentally).

Samples	Concentrations of In_2O_3 NPs wt.%	Values for allowed energy gap of the indirect transition (eV)
(PEO)	**0**	**4.5**
(PEO-NiO) Nanocomposites	**0**	**4.2**
(PEO-NiO-In_2O_3) Nanocomposites	**1.8**	**3.9**
(PEO-NiO-In_2O_3) Nanocomposites	**3.6**	**3.21**
(PEO-NiO-In_2O_3) Nanocomposites	**5.4**	**2.1**

Table (4.9): The energy gaps for forbidden indirect transitions of (PEO-CuO-In_2O_3) nanocomposites (experimentally).

Samples	Concentrations of In_2O_3 NPs wt.%	Values for forbidden energy gap of indirect transition (eV)
(PEO)	**0**	**4.15**
(PEO-NiO) Nanocomposites	**0**	**2.95**
(PEO-NiO-In_2O_3) Nanocomposites	**1.8**	**2.79**
(PEO-NiO-In_2O_3) Nanocomposites	**3.6**	**2.35**
(PEO-NiO-In_2O_3) Nanocomposites	**5.4**	**2.1**

Table (4.10): The energy gaps for forbidden indirect transitions of (PEO-NiO-In_2O_3) nanocomposites (experimentally)

Samples	Concentrations of In_2O_3 NPs wt.%	Values for forbidden energy gap of indirect transition (eV)
(PEO)	**0**	**4.19**
(PEO-NiO) Nanocomposites	**0**	**3.65**
(PEO-NiO-In_2O_3) Nanocomposites	**1.8**	**3.59**
(PEO-NiO-In_2O_3) Nanocomposites	**3.6**	**2.8**
(PEO-NiO-In_2O_3) Nanocomposites	**5.4**	**1.43**

4.5.4 Extinction Coefficient of (PEO-CuO- In_2O_3) and (PEO-NiO- In_2O_3) Nanocomposites

Extinction coefficient (k) is calculated using the equation (2-34). Figures (4.44-4.46) show the variation of the extinction coefficient as a function of wavelength (λ) for (PEO-CuO-In_2O_3) and(PEO-NiO-In_2O_3) nanocomposites, respectively. The extinction coefficient of (PEO-CuO-In_2O_3) and (PEO-NiO-In_2O_3) nanocomposites increases with increasing wavelength of incident light in the UV region, as shown in the figures. This is due to the strong absorption of all synthesized nanocomposites in these regions. Furthermore, the extinction coefficient of nanocomposites increases in the visible and near-infrared regions, which could be explained by the fact that the absorption coefficient of nanocomposites in the visible and near-infrared regions is nearly constant. According to equation (2.34)[126], the extinction coefficient is dependent on the wavelength. The extinction coefficient of (PEO-CuO) and (PEO-NiO) nanocomposites rises when the concentration of In_2O_3 nanoparticles rises, which is connected to the nanocomposites' enhanced absorption coefficient[127].

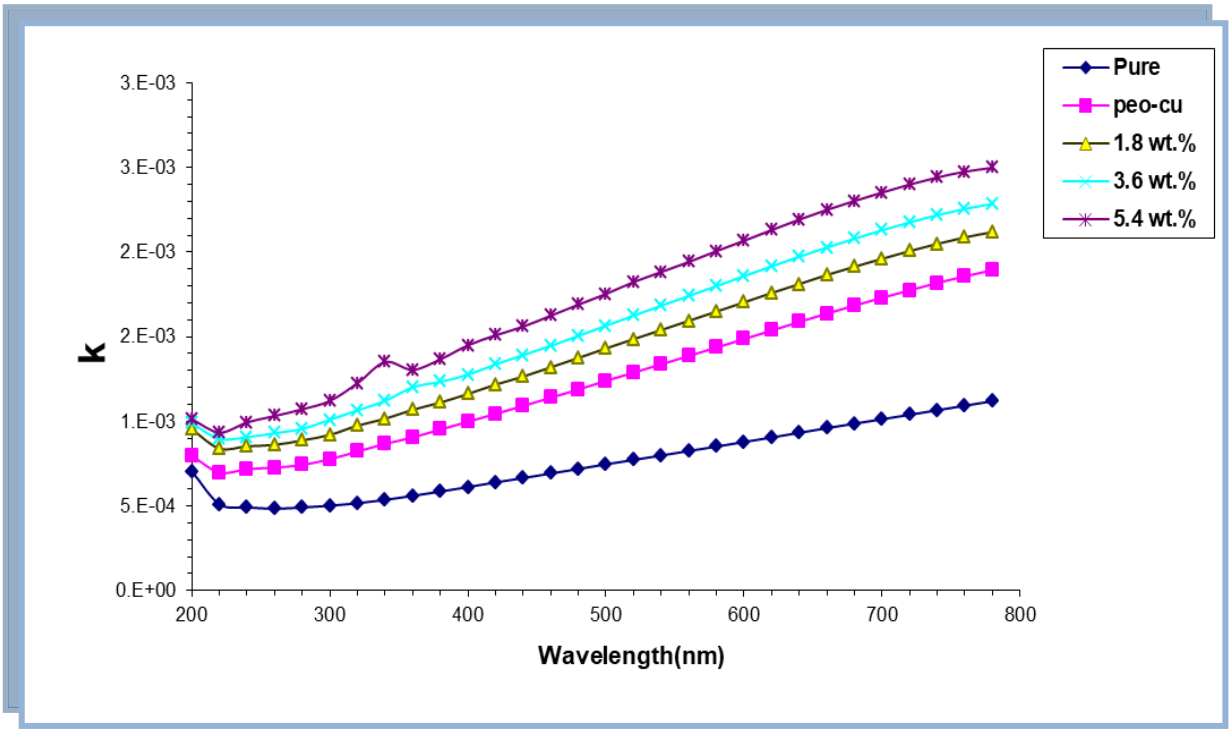

Figure (4.44): Variation of extinction coefficient for (PEO-CuO-In_2O_3) nanocomposites with wavelength.

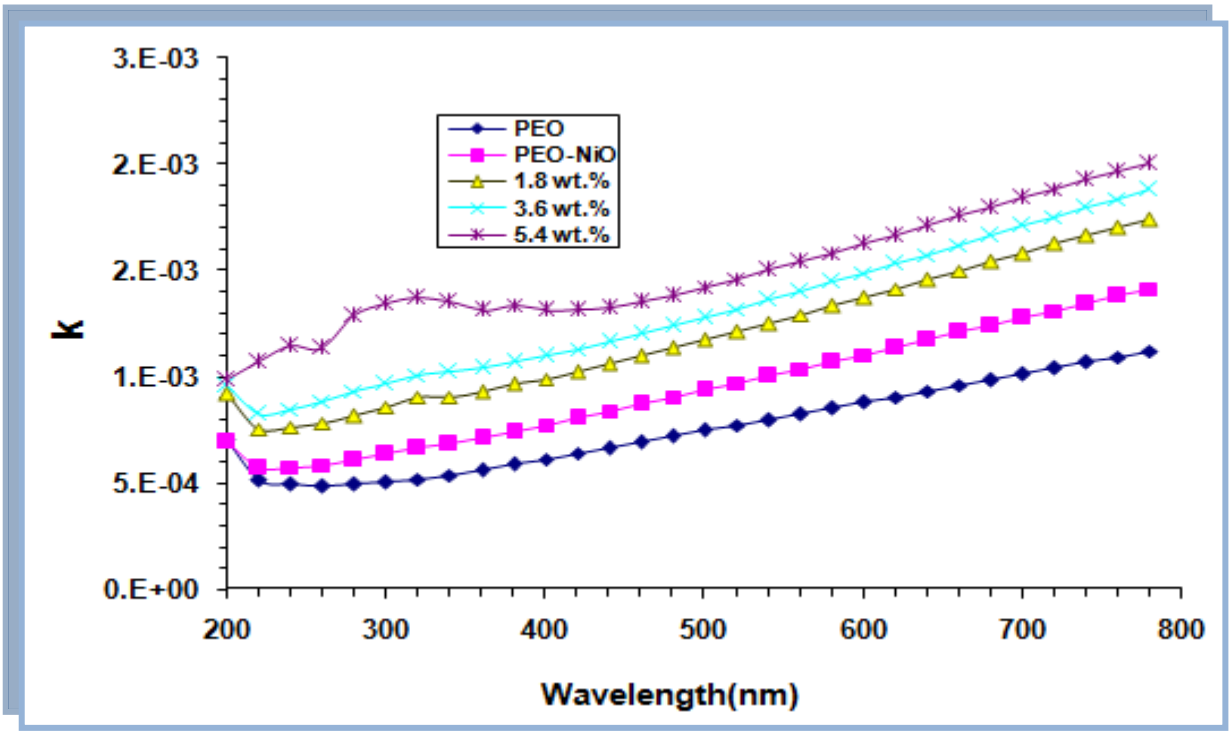

Figure (4.45): Variation of extinction coefficient for (PEO-NiO-In_2O_3) nanocomposites with wavelength.

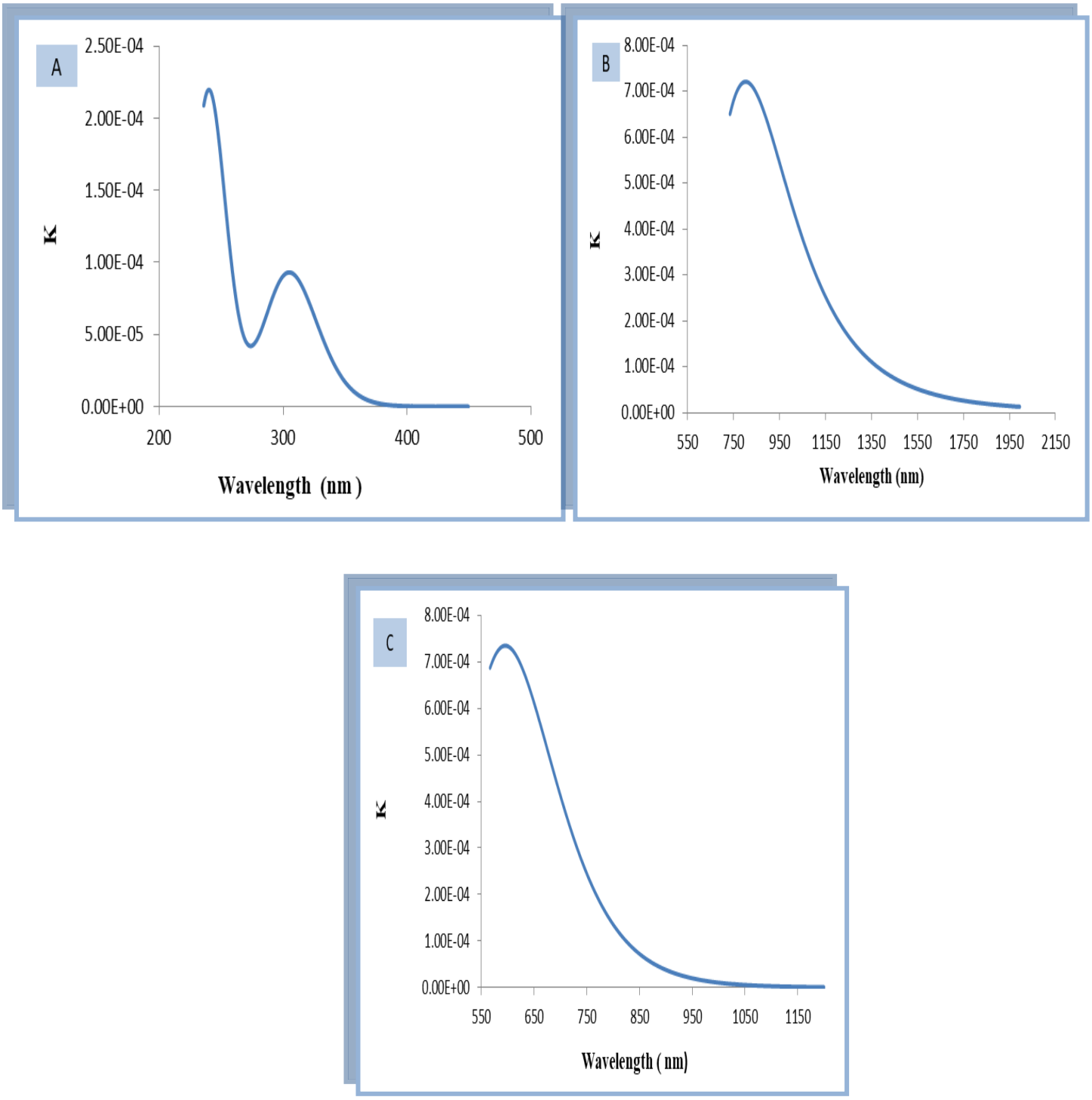

Figure (4.46): Variation extinction coefficient (A). for PEO (B).for(PEO-CuO-In_2O_3) (C). for (PE-ONiO-In_2O_3) nanocomposites (Theoretically).

4.5.5 The Refractive Index of (PEO-CuO-In_2O_3) and (PEO-NiO-In_2O_3) Nanocomposite

The refractive index is measured using equation (2.32). Figures (4.47-4.49) show the refractive index of (PEO-CuO-In_2O_3) and (PEO-NiO-In_2O_3) nanocomposites as a function of wavelength experimental and theoretical, respectively. The refractive index of all created nanocomposites increases as the wavelength of incident light increases, as seen in the figures. Furthermore, as the concentration of In_2O_3 nanoparticles increases, the refractive index of nanocomposites decreases. This result can be explained by the high absorbance of all nanocomposites samples, which reduces reflection and transmission[128]. The values of refractive index of nanocomposites can be useful in many optical applications. At visible and near-infrared regions, the refractive index is approximately constant[129].

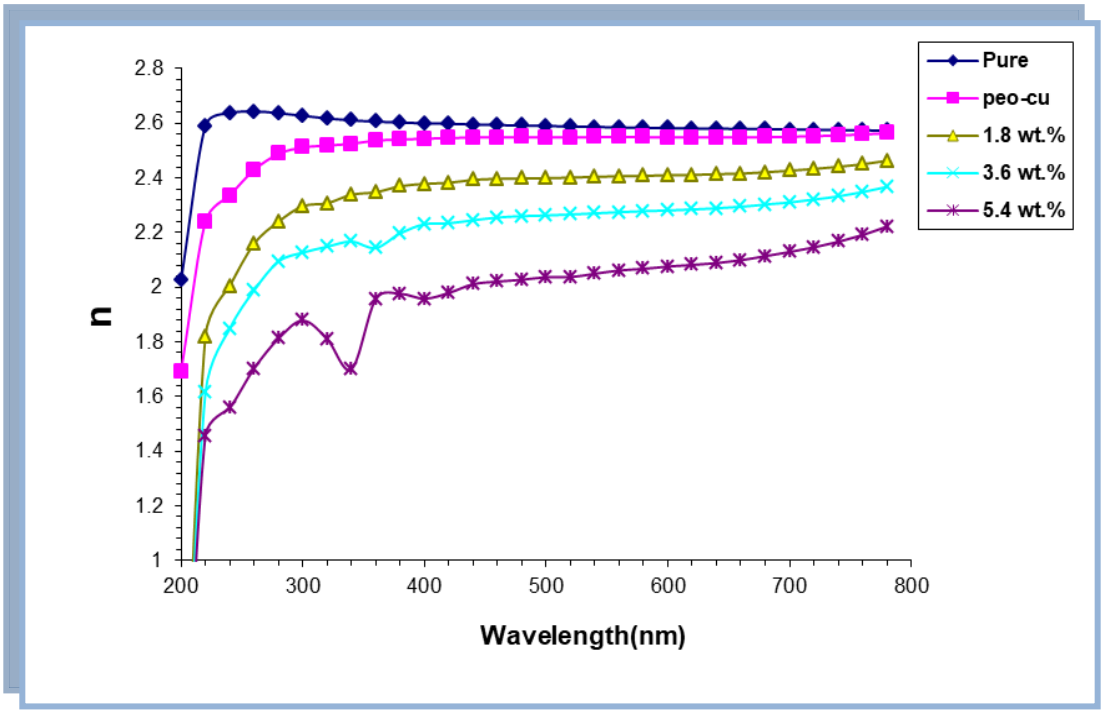

Figure (4.47): Variation of refractive index for (PEO-CuO-In_2O_3) nanocomposites with wavelength.

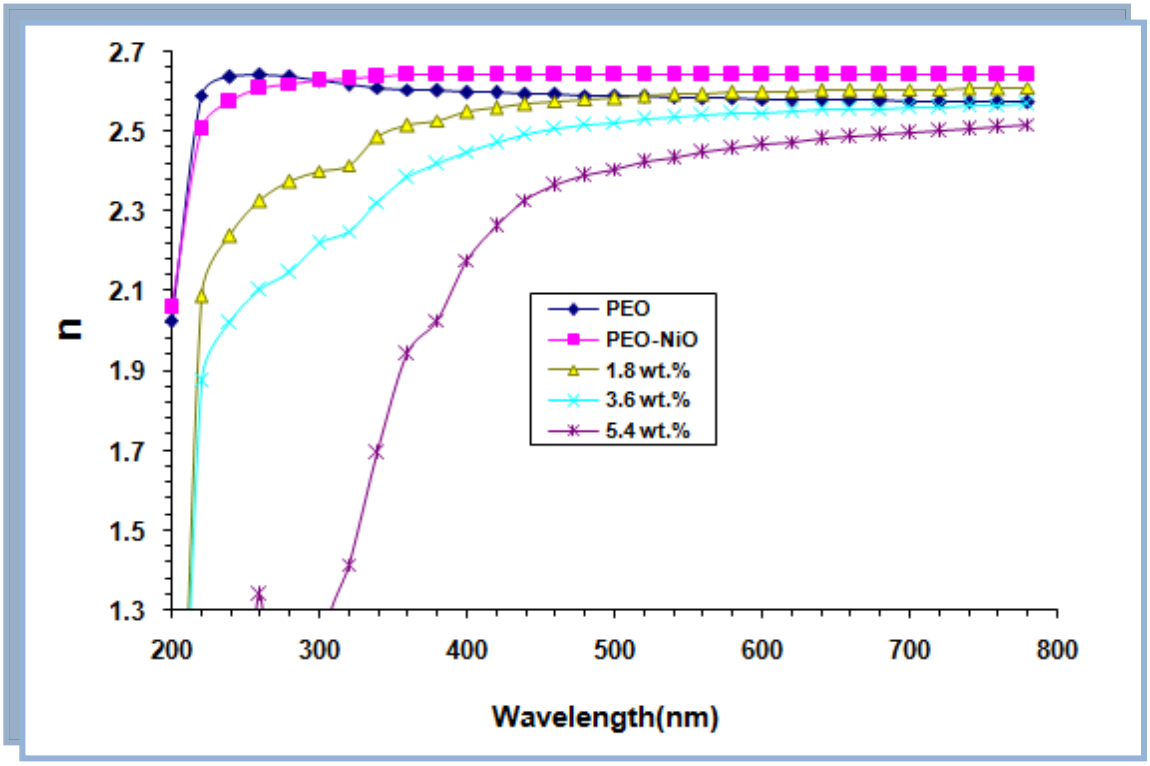

Figure (4.48): Variation of refractive index for (PEO-NiO-In_2O_3) nanocomposites with wavelength

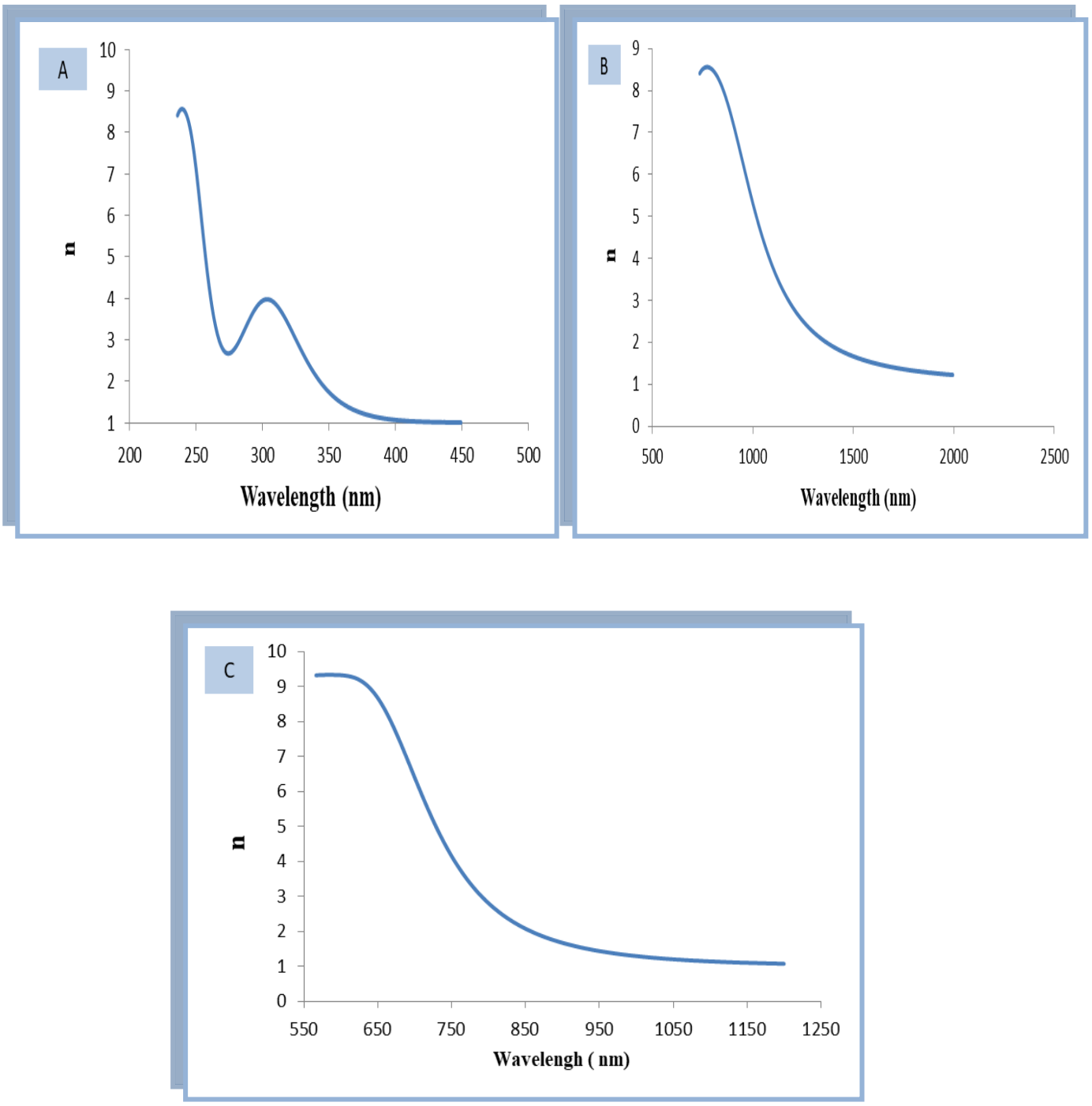

Figure (4.49): Variation of refractive index (A). for PEO (B).for(PEO-CuO-In_2O_3) (C). for (PE-ONiO-In_2O_3)nanocomposites(Theoretically).

4.5.6 The Real and Imaginary Parts of Dielectric Constant of (PEO-CuO-In_2O_3) and (PEO-NiO-In_2O_3) Nanocomposite

The real and imaginary parts of dielectric constant were calculated by using equations (2.37) and (2.38), respectively. Figures (4.50-4.52) display the fluctuation of the real part of dielectric constant (ε_1) with the wavelength for (PEO-CuO-In_2O_3) and (PEO-NiO-In_2O_3) nanocomposites experimental and theoretical, respectively. The effect of In_2O_3 nanoparticles on the imaginary part of dielectric constant (ε_2) are shown in Figures (4.53-4.55) for (PEO-CuO) and (PEO-NiO) nanocomposites respectively. The behavior of the real part of the dielectric constant is similar to that of the refractive index (n) because the value of extinction coefficient (k^2) is very small compared with refractive index (n^2), while the imaginary part of the dielectric constant is essentially In_2O_3 proportional with extinction coefficient (k) values [130]. As demonstrated in Figures (4.50-4.52), increasing the concentrations of In_2O_3 nanoparticles lowers the real part of the dielectric constant of (PEO), (PEO-CuO), and (PEO-NiO) nanocomposites, which is attributable to lower incident photon scattering. The imaginary component of the dielectric constant of nanocomposites increases as the concentration of In_2O_3 nanoparticles increases, owing to the higher absorption coefficient of nanocomposites. The real and imaginary parts of the dielectric constant of nanocomposites increase with increasing wavelength of incident photon, as shown in these figures. This is because the real part of the dielectric constant is proportional to the refractive index, while the imaginary part is dependent on the extinction coefficient.

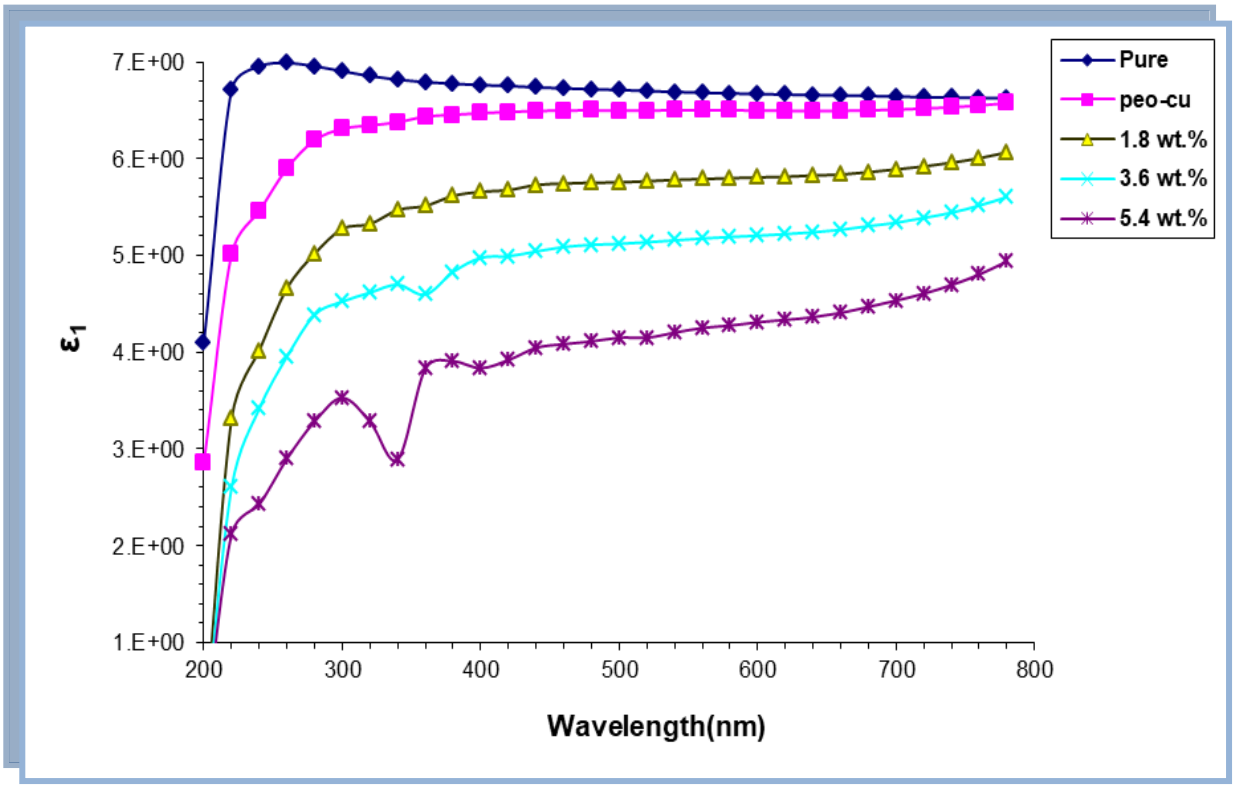

Figure (4.50): Variation of real part of dielectric constant for (PEO-CuO-In_2O_3) nanocomposites with wavelength.

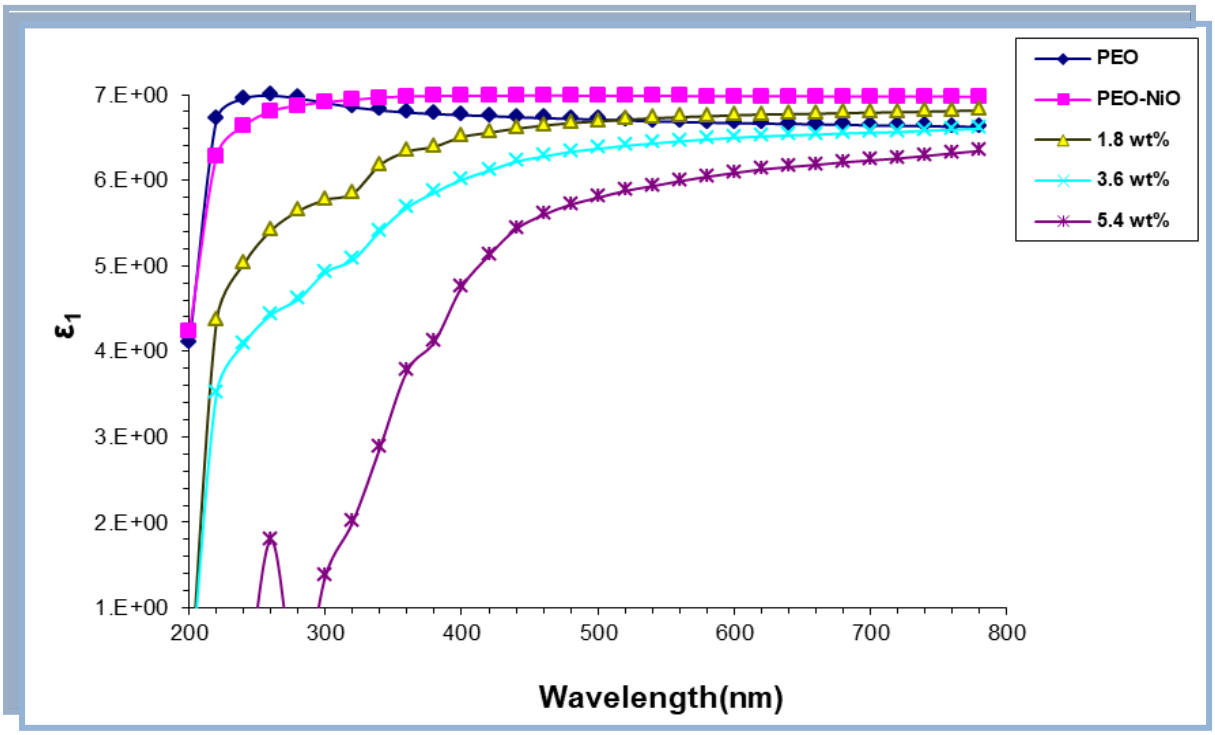

Figure (4.51): Variation of real part of dielectric constant for (PEO-NiO- In_2O_3) nanocomposites with wavelength.

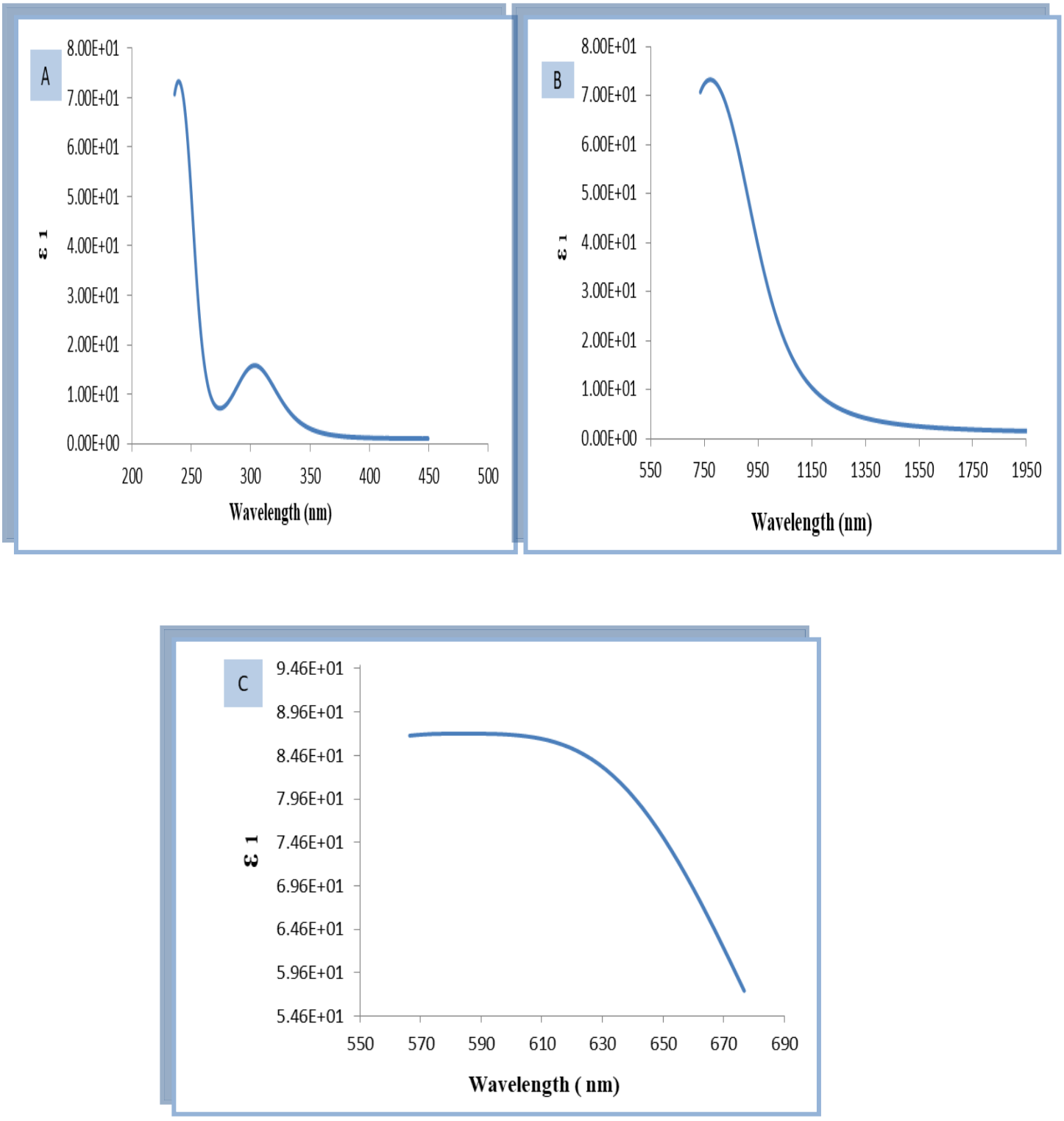

Figure (4.52): Real part of dielectric constant as a function of wavelength (A). for PEO (B).for (PEO-CuO-In_2O_3) (C). for (PEO-NiO-In_2O_3) nanocomposites(Theoretically).

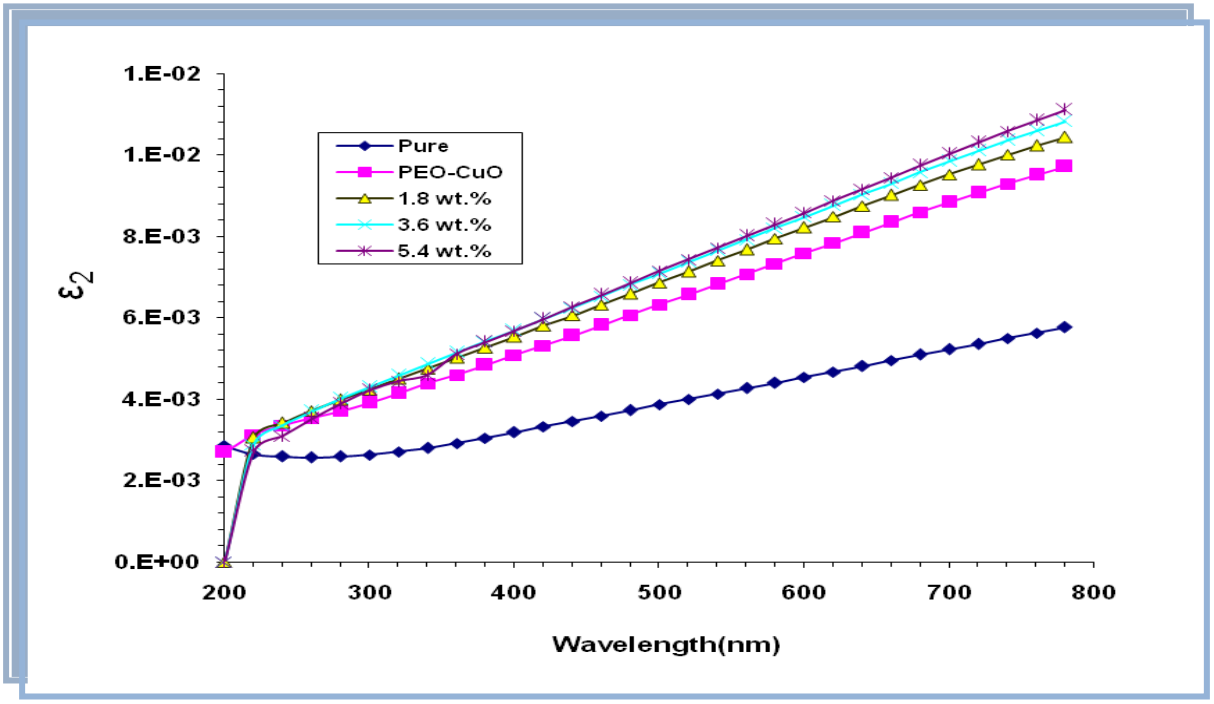

Figure (4.53): Variation of imaginary part of dielectric constant for (PEO-CuO-In_2O_3) nanoosites with wavelength.

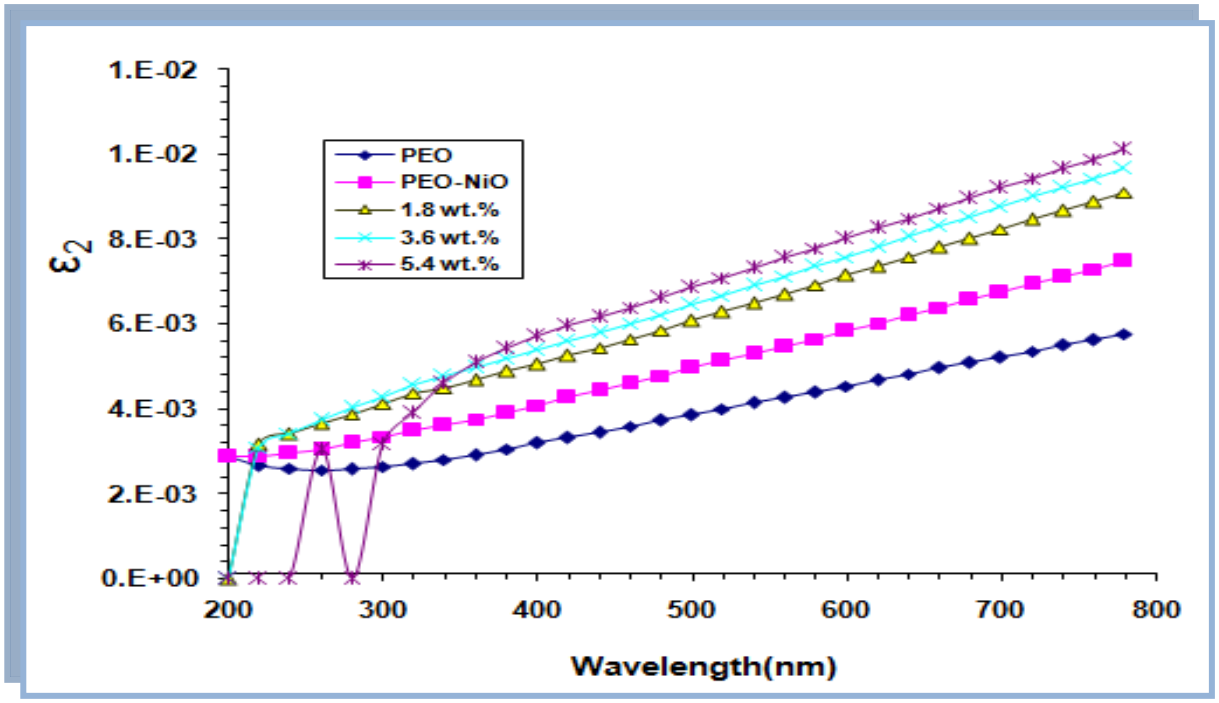

Figure (4.54): Variation of imaginary part of dielectric constant for (PEO-NiO-In_2O_3) nanocomposites with wavelength

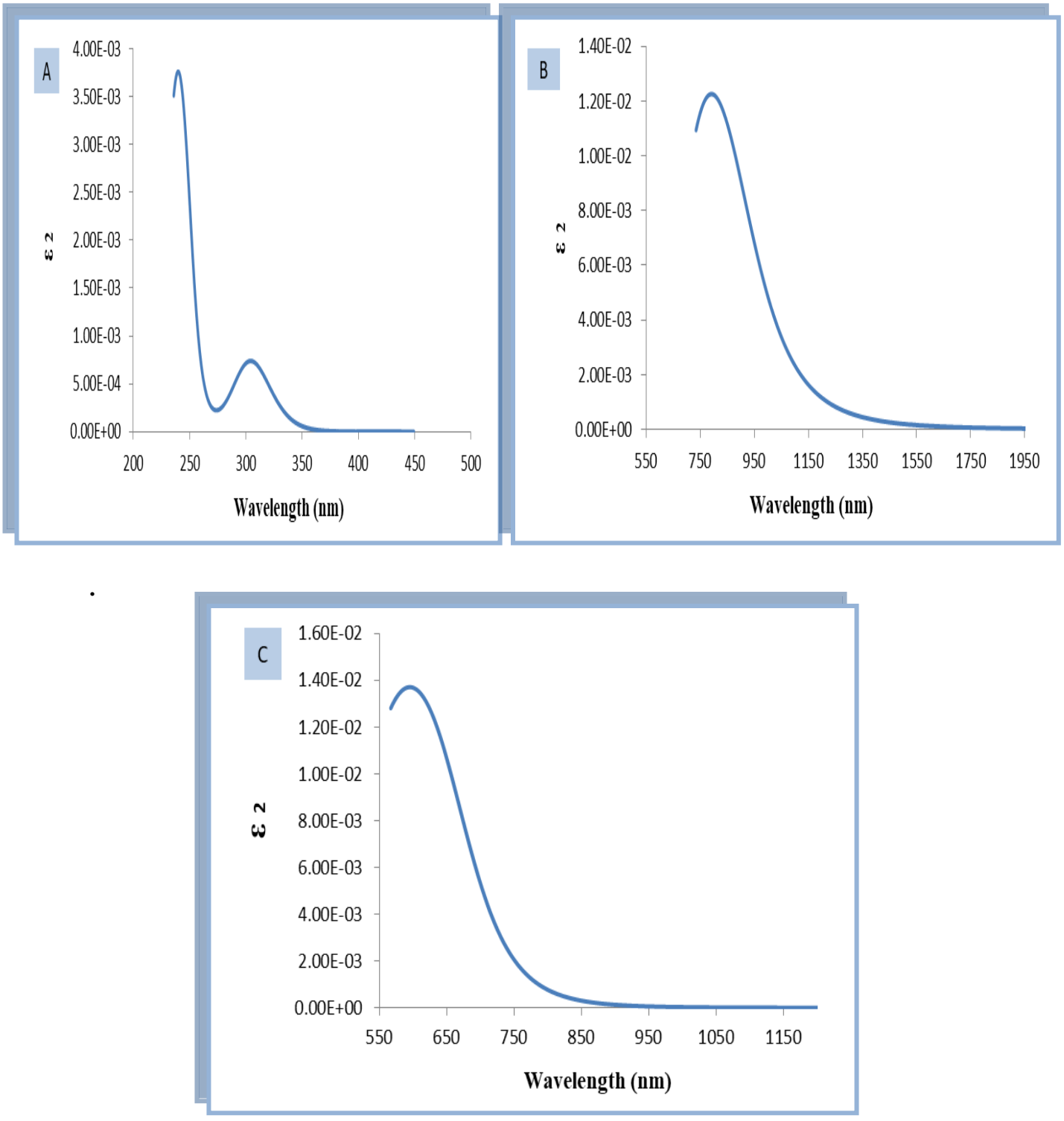

Figure (4.55): Imaginary dielectric constant as a function of wavelength (A). for PEO (B).for (PEO-CuO-In_2O_3) (C). for (PEO-NiO-In_2O_3)nanocomposites(Theoretically).

4.5.7 The Optical Conductivity of (PEO-CuO-In_2O_3) and (PEO-NiO-In_2O_3) Nanocomposite

The optical response of a material is mostly investigated in terms of optical conductivity, which can be determined using the equation (2.39). Figures (4.56-4.58) show how the optical conductivity of (PEO-CuO-In_2O_3) and (PEO-NiO-In_2O_3) nanocomposites varies with wavelength experimental and theoretical. The optical conductivity of all prepared nanocomposites increases with increasing In_2O_3 nanoparticle concentrations, a behavior attributed to the formation of localized levels in the energy gap; increasing In_2O_3 nanoparticle concentrations causes an increase in the density of localized levels in the energy gap, resulting in an increase in the absorption coefficient, and thus increasing the optical conductivity of nanocomposites[131]. The optical conductivity of nanocomposites decreases as the wavelength of the incident photon increases, as the optical conductivity of nanocomposites is largely dependent on the wavelength of the incident photon. All prepared nanocomposites have strong optical conductivity in the UV area; the rise in optical conductivity at low photon wavelengths is related to the high absorption of all generated nanocomposites in that region, resulting in an increase in charge transfer excitations. The samples are transmittance in the visible and near infrared areas, according to the optical conductivity spectrum[132,133].

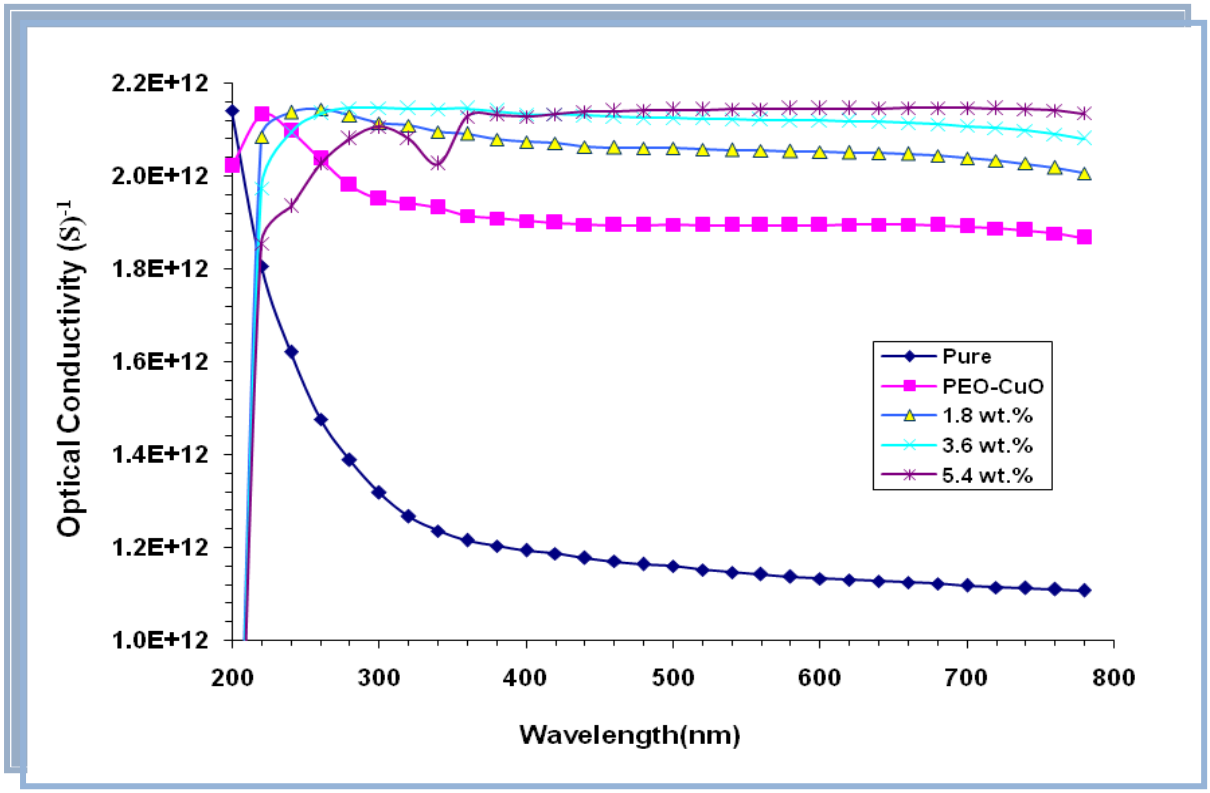

Figure (4.56): Variation of optical conductivity for (PEO-CuO- In_2O_3) nanocomposites with wavelength

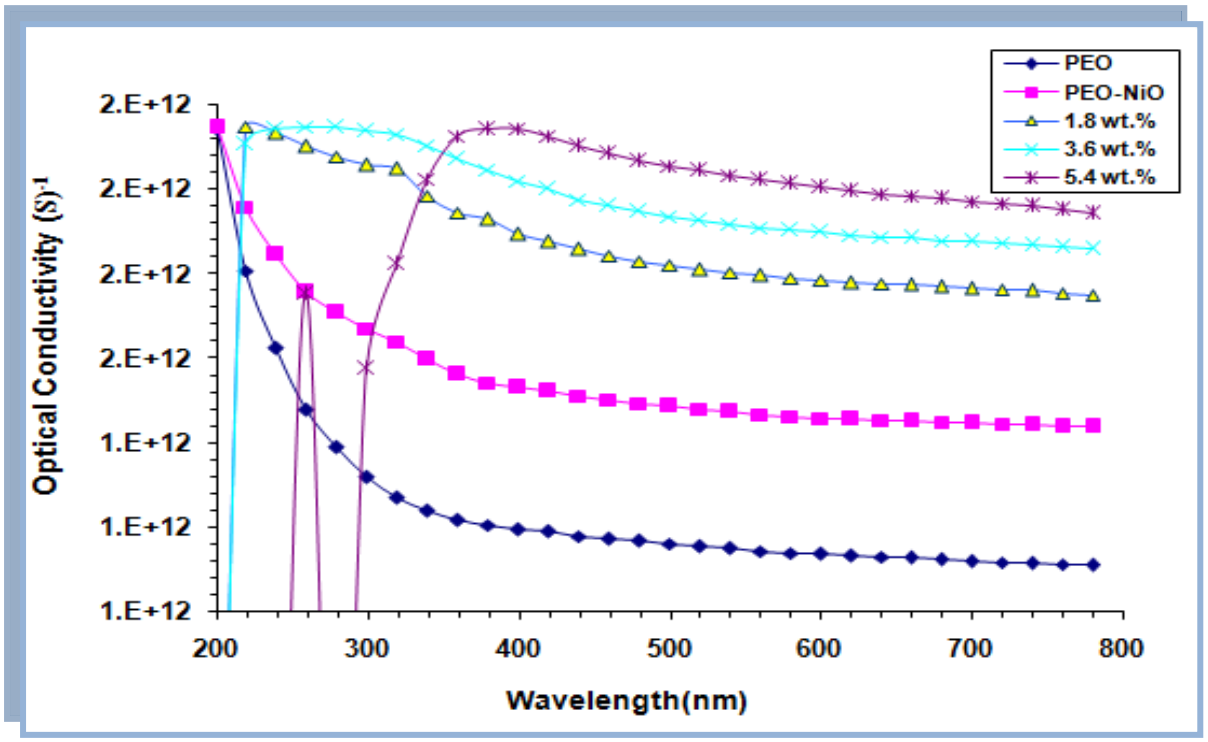

Figure (4.57): Variation of optical conductivity for (PEO-NiO-In_2O_3) nanocomposites with wavelength.

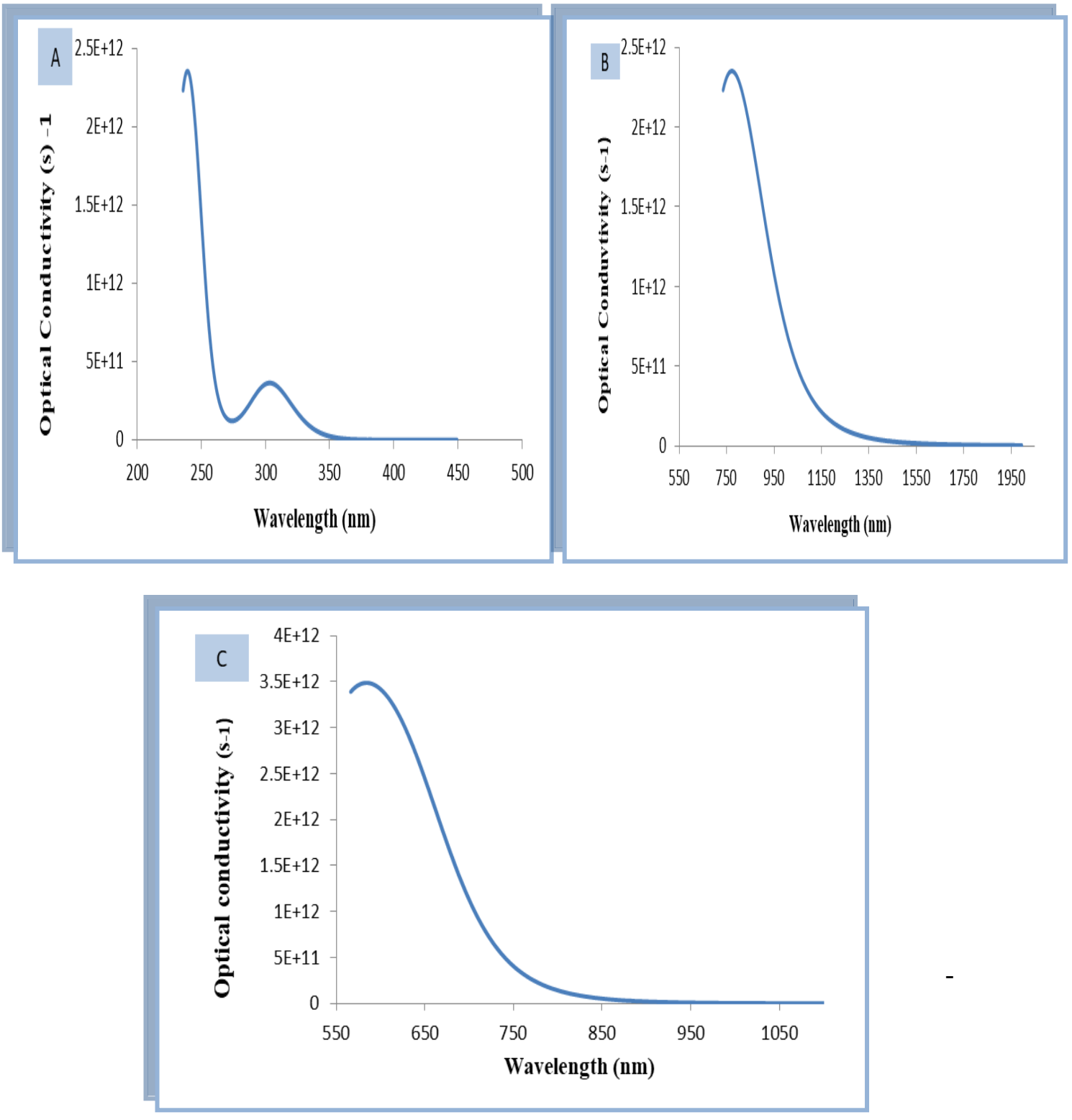

Figure (4.58): Variation of optical conductivity as a function of wavelength (A). for PEO (B).for(PEO-CuO-In_2O_3) (C). for (PEO-NiO-In_2O_3)nanocomposites(Theoretically).

4.6 The Applications (PEO-CuO-In_2O_3) and (PEO-NiO-In_2O_3) Nanocomposites

4.6.1 Application of Nanocomposites for Photocatalytic Activity

The photocatalytic activity of the produced samples for (PEO), (PEO-CuO), (PEO-CuO-In_2O_3), (PEO-NiO) and (PEO-NiO-In_2O_3) nanocomposites was investigated using the photodegradation percentage of methylene orange (MO) dye as a pollutant model, as indicated in section (2.16.2). The absorbance of MO dye is used to determine how quickly it degrades. Figures (4.59-4-68) shows the photodegradation of MO dye in (PEO), (PEO-CuO), (PEO-CuO-In_2O_3), (PEO-NiO), and (PEO-NiO-In_2O_3) nanocomposites at wavelengths ranging from 400 to 520 nm. Figure below shows the variation of absorbance for methyl orange dye with wavelength for different concentrations of nanoparticles at times (0, 30, 60 and 90) min. The photo-degradation of methyl orange dye increases as the nanoparticles concentrations and irradiation time increase where the best photocatalytic activity for (PEO-CuO-In_2O_3) and (PEO-NiO-In_2O_3) nanocomposites was 90% and 87% respectively within 90 minutes at concentration 5.4%wt of In_2O_3 nanoparticles. The absorbance of methyl orange dye as a function of UV irradiation time at (λ=460 nm) are shown in Figures (4.69-4.70). As seen in the figure, the photodegradation of methyl orange dye increases with increase in the irradiation period. Figures (4.71-4.72) shows the variation of absorbance of methyl orange dye with nanoparticles concentrations for different irradiation times at (λ=460 nm). The photo-degradation ratio increases when the irradiation time is extended; this is due to an increase of electron–hole pairs and a decrease in the recombination of these pairs, which leads to an increase in the decomposition percentages and thus an increase in the photocatalytic activity[104]. Figures (4.73-4.74) show the image of photodegradation performance sample. The sample of (PEO-CuO-In_2O_3)

nanocomposites with 5.4wt% concentration of In_2O_3 nanoparticles are considered as the optimized sample, show more absorbance decay than that of the other samples. This result indicates that the presence of the photocatalyst increased the efficiency of hydrogen peroxide decomposition, and consequently the MO dye degradation.

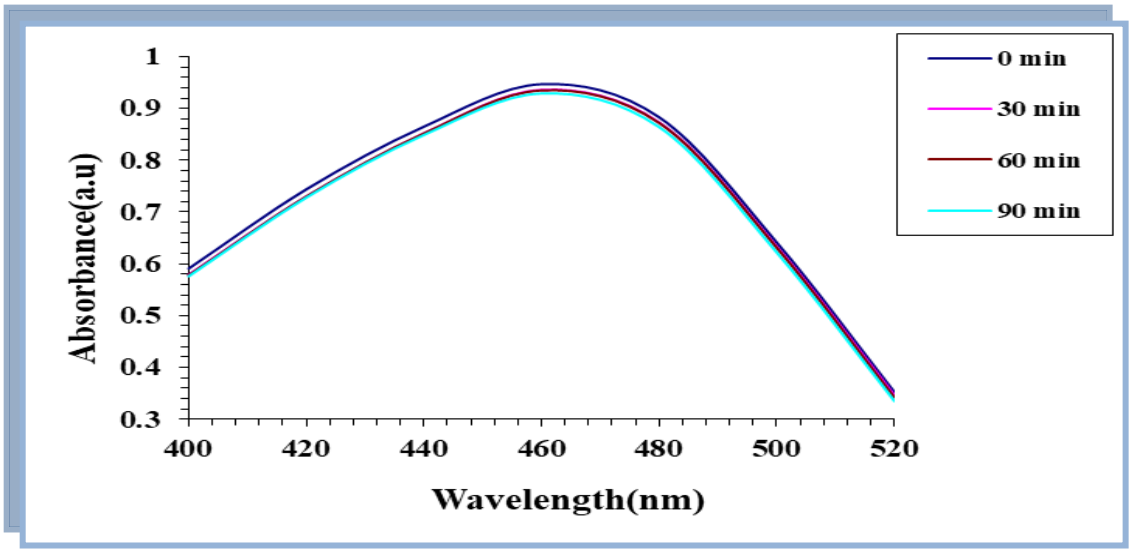

Figure (4.59): Photo-degradation performance of variation of absorbance spectra of MO dye with wavelength (nm).

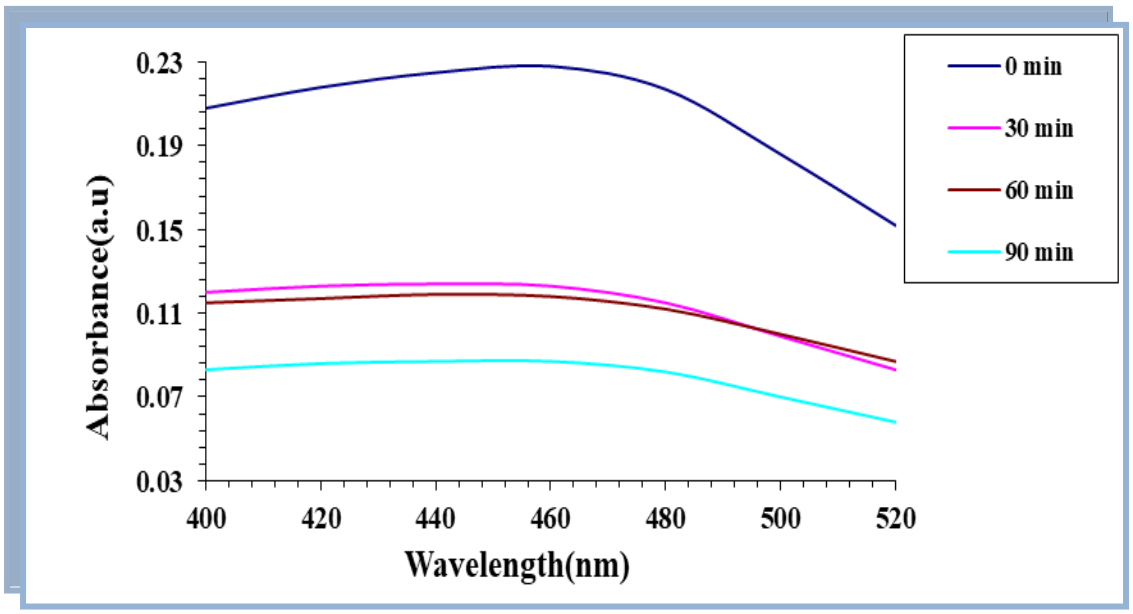

Figure (4.60): Variation of absorbance spectra of MO dye solution for (PEO) with wavelength (nm).

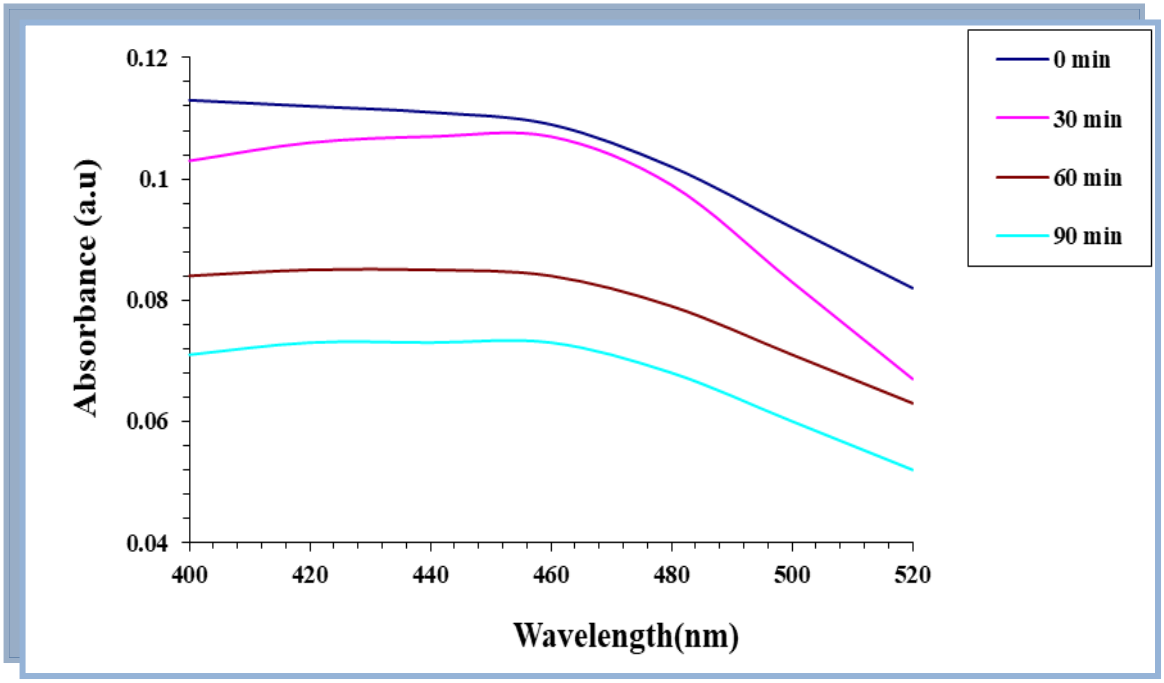

Figure (4.61): Variation of absorbance spectra of MO dye solution for (PEO-CuO) nanocomposite with wavelength (nm).

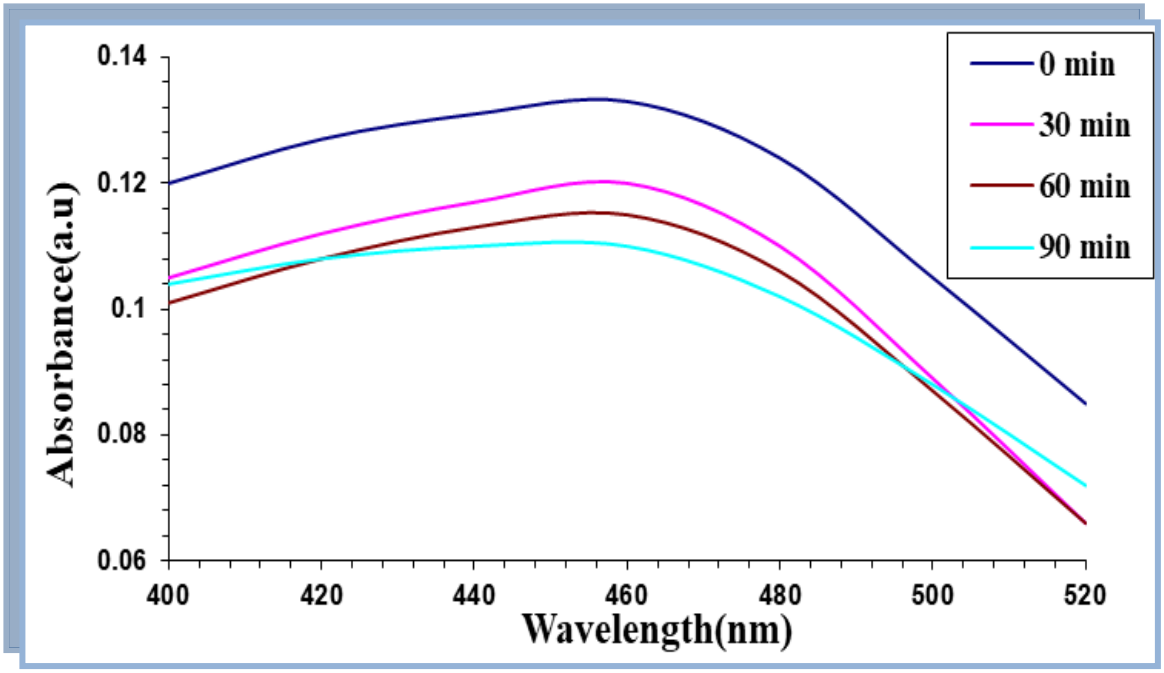

Figure (4.62): Variation of absorbance spectra of MO dye solution for (PEO-CuO-In_2O_3) nanocomposites for 1.8wt% concentration of In_2O_3 nanoparticles with wavelength (nm).

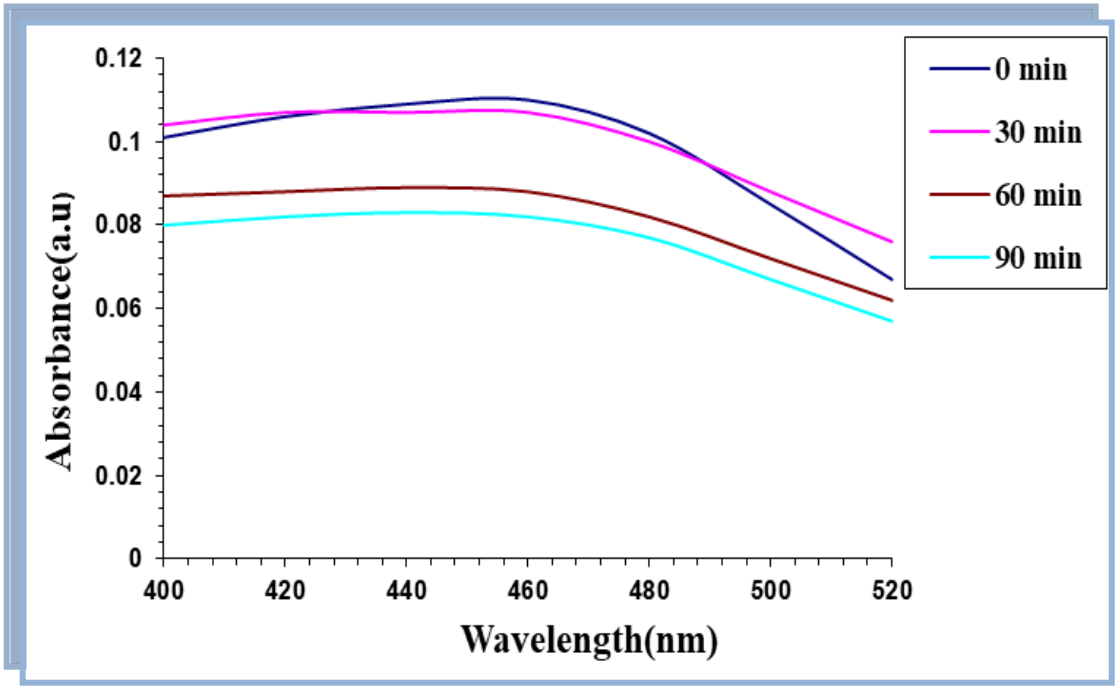

Figure (4.63): Variation of absorbance spectra of MO dye solution for (PEO-CuO-In_2O_3) nanocomposites for 3.6 wt% concentration of In_2O_3 nanoparticles with wavelength (nm).

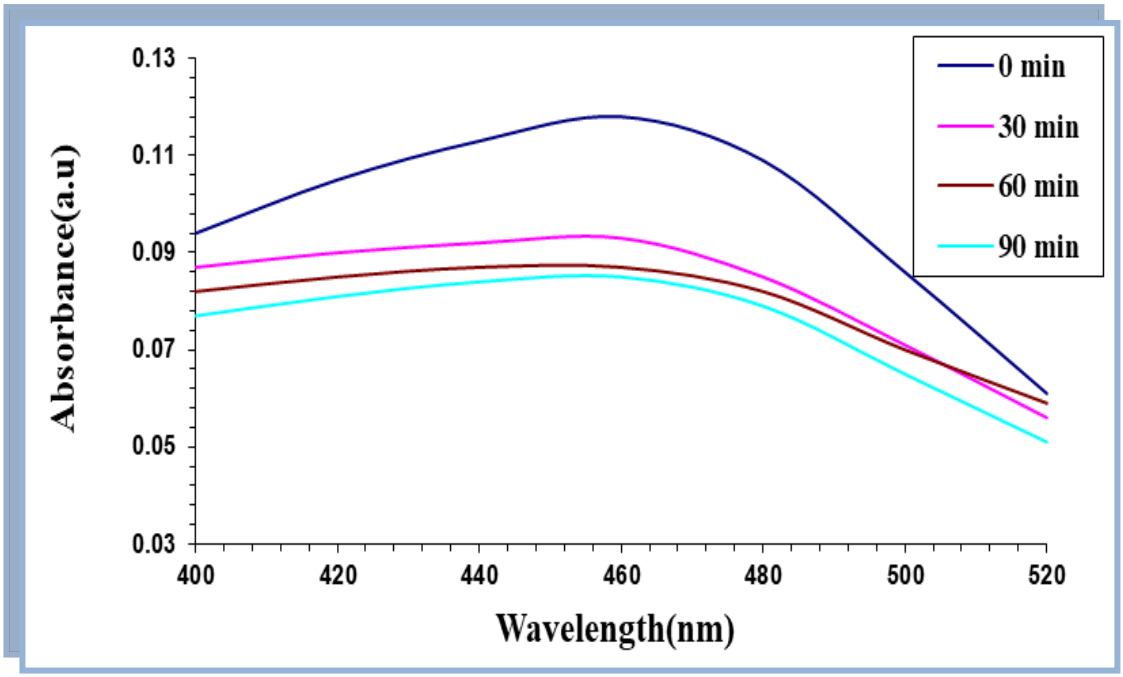

Figure (4.64): Variation of absorbance spectra of MO dye solution for (PEO-CuO-In_2O_3) nanocomposites for 5.4 wt% concentration of In_2O_3 nanoparticles with wavelength (nm).

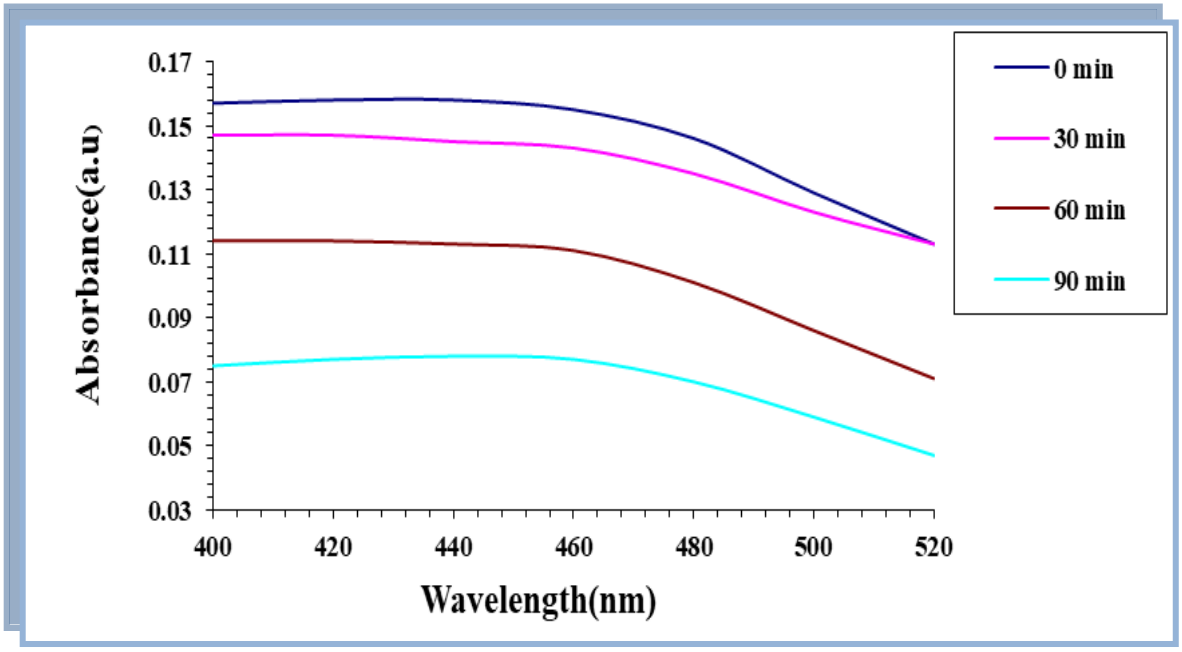

Figure (4.65): Variation of absorbance spectra of MO dye solution for (PEO-NiO) nanocomposite with wavelength (nm).

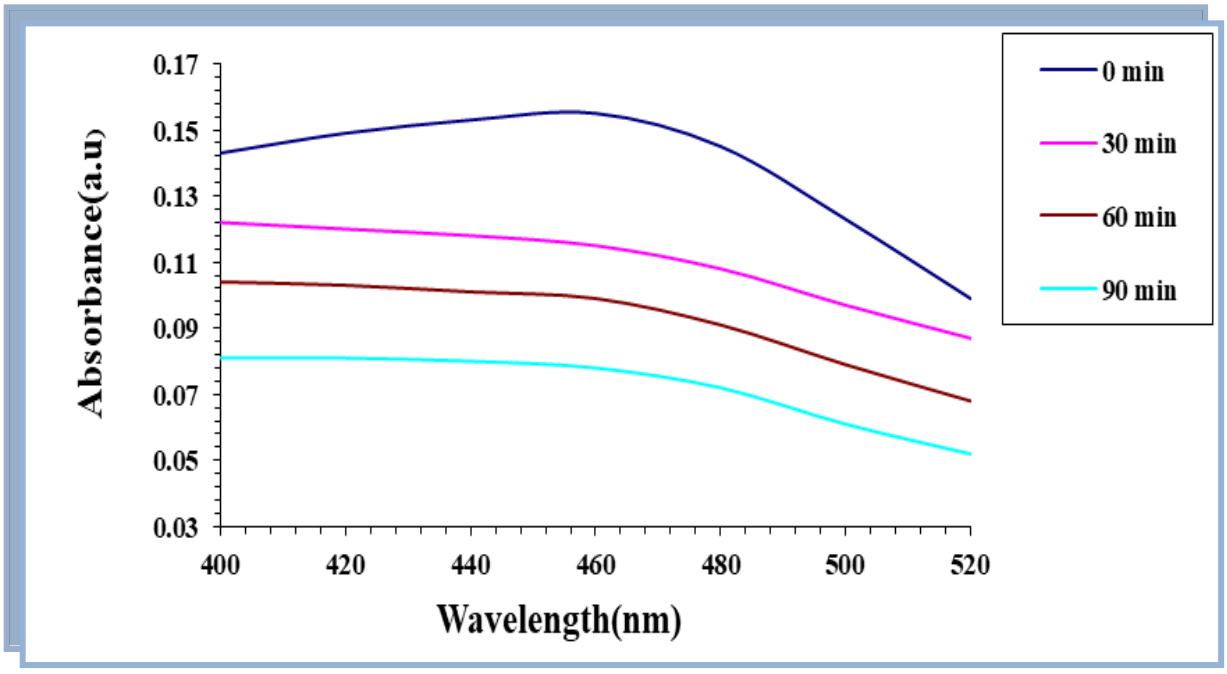

Figure (4.66): Variation of absorbance spectra of MO dye solution for (PEO–NiO-In_2O_3) nanocomposites for 1.8wt% concentration of In_2O_3 nanoparticles with wavelength (nm).

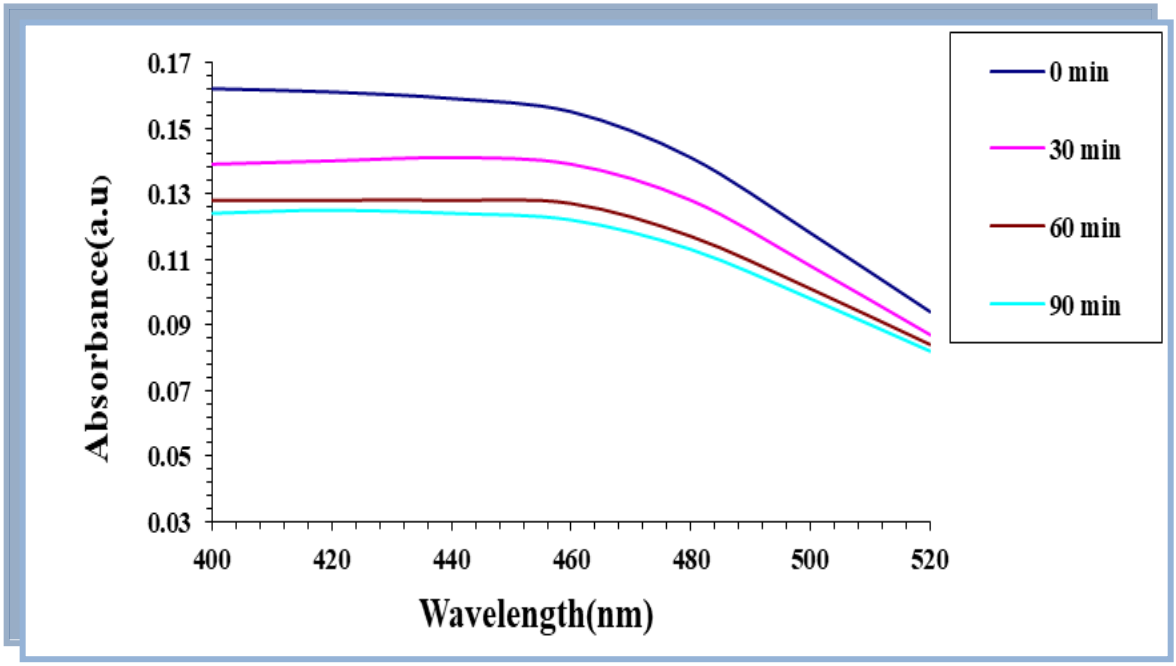

Figure (4.67): Variation of absorbance spectra of MO dye solution for (PEO-NiO-In_2O_3) nanocomposites for 3.6 wt% concentration of In_2O_3 nanoparticles with wavelength (nm).

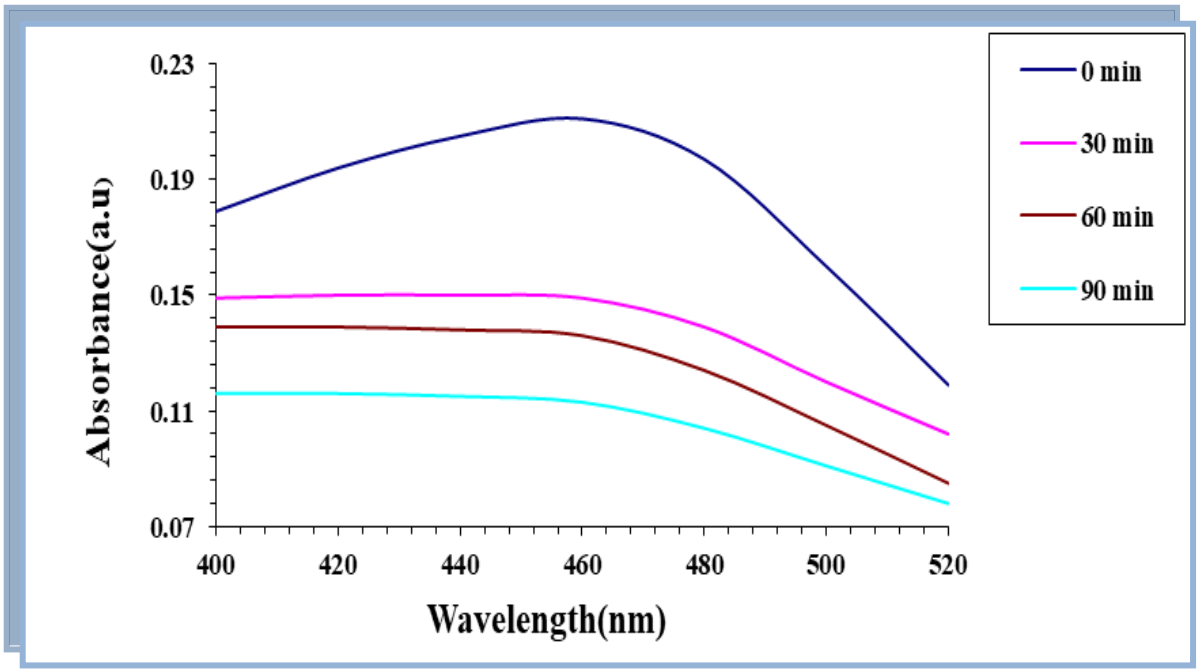

Figure (4.68): Variation of absorbance spectra of MO dye solution for (PEO-NiO-In_2O_3) nanocomposites for 5.4 wt% concentration of In_2O_3nanoparticles with wavelength(nm).

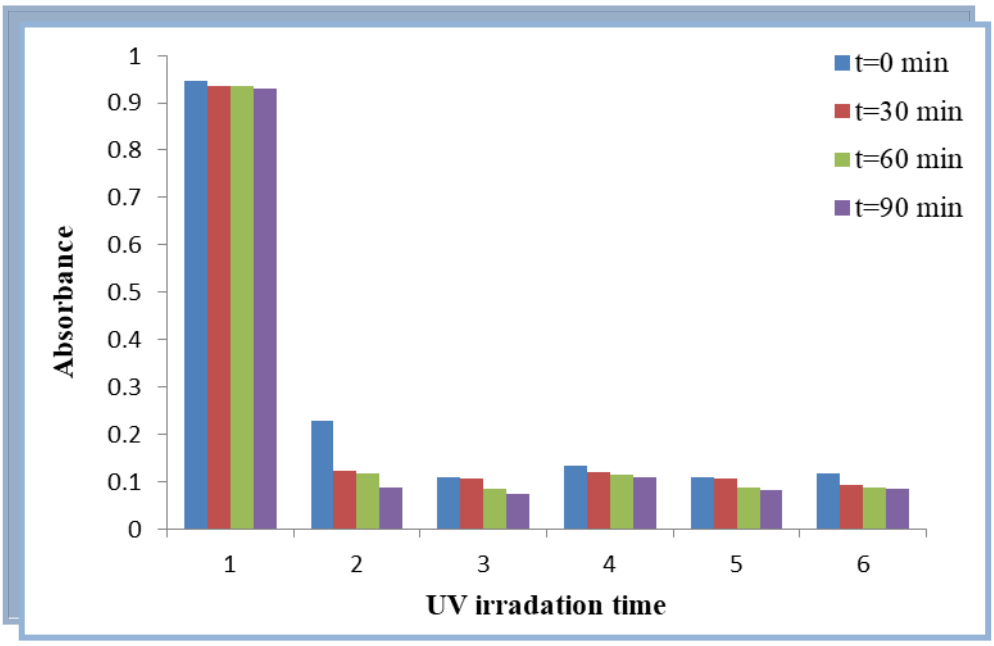

Figure (4. 69): Effect of UV-irradiation time on absorbance spectra of 1- MO dye 2-(MO-PEO) 3-(MO-PEO-CuO) 4-(MO-PEO-CuO-In_2O_3)for 1.8wt%In_2O_3 5-(MO-PEO-CuO-In_2O_3) for 3.6wt% In_2O_3 6-(MO-PEO-CuO-In_2O_3) for 5.4wt% In_2O_3 at 460 (nm).

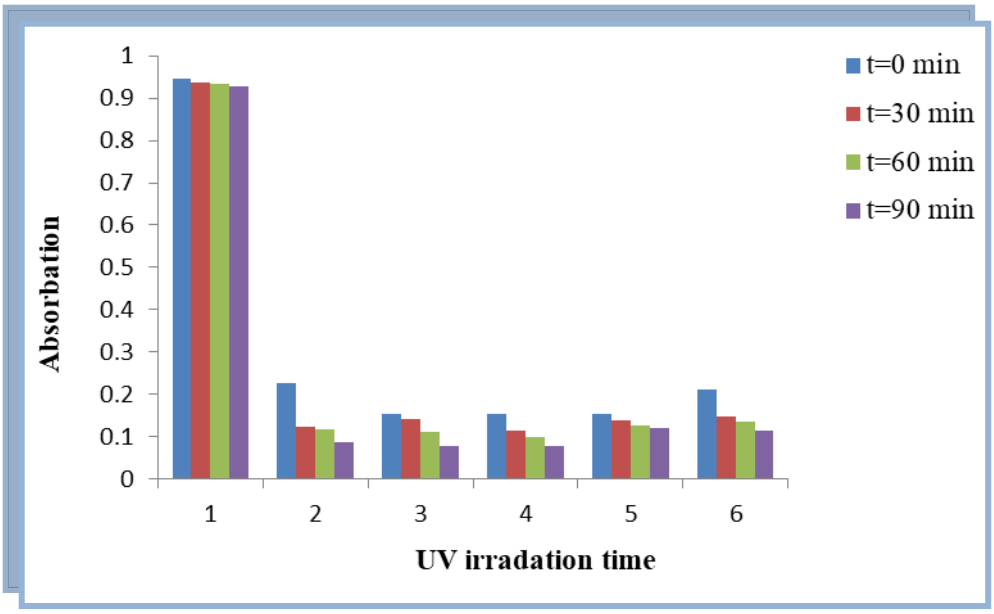

Figure (4. 70): Effect of UV-irradiation time on absorbance spectra of 1- MO dye 2-(MO-PEO) 3-(MO-PEO-NiO) 4-(MO-PEO-NiO-In_2O_3)for 1.8wt%In_2O_3 5-(MO-PEO-NiO-In_2O_3) for 3.6wt% In_2O_3 6-(MO-PEO-NiO-In_2O_3) for 5.4wt% In_2O_3 at 460 (nm).

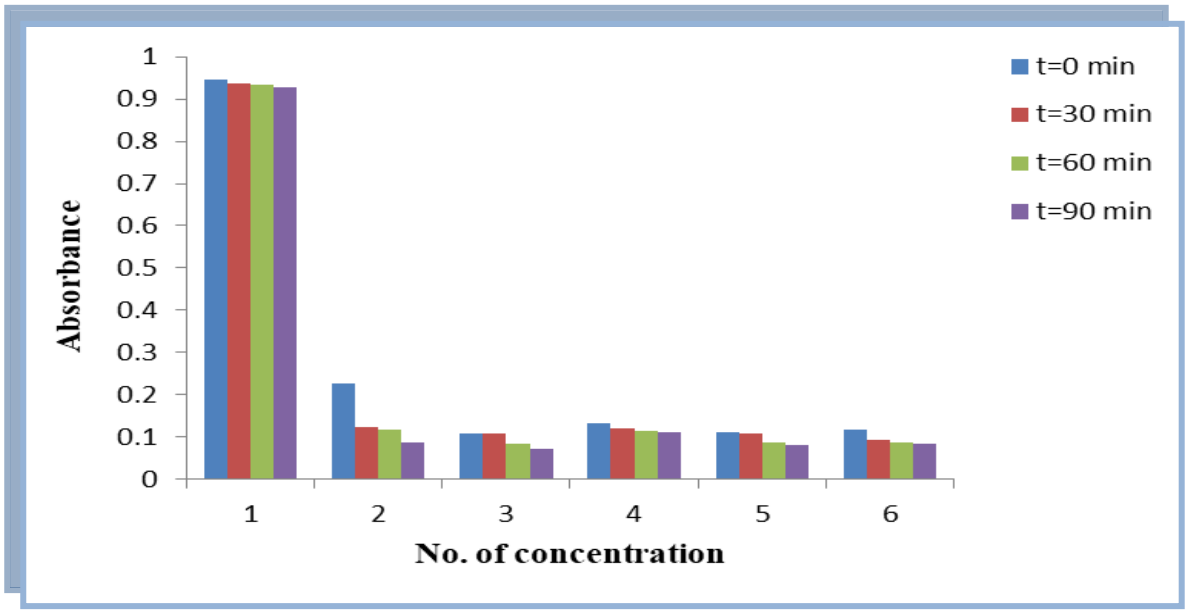

Figure (4. 71): Photodegradation performance for (PEO-CuO-In_2O_3) nanocomposites against MO dye with no. of concentration 1- MO dye 2-PEO 3- PEO-CuO 4- 1.8wt%In_2O_3 5- 3.6 wt%In_2O_3 6-5.4wt%In_2O_3

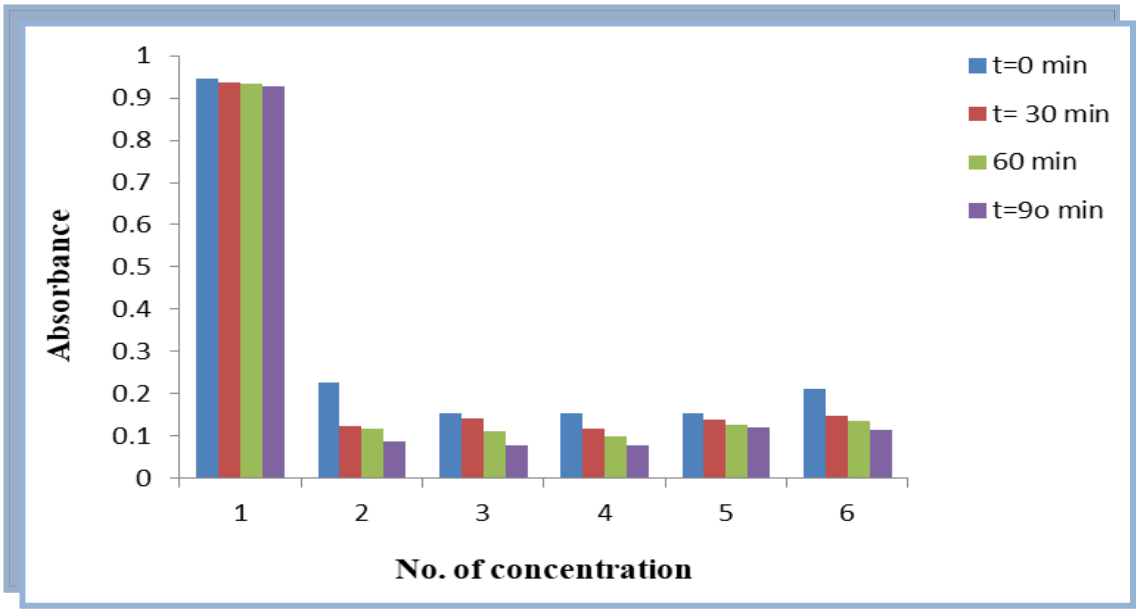

Figure (4. 72): Photodegradation performance for (PEO-NiO-In_2O_3) nanocomposites against MO dye with no. of concentration 1- MO dye 2-PEO 3- PEO-NiO 4- 1.8wt%In_2O_3 5- 3.6 wt%In_2O_3 6- 5.4wt%In_2O_3

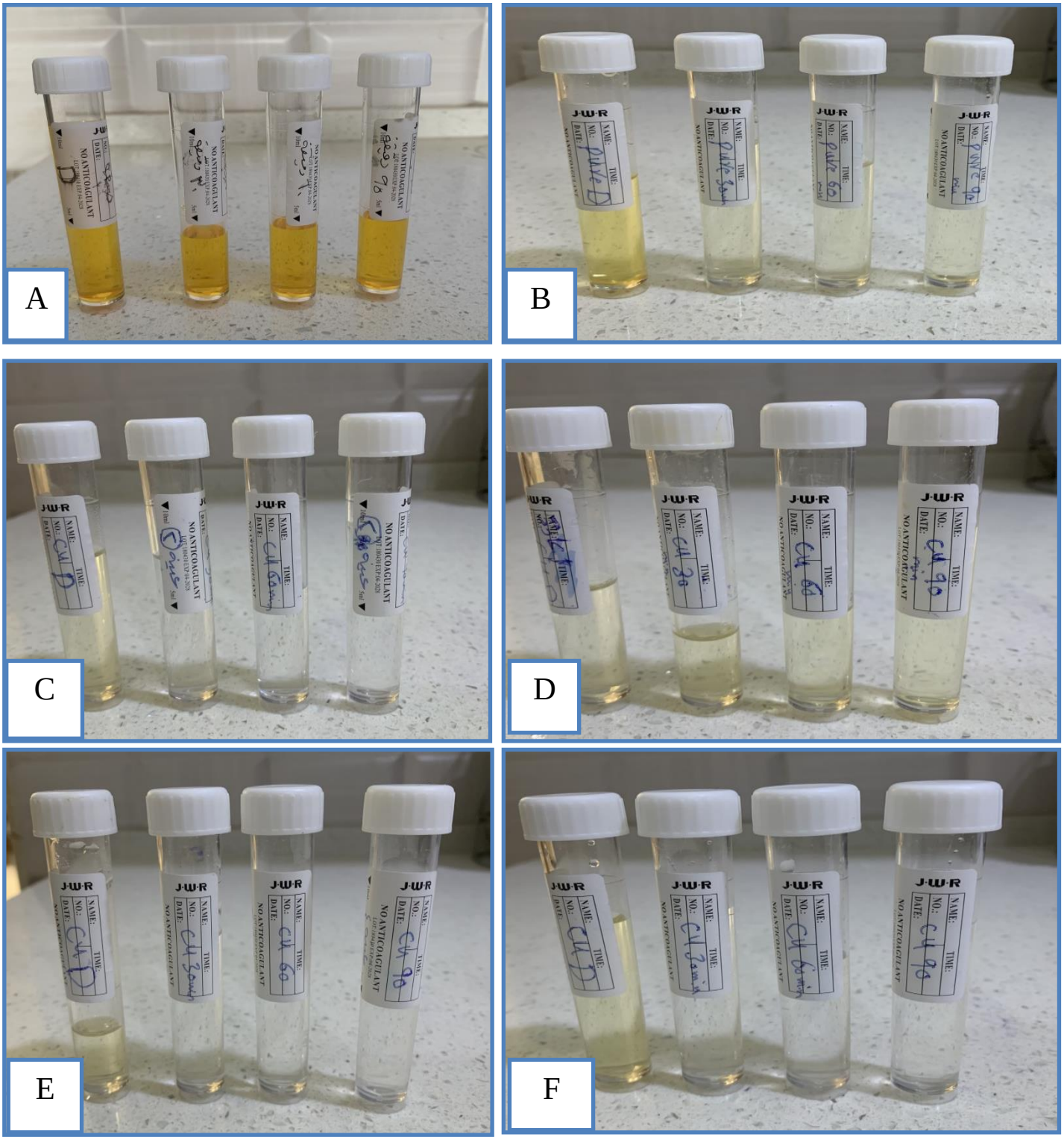

Figure(4.73):Image Photodegradation performance for sample:(A) for dye(MO) (B) for MO-PEO (C) for MO-PEO-CuO (D) for MO-1.8 wt.% In_2O_3 nanoparticles (E) for MO-3.6 wt.% In_2O_3 nanoparticles (F)for MO- 5.4 wt.% In_2O_3 nanoparticles.

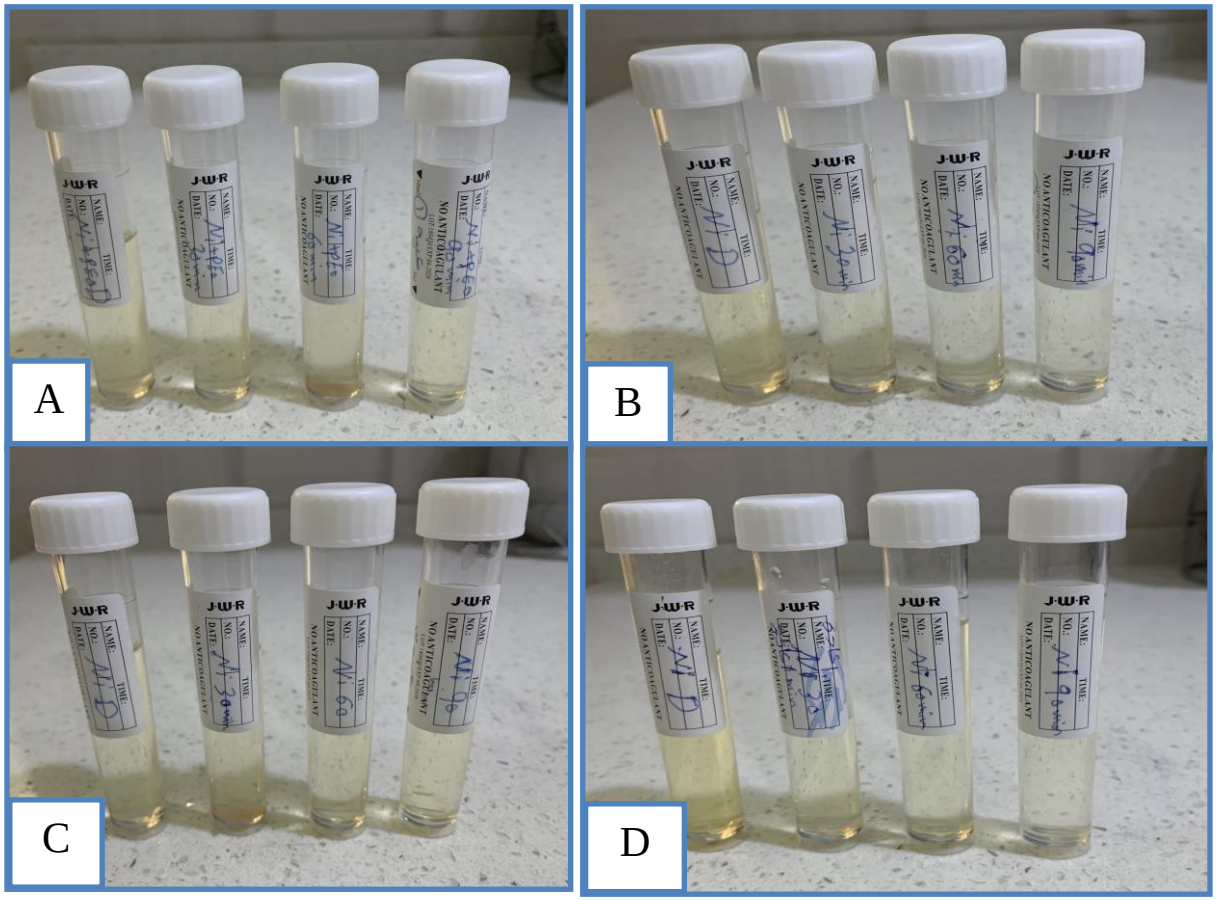

Figure (4.74):Image Photodegradation performance for sample: (A) for MO-PEO-NiO-(B) for MO-1.8 wt.% In_2O_3 nanoparticles (C) for MO-3.6 wt.% In_2O_3 nanoparticles(D) for MO-5.4 wt.% In_2O_3 nanoparticles.

4.6.2 Application of (PEO-CuO-In_2O_3) and (PEO-NiO-In_2O_3) nanocomposites for Antibacterial Activity

The antibacterial activity of the (PEO-CuO-In_2O_3) and (PEO-NiO-In_2O_3) nanocomposites samples tested against gram-negative (Salmonella) and gram-positive (Bacillus cereus) and the obtained data are presented in Figures (4.75-4.79). According to the statistics, the inhibition zone grows with the increasing of concentrations of (In_2O_3 NPS). Although some technologies, such as ionizing radiation, can make polymers antimicrobial, they can still be contaminated by microorganisms while in use. Melt mixing of polymers with

antibacterial chemicals is the best and easiest approach to create antibacterial polymers[131].

The presence of reactive oxygen species (ROS) formed with varying quantities of nanoparticles is the explanation for the bactericidal activity of the (PEO-CuO-In_2O_3) and (PEO-NiO-In_2O_3) nanocomposites[134]. The antibacterial activity of nanocomposites could be due to a chemical interaction between hydrogen peroxide and membrane proteins, or between the chemical generated in the presence of nanocomposites and the outer bilayer of bacteria. The hydrogen peroxide created destroys bacteria by entering their cell membrane. Once the hydrogen peroxide is created, the (PEO-CuO-In_2O_3) and (PEO-NiO-In_2O_3) nanocomposites continue to engage with dead bacteria, foiling future bacterial action and continuing to manufacture and release hydrogen peroxide into the medium[135].

Another mode of action is that the nanoparticles in nanocomposites have positive charges, while the bacteria have negative charges, resulting in an electromagnetic attraction between the nanoparticles and germs. The bacteria are oxidized and perish as soon as the attraction is made[136].

The main mechanism that caused the antibacterial activity of nanocomposites by the nanoparticles might be through oxidative stress caused by ROS. ROS includes radicals like super oxide radicals (O^{-2}), hydroxyl radicals (–OH) and hydrogen peroxide (H_2O_2); and singlet oxygen ($^1O_2$) could be the reason damaging the proteins and DNA in the bacteria. ROS could have been produced by the present the (PEO-CuO-In_2O_3) and (PEO-NiO-In_2O_3) nanocomposites leading to the inhibition of most pathogenic bacteria like Salmonella and Bacillus cereus[137,138].

The interaction of particles with the cell wall of bacteria decreases at low concentrations of nanoparticles, while the aggregation probability of particles increases at high concentrations of particles. As a result, the effective surface to volume ratio of particles increases, and the resulting interaction between

particles and the cell wall of bacteria decreases[139]. It is clearly evident from the result that the antibacterial activity of the samples was notably stronger against gram negative bacteria (Salmonella) than gram positive bacteria (Bacillus cereus) on nanoparticles. This is due to the gram positive bacteria possess a thick cell wall containing many layers of peptidoglycan. In contrast, gram negative bacteria have a relatively thin cell wall consisting of a few layers of peptidoglycan. Thus, a higher weight ratio of nanoparticles is required to kill (Bacillus cereus**)** compared (Salmonella**).** It can be concluded that the PEO-In_2O_3 nanocomposite blend that has been prepared is an effective agent against gram positive and gram negative bacteria (which is our case), taking into account that the In_2O_3 nanoparticles are uniformly dispersed in the (PEO) polymer. These results are in agreement with[140,141]. We note from the Table that the nanocomposite (PEO-NiO-In_2O_3) is more inhibiting for bacteria than the nanocomposite (PEO-CuO-In_2O_3), especially for bacteria of the type salmonella.

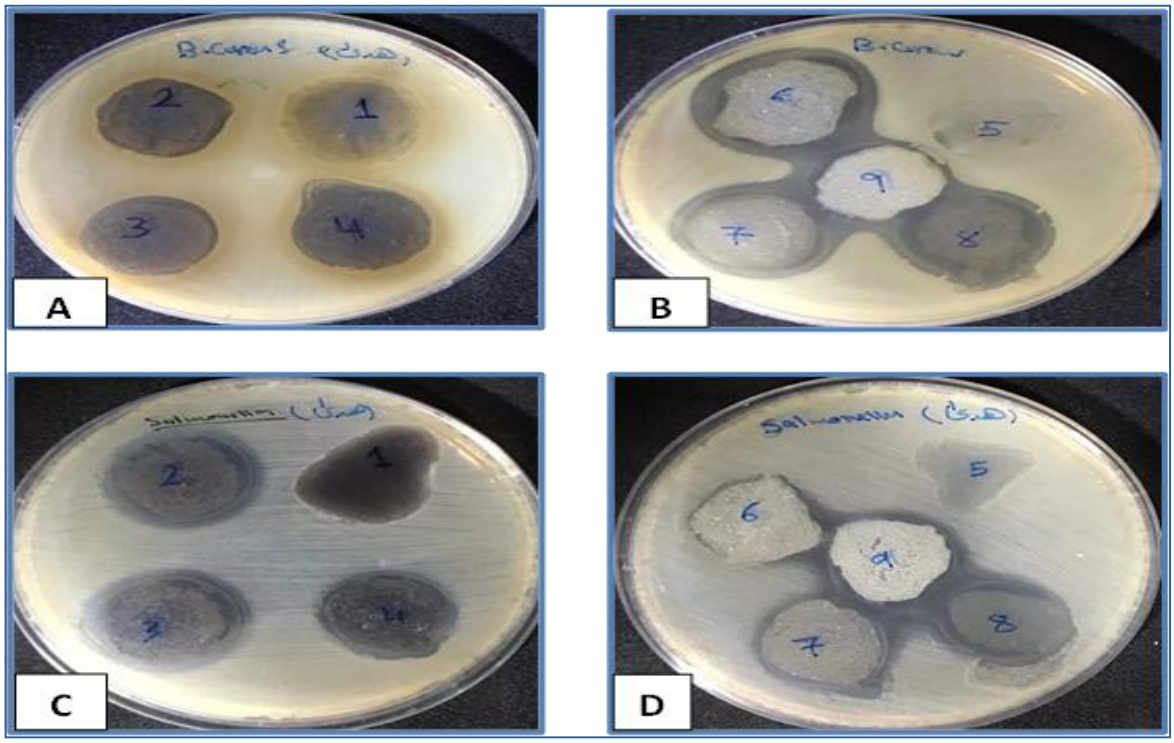

Figure (4.75):Image Antibacterial activity for (PEO-CuO-In_2O_3) and (PEO-NiO-In_2O_3) nanocomposite blend against (A) (B) (Bacillus cereus (C) (D)(Salmonella) Numbers (1-9) refers to (0,1.8,3.6,5.4) wt.% of In_2O_3 NPs.

Table (4.11): Antibacterial activity of (PEO-CuO-In_2O_3) and (PEO-NiO-In_2O_3) nanocomposite blend against pathogen.

Samples	Concentrations of In_2O_3 NPs wt.%	Bacillus cereus bacteria	Salmonella bacterial
(PEO)	0	0	0
(PEO-CuO) Nanocomposites	0	0	0
(PEO-CuO-In_2O_3) Nanocomposites	1.8	22	24
(PEO-Cu-In_2O_3) Nanocomposites	3.6	22	24
(PEO-Cu-In_2O_3) Nanocomposites	5.4	22	24
(PEO-NiO) Nanocomposites	0	23	23
(PEO-NiO-In_2O_3) Nanocomposites	1.8	23	25
(PEO-NiO-In_2O_3) Nanocomposites	3.6	25	25
(PEO-NiO-In_2O_3) Nanocomposites	5.4	26	27

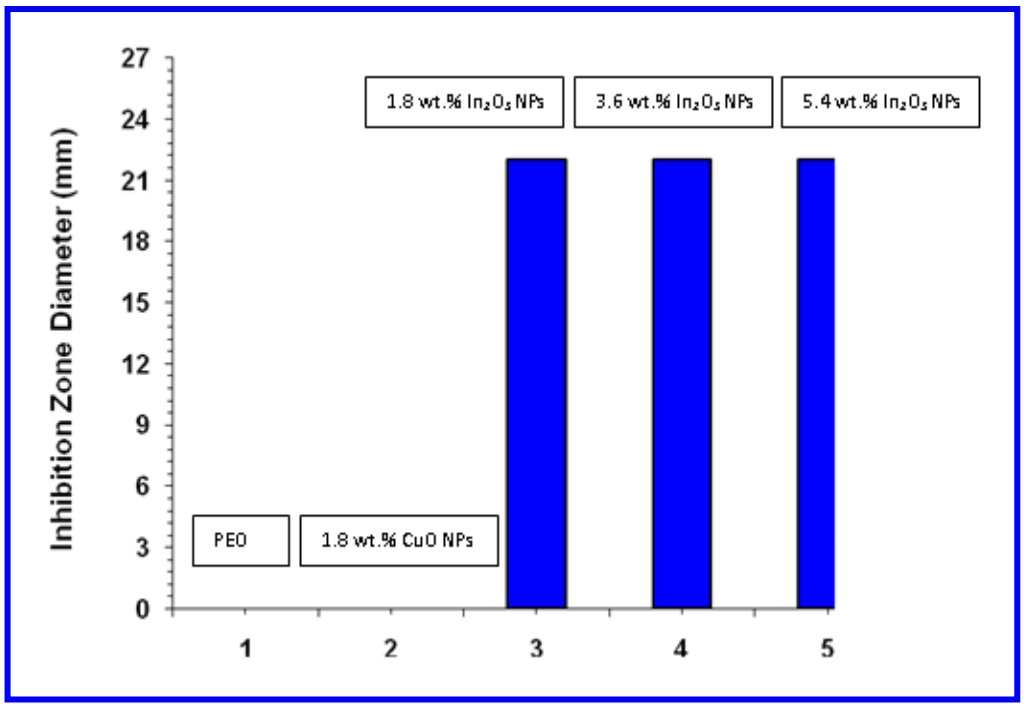

Figure (4. 76): Antibacterial activity of (PEO-/CuO-In_2O_3) nanocomposites against gram positive organisms (Bacillus cereus).

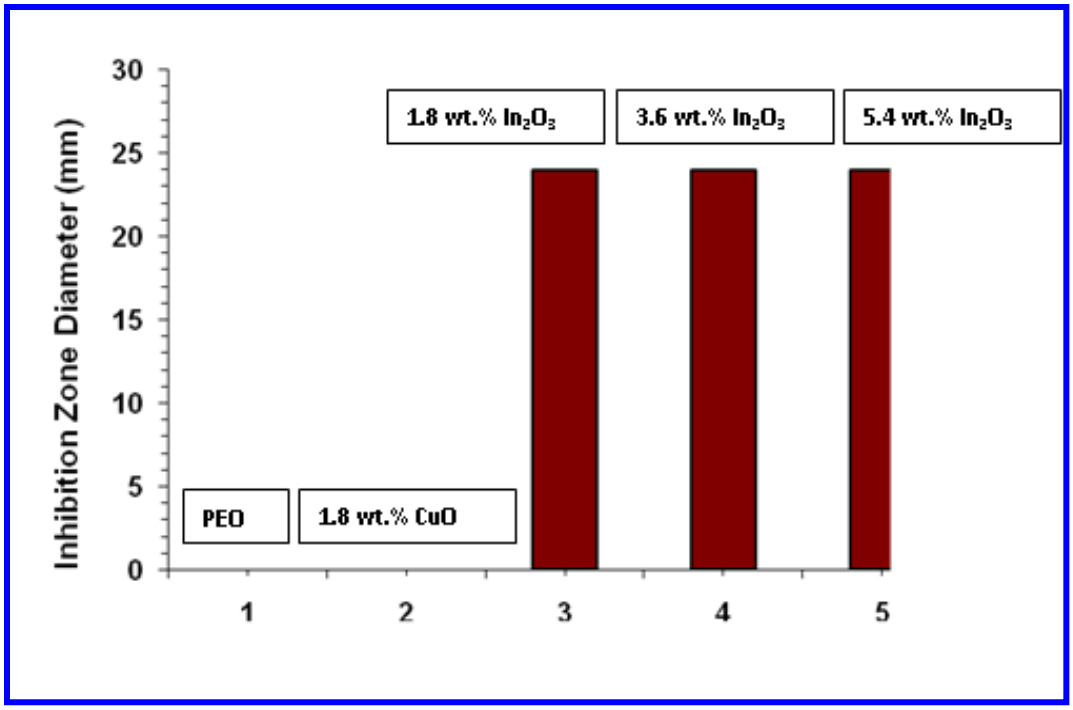

Figure (4.77): Antibacterial activity of (PEO-CuO-In_2O_3) nanocomposites against gram negative organisms (Salmonella).

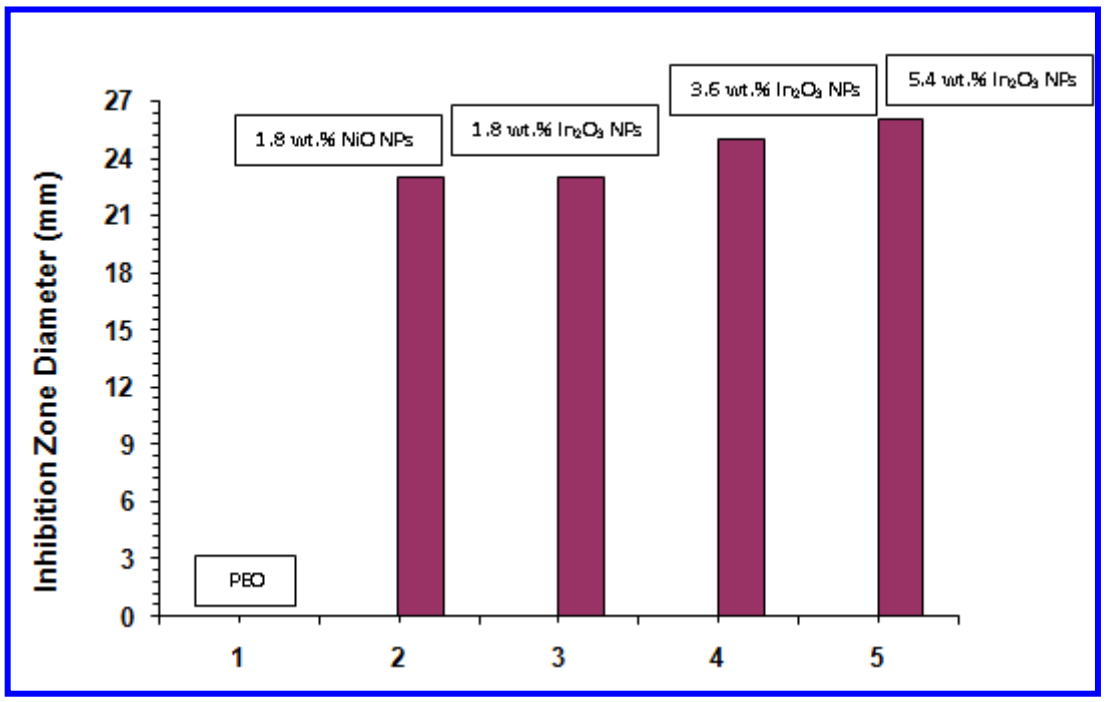

Figure (4.78): Antibacterial activity of (PEO-NiO-In_2O_3) nanocomposites against gram positive organisms (Bacillus cereus).

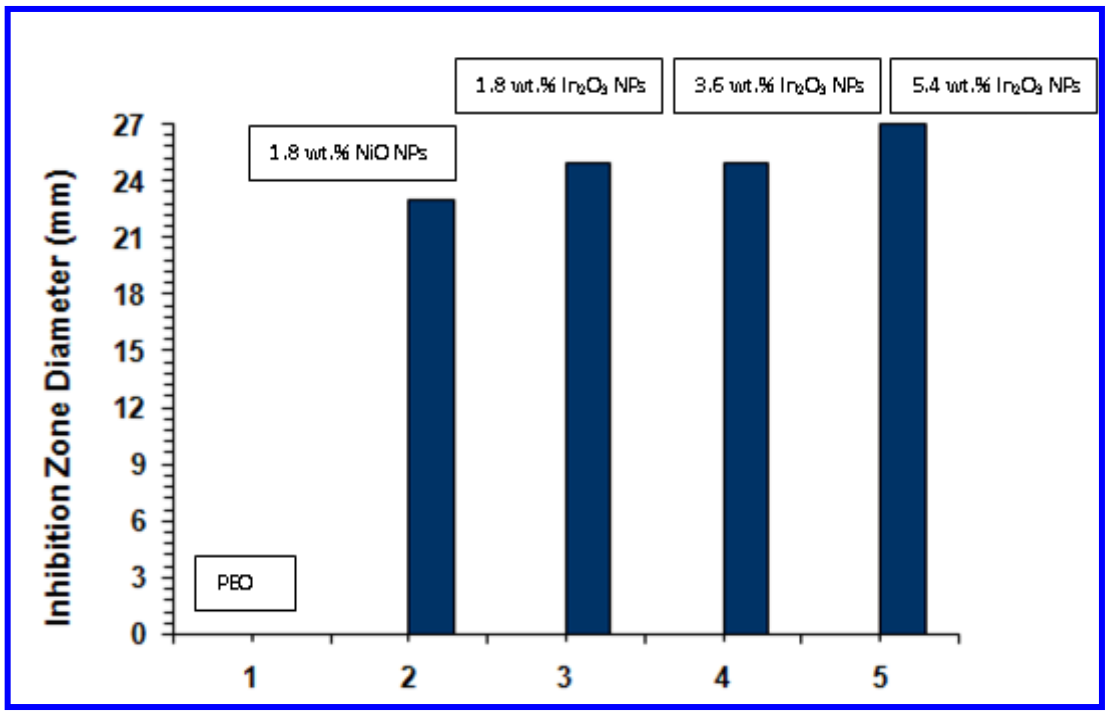

Figure (4.79): Antibacterial activity of (PEO-NiO-In_2O_3) nanocomposites against gram negative organisms (Salmonella).

5.1 Conclusions

In our study, the following Conclusions were obtained:

1. By using the B3LYP-DFT with a suitable SDD basis set, good relaxation was obtained for the investigated substances. Experimental and other theoretical research agree well with the predicted values of geometrical parameters of nanocomposites.
2. Total ground state energy of nanocomposites is lower than that for pure PEO so, the total energy of the produce nanocomposites was linearly decrease with increase of the number of atoms added.
3. All nanocomposites show LUMO destabilization and HOMO stabilization, and both changed significantly, suggesting that various structures play key roles in electrical characteristics.
4. One of the most significant outcomes of this research is the reduction in the energy gap in theoretical and experimental results. Because the HOMO and LUMO levels become more adjacent, this announces that these molecules are the closest to the semiconductor. These global outcomes resulted in significant electronic applications.
5. All of the nanocomposites analyzed require very little energy to become cations since the ionization potential decreases as the number of atoms increases, but the electronic affinity increases.
6. High occupation molecular orbitals have a higher density of states than lower unoccupied molecular orbitals. When these nanocomposites interact with other molecules or species, this characteristic allows them to behave as appropriate electronic applications.
7. The absorbance, absorption coefficient, extinction coefficient, refractive index, real and imaginary dielectric constants and optical conductivity of

(PEO-CuO-In_2O_3) and (PEO-NiO-In_2O_3) nanocomposites increase with an increase in In_2O_3 NPS concentrations. The transmittance decrease with increase of the In_2O_3NPS concentrations. The (PEO-CuO-In_2O_3) and (PEO-NiO-In_2O_3) nanocomposites experimental have high absorbance in the UV-region and extends towards the visible area theoretical. From the results of optical properties showed that the (PEO-CuO-In_2O_3) and (PEO-NiO-In_2O_3) nanocomposites can be used photocatalytic and an antibacterial applications.

8. The absorbance of methylene orange dye solution for (PEO-CuO-In_2O_3) and (PEO-NiO-In_2O_3) nanocomposites decreases with increasing the concentrations of In_2O_3 nanoparticles. The absorbance of methylene orange dye solution for (PEO-CuO-In_2O_3) and (PEO-NiO-In_2O_3) nanocomposites decreases with increasing the time of the irradiation. The photodegradation percentage of MO dye increases with increasing the time of the irradiation which leads to increase in the photocatalytic reaction and reduced electron/hole recombination. The best photocatalytic activity for (PEO-CuO-In_2O_3) nanocomposite was 27% at concentration 5.4%wt of In_2O_3 nanoparticles.
9. The results of antibacterial application for (PEO-CuO-In_2O_3) and (PEO-NiO-In_2O_3) nanocomposites showed that the inhibition zone for Bacillus cereus and Salmonella increases with an increase concentrations of In_2O_3 nanoparticles which may be used it for antibacterial with high activity.

5.2 Future Work

The suggestion work for future work can be summarize in the following:

1- Study of the effect of In_2O_3 nanoparticles on the electrical and thermal properties of (PEO-CuO) and (PEO-NiO) nanocomposites.

2- Study of the mechanical properties of (PEO-CuO-In_2O_3) and (PEO-NiO- In_2O_3) nanocomposites.

3- Study the electronic and optical properties of PEO with other metal oxides such as Fe_2O_3.

4- Study of the D.C electrical conductivity at different temperatures of (PEO-CuO-In_2O_3) and (PEO-NiO- In_2O_3) nanocomposites.

5- Study of the humidity sensors application of (PEO-CuO-In_2O_3) and (PEO-NiO- In_2O_3) nanocomposites.

1) Madkour, Loutfy H. "Introduction to nanotechnology (NT) and nanomaterials (NMs)." *Nanoelectronic Materials. Springer, Cham*, 1-47,(2019).
2) Paul, Donald R., and Lioyd M. Robeson. "Polymer nanotechnology: nanocomposites." Polymer 49.15, 3187-3204 (2008).
3) Muthuraj, Rajendran, Manjusri Misra, and Amar Kumar Mohanty. "Biodegradable compatibilized polymer blends for packaging applications: A literature review." *Journal of Applied Polymer Science* 135.24, 45726 (2018).
4) Alkhayatt, Adel H. Omran, Ali H. Al-Azzawi, and Zahraa Alakayashi. "Rheological and optical characterization of Polyvinylpyrrolidone (PVP)-Polyethylene glycol (PEG) polymer blends." *Journal of Kufa-Physics* 11.02, (2019).
5) Hajar, MD Siti, A. G. Supri, and A. J. Jalilah. "Effect of Poly (Ethylene Glycol) Diglycidyl Ether as Surface Modifier on Conductivity and Morphology of Carbon Black Filled Poly (Vinyl Chloride)/Poly (Ethylene Oxide) Conductive." *Journal of Advanced Research in Materials Science*, ISSN 2289-7992, (2015).
6) Abdelghany, A. M., Abdelrazek, E. M., Badr, S. I., and Morsi, M. A. "Effect of gamma-irradiation on (PEO/PVP)/Au nanocomposite: materials for electrochemical and optical applications." *Materials and Design* 97 532-543(2016).
7) Robeson, Lloyd. "Historical perspective of advances in the science and technology of polymer blends." Polymers 6.5 ,1251-1265, (2014).
8) Tyagi, Monika, and Dhruv Tyagi. "Polymer nanocomposites and their applications in electronics industry." *Int J Electron Electr Eng* 7.6,603-608,(2014).

9) Rahman, M. T., Hoque, M. A., Rahman, G. T., Gafur, M. A., Khan, R. A., and Hossain, M. K. "Study on the mechanical, electrical and optical properties of metal-oxide nanoparticles dispersed unsaturated polyester resin nanocomposites." Results in Physics 13,102264, (2019).

10) R. Divya, M. Meena, C. Mahadevan and C. Padma, "Investigation on CuO dispersed PVA polymer films", *J Eng Res Appl*, 4(5),1-7, (2014).

11) V. Sangawar, M. Golchha, "Evolution of the optical properties of Polystyrene thin films filled with Zinc Oxide nanoparticles", *Int J Sci Eng Res*, 4(6), 2700-2705, (2013).

12) Z. Ali, M. Helal, H. Saleh, A. Zikry and Y. Darwish, "Silverpolymer blend nanocomposite", N Y Sci J 7, 84-94, (2014).

13) M. Biercuk, M. Llaguno, H. Radosvljevicm, "Carbon nanotube composites for thermal management", *Applied Physics Letters*, 80(15), 2767-2769, (2002).

14) Sundaramahalingam, K., Vanitha, D., Nallamuthu, N., Manikandan, A., and Muthuvinayagam, M. "Electrical properties of lithium bromide poly ethylene oxide/poly vinyl pyrrolidone polymer blend elctrolyte." Physica B: Condensed Matter 553, 120-126, (2019).

15) Kashmola, Talib Omer, and Estabraq Saad Kamil. "Structure rheology of polyethylene oxide solution." *Iraqi Journal of Chemical and Petroleum engineering* 15.1, 23-32, (2014).

16) Morsi, M. A., and A. M. Abdelghany. "UV-irradiation assisted control of the structural, optical and thermal properties of PEO/PVP blended gold nanoparticles." *Materials Chemistry and Physics* 201, 100-112 (2017).

17) Wang, S. B., Hsiao, C. H., Chang, S. J., Lam, K. T., Wen, K. H., Young, S. J., ... and Huang, B. R. "CuO nanowire-based humidity sensor." *IEEE Sensors Journal* 12.6, 1884-1888, (2011).

18) Verma, Monu, Vinod Kumar, and Akash Katoch. "Sputtering based synthesis of CuO nanoparticles and their structural, thermal and optical studies." *Materials Science in Semiconductor Processing* 76, 55-60 ,(2018).

19) Nesa, Meherun, et al. "Structural, optical and electronic properties of CuO and Zn doped CuO: DFT based First-principles calculations." *Chemical Physics* 528, 110536 ,(2020).

20) Menazea, A. A. "One-Pot Pulsed Laser Ablation route assisted copper oxide nanoparticles doped in PEO/PVP blend for the electrical conductivity enhancement." *Journal of Materials Research and Technology* 9.2, 2412-2422 (2020).

21) Shankar, Prabakaran, and John Bosco Balaguru Rayappan. "Gas sensing mechanism of metal oxides: The role of ambient atmosphere, type of semiconductor and gases-A review." Sci. Lett. J 4.4, 126 ,(2015).

22) Özerli, Halil, et al. "Electrical and photovoltaic properties of Ag/p-Si structure with GO doped NiO interlayer in dark and under light illumination." *Journal of Alloys and Compounds* 718, 75-84, (2017).

23) Sk, M. M., Yue, C. Y., Ghosh, K., and Jena, R. K.. "Review on advances in porous nanostructured nickel oxides and their composite electrodes for high-performance supercapacitors." *Journal of Power Sources* 308 (2016): 121-140.

24) Al Boukhari, Jamalat Hisham. "Effect of Rare Earth Elements on NiO Nanoparticles Behavior." (2020).

25) Junejo, A. R., S. Memon, and S. Pathan. "A Novel Precursor in Preparation and Characturization of Nickel Oxide (NIO) and Cobalt Oxide (CO3O4) Nanoparticals (NPS) Via Aqueous Chemical Growth (ACG) Techniques." Advanced Nanoscience and Technology: *An Internation al Journal* (ANTJ) 2.1,1-7 (2016).

26) Rasheed, R. T. , Theoretical Structures Study of Indium Oxide (In2O3) Cluster Using DFT Calculations. *Asian Journal of Materials Chemistry*, 2(1), 26-29 (2017).

27) Yang, Hongxiao, Shuping Wang, and Yanzhao Yang. "Zn-doped In_2O_3 nanostructures: preparation, structure and gas-sensing properties." CrystEngComm 14.3, 1135-1142 (2012).

28) Zhanpeisov, Nurbosyn U., Hiroaki Nakatani, and Hiroshi Fukumura. "Theoretical DFT study of the structure and chemical activity of small indium (III) oxide clusters." *Research on Chemical Intermediates* 37.6,647-658. (2011).

29) Zhang, Y., Li, Q., Tian, Z., Hu, P., Qin, X., and Yun, F. "Gas-sensing properties of ITO materials with different morphologies prepared by sputtering." *SN Applied Sciences* 2.2, 1-11, (2020).

30) Mohan, V. M., Bhargav, P. B., Raja, V., Sharma, A. K., and Narasimha Rao, V. V. R. "Optical and electrical properties of pure and doped PEO polymer electrolyte films." Soft Materials 5.1, 33-46 (2007).

31) Kumar, K. K., Pavani, Y., Ravi, M., Bhavani, S., Sharma, A. K., and Rao, V. N. "Effect of complexation of NaCl salt with polymer blend (PEO/PVP) electrolytes on ionic conductivity and optical energy band gaps." AIP Conference Proceedings. Vol. 1391. No. 1. *American Institute of Physics*, (2011).

32) Kesavan, K., S. Rajendran, and Chithra M. Mathew. "Studies on poly (vinyl pyrrolidone) based solid polymer blend electrolytes complexed with various lithium salts." *Polymer Science Series* B 56.4, 520-529 (2014).

33) Abdullah, Omed Gh, Dlear R. Saber, and Luqman O. Hamasalih. "Complexion formation in PVA/PEO/CuCl2 solid polymer electrolyte." *Universal Journal of Materials Science* 3.1, 1-5 (2015).

34) Hashim, Ahmed, Majeed Ali Habeeb, and Aseel Hadi. "Synthesis of novel polyvinyl alcohol–starch-copper oxide nanocomposites for humidity sensors applications with different temperatures." Sensor Letters 15.9, 758-761 (2017).

35) Choudhary, Shobhna, and R. J. Sengwa. "Morphological, structural, dielectric and electrical properties of PEO–ZnO nanodielectric films." *Journal of Polymer Research* 24.3, 1-12 (2017).

36) E. M. Abdelrazek, A.M. Abdelghany, S. I. Badr and M. A. Morsi,"Structural, optical, morphological and thermal properties of PEO/PVP blend containing different concentrations of biosynthesized Au nanoparticles." *Journal of materials research and technology* 7.4, 419-431 (2018).

37) Ramesan, M. T., Nushhat, K., Parvathi, K., and Anilkumar, T. "Nickel oxide and polyindole/phenothiazine blend nanocomposites: preparation, characterization, thermal, electrical properties and gas sensing applications." *Journal of Materials Science: Materials in Electronics* 30.14, 13719-13728, (2019).

38) Abutalib, M. M., and A. Rajeh. "Influence of ZnO/Ag nanoparticles doping on the structural, thermal, optical and electrical properties of PAM/PEO composite." Physica B: Condensed Matter 578, 411796 ,(2020).

39) Farea, M. O., A. M. Abdelghany, and A. H. Oraby. "Optical and dielectric characteristics of polyethylene oxide/sodium alginate-modified gold nanocomposites." RSC Advances 10.62, 37621-37630 (2020).

40) Hazim, Angham, Hayder M. Abduljalil, and Ahmed Hashim. "Structural, spectroscopic, electronic and optical properties of novel platinum doped (PMMA/ZrO2) and (PMMA/Al2O3) nanocomposites for electronics

devices." *Transactions on Electrical and Electronic Materials* 21.6, 550-563 (2020).

41) Hadi, Aseel, Ahmed Hashim, and Yahya Al-Khafaji. "Structural, optical and electrical properties of PVA/PEO/SnO2 new nanocomposites for flexible devices." *Transactions on Electrical and Electronic Materials* 21.3, 283-292, (2020).

42) Mansor, Eman S., Heba Ali, and Ahmed Abdel-Karim. "Efficient and reusable polyethylene oxide/polyaniline composite membrane for dye adsorption and filtration." Colloid and Interface Science Communications 39, 100314 ,(2020).

43) Muhammed, D. S., Brza, M. A., M Nofal, M., B Aziz, S., A Hussen, S., and Abdulwahid, R. T. "Optical dielectric loss as a novel approach to specify the types of electron transition: XRD and UV-vis as a non-destructive techniques for structural and optical characterization of PEO based nanocomposites." Materials 13.13, 2979 (2020).

44) Ahmed, Hind, and Ahmed Hashim. "Geometry optimization, optical and electronic characteristics of novel PVA/PEO/SiC structure for electronics applications." Silicon 13.8, 2639-2644 (2021).

45) Abutalib, M. M., and A. Rajeh. "Enhanced structural, electrical, mechanical properties and antibacterial activity of Cs/PEO doped mixed nanoparticles (Ag/TiO_2) for food packaging applications." Polymer Testing 93,107013, (2021).

46) Al-Muntaser, A. A., Pashameah, R. A., Sharma, K., Alzahrani, E., Farea, M. O., and Morsi, M. A"α-MoO_3 nanobelts/CMC-PVA nanocomposites: hybrid materials for optoelectronic and dielectric applications." *Journal of Polymer Research* 29.7, 1-11 (2022).

47) M. Utkarsh , K. Ji-Yeong , S. Ji-Young , K. Jae-Sung , and C. SungHwan, " Novel Poly(Methyl Methacrylate) Containing Nanodiamond to Improve the Mechanical Properties and Fungal Resistance", Materials (Basel), 12(20), 3438, (2019).

48) M. G. Mohammed, M. A. Ahmad, R. Ahmed, A. Reem, A. A. Fahad, and A. Sultan, "Reinforcement of PMMA Denture Base Material with a Mixture of ZrO2 Nanoparticles and Glass Fibers", Int J Dent, 2019, 2489393, (2019).

49) S. Ahmed, M. Hussein, S. Hadi and S. A. Mohammed, "Study the Effect of Thickness on Optical Properties of Polymer PMMA Thin Films Preparated by Spin Coating Method", *Journal of University of Babylon*, 27, 4, (2019).

50) Kaupp, Martin. "Buchbesprechung: A Chemist's Guide to Density Functional Theory. Von Wolfram Koch und Max C. Holthausen." 989-990 (2001).

51) Rogers, Donald W. Computational Chemistry using the PC. John Wiley and Sons, (2003).

52) Pham, N. K., Vu, N. H., Van Pham, V., Ta, H. K. T., Cao, T. M., Thoai, N., and Tran, V. C. "Comprehensive resistive switching behavior of hybrid polyvinyl alcohol and TiO_2 nanotube nanocomposites identified by combining experimental and density functional theory studies." *Journal of Materials Chemistry* C 6.8, 1971-1979 (2018).

53) Leach, Andrew R., and Andrew R. Leach. Molecular modelling: principles and applications. Pearson education, (2001).

54) Sholl, David S., and Janice A. Steckel. Density functional theory: a practical introduction. John Wiley and Sons, (2011).

55) Young, D. C. A Practical Guide for Applying Techniques to Real-World Problems, ISBN 0-471-33368-9, 434 page,(2001).

56) Marenich, A. V., Ho, J., Coote, M. L., Cramer, C. J., & Truhlar, D.G. "Computational electrochemistry: prediction of liquid-phase reduction potentials." *Physical Chemistry Chemical Physics* 16.29, 15068-15106 (2014).

57) Valone, Steven M. "Quantal Density Functional Theory II. Approximation Methods and Applications." 11387-11388, (2010).

58) Fitts, Donald D. Principles of quantum mechanics: as applied to chemistry and chemical physics. Cambridge University Press, (1999).

59) Clementi, E., André, J. M., and McCammon, J. A. (Eds.). Theory and Applications in Computational Chemistry: The First Decade of the Second Millennium. American Institute of Physics, ISBN 978-0-7354-1057-2, 275 page (2012).

60) Frisch, M. J., et al. "KN Kudin, JC Burant, JM Millam, SS Iyengar, J." (2003).

61) Mueller, M. P. Fundamentals of quantum chemistry: molecular spectroscopy and modern electronic structure computations. Springer Science and Business Media, ISBN-0- 306-47566-9, 262 page, (2007).

62) Gotwals Jr, Robert R. "Integrating Computational Chemistry (Molecular Modeling) into the General Chemistry Curriculum." North Carolina School of Science and Mathematics, 1-11 (2008).

63) Gauld, James W. "Reviews in Computational Chemistry, Volume 20 Edited by Kenny B. Lipkowitz (North Dakota State University), Raima Larter (Indiana University-Purdue University), Thomas R. Cundari (University of North Texas), and Donald B. Boyd, Editor Emeritus (Indiana University− Purdue University). John Wiley and Sons, Inc.: Hoboken, NJ. 2004. xxvi+ 458 pp. $150.00. ISBN 0-471-44525-8." 3233-3233 (2005).

64) Gaussian09, Revision A. "1, mj frisch, gw trucks, hb schlegel, ge scuseria, ma robb, jr cheeseman, g. Scalmani, v. Barone, b. Mennucci, ga petersson et al., gaussian." Inc., Wallingford CT 121, 150-166 (2009).

65) Peverati, Roberto, and Donald G. Truhlar. "M11-L: A local density functional that provides improved accuracy for electronic structure calculations in chemistry and physics." *The Journal of Physical Chemistry Letters* 3.1, 117-124 (2012).

66) Hinchliffe, Alan. Molecular modelling for beginners. John Wiley and Sons, (2003).

67) Zhao, Yan, and Donald G. Truhlar. "Design of density functionals that are broadly accurate for thermochemistry, thermochemical kinetics, and nonbonded interactions." *The Journal of Physical Chemistry* A 109.25, 5656-5667, (2005).

68) Wodrich, Matthew D., Clémence Corminboeuf, and Paul von Ragué Schleyer. "Systematic errors in computed alkane energies using B3LYP and other popular DFT functionals." Organic letters 8.17, 3631-3634 (2006).

69) Abdulsattar, Mudar A. "Size effects of semiempirical large unit cell method in comparison with nanoclusters properties of diamond-structured covalent semiconductors." Physica E: Low-dimensional Systems and Nanostructures 41.9, 1679-1688, (2009).

70) Judson, R. S., Jaeger, E. P., Treasurywala, A. M., and Peterson, M.L."Conformational searching methods for small molecules. II. Genetic algorithm approach." *Journal of Computational Chemistry* 14.11, 1407-1414, (1993).

71) Sabin, J. R., Trickey, S. B., Apell, S. P., and Oddershede, J."Molecular shape, capacitance, and chemical hardness." *International Journal of Quantum Chemistry* 77.1, 358-366, (2000).

72) Camargo, A. J., Honório, K. M., Mercadante, R., Molfetta, F. A., Alves, C. N., and da Silva, A. B."A study of neolignan compounds with biological activity against Paracoccidioides brasiliensis by using quantum chemical and chemometric methods." *Journal of the Brazilian Chemical Society* 14, 809-814, (2003).

73) Shenghua, Li, Yang He, and Jin Yuansheng. "Lubrication chemistry viewed from DFT-based concepts and electronic structural principles." *International Journal of Molecular Sciences* 5.1, 13-34,(2003).

74) Barnes, Craig E. "Inorganic Chemistry (Catherine E. Housecroft and Alan G. Sharpe)." *Journal of Chemical Education* 80.7, 747, (2003).

75) Oftadeh, M., S. Naseh, and M. Hamadanian. "Electronic properties and dipole polarizability of thiophene and thiophenol derivatives via density functional theory." *Computational and Theoretical Chemistry* 966,1-3, 20-25 (2011).

76) Sadasivam, K., and R. Kumaresan. "Theoretical investigation on the antioxidant behavior of chrysoeriol and hispidulin flavonoid compounds–A DFT study." *Computational and Theoretical Chemistry* 963.1, 227-235, (2011).

77) Al-Mudhaffer, Mohammed F., Maged A. Nattiq, and Mohammed Ali Jaber. "Linear optical properties and energy loss function of Novolac: epoxy blend film." Archives of Applied Science Research 4.4, (2012) 1731-7140.

78) Ilıcan, Saliha, Müjdat Çağlar, and Yasemin Çağlar. "The effect of deposition parameters on the physical properties of Cd xZn1-xS films deposited by spray pyrolysis method." (2007).

79) Hamad, T. K., Yusop, R. M., Abdullah, B., and Yousif, E. "Laser induced modification of the optical properties of nano-ZnO doped PVC films." *International Journal of Polymer Science* 2014 (2014).

80) Abdullah, Omed Gh, and S. R. Saeed. "Effect of NaI doping on same physical characteristic of (PVA) 0.9-(KHSO4) 0.1 composite films." *Chemistry and Materials Research* 3.11, 19-24 (2013).

81) Sangawar, V., and M. Golchha. "Evolution of the optical properties of polystyrene thin films filled with zinc oxide nanoparticles." International *Journal of Scientific and Engineering Research* 4.6, 2700-2705 (2013).

82) Nathan, Abutu A., A. Onoja, and A. Amah. "Influence of PVA, PVP on crystal and optical properties of europium doped strontium aluminate nanoparticles." Amer. J. Eng. Res 4.4 (2015).

83) Begum, Anayara, Amir Hussain, and Atowar Rahman. "Optical and electrical properties of doped and undoped Bi2S3–PVA films prepared by chemical drop method." Mater. Sci. Appl. 2, 163-168, (2011).

84) S.WeiFu. Research on the characterization of hydrogenated silicon thin film using constant photocurrent method. Thesis M.Sc, Department of Optics and Photonics, National Central University, China (2009) .

85) Lalithambika, K. C., K. Shanthakumari, and Sriram Sriram. "Optical properties of CdO thin films deposited by chemical bath method." *International Journal of ChemTech Research* 6.5 ,3071-3077, (2014).

86) Abdullah, Omed Gh, Bakhtyar K. Aziz, and Sarkawt A. Hussen. "Optical characterization of polyvinyl alcohol-ammonium Nitrate polymer electrolytes films." *Chemistry and Materials Research* 3.9, 84-90,(2013).

87) Andriesh, A. M., M. S. Iovu, and S. D. Shutov. "Chalcogenide non-crystalline semiconductors in optoelectronics." *Journal of Optoelectronics and Advanced Materials* 4.3 ,631-647, (2002).

88) Nahida, J. H. "Spectrophotometric analysis for the UV-irradiated (PMMA)." *International Journal of Basic and Applied Sciences* 12.2 (2012): 58-67.

89) Abdullah, O. G., Tahir, D. A., Ahmad, S. S., and Ahmad, H. T."Optical properties of PVA: CdCl2. H2O polymer electrolytes." *IOSR J. Appl. Phys* 4.3 ,52-57, (2013).

90) Tintu, R., Saurav, K., Sulakshna, K., Nampoori, V. P. N., Radhakrishnan, P. and Thomas, S. "Ge28Se60Sb12/PVA composite films for photonic applications." *Journal of Non-Oxide Glasses* 2.4 ,167-174, (2010).

91) Hassouni, M. H., Mishjil, K. A., Chiad, S. S. and Habubi, N. F."Effect of gamma irradiation on the optical properties of Mg doped CdO Thin films deposited by Spray Pyrolysis." *International Letters of Chemistry, Physics and Astronomy* 11, 26-37, (2013).

92) Ezema, F. I. "Growth and Optical Properties of Ag." Journal of the University of Chemical Technology and Metallurgy 42.2 (2007): 217-222.Ag." *Journal of the University of Chemical Technology and Metallurgy* 42.2, 217-222 ,(2007).

93) Ahmadi, F., Rahimi-Nasrabadi, M., Fosooni, A., and Daneshmand, M. "Synthesis and application of CoWO4 nanoparticles for degradation of methyl orange." *Journal of Materials Science: Materials in Electronics* 27.9, 9514-9519,(2016).

94) Tuğrul, A. B., Altinsoy, N., Demir, E., Erentürk, S. A., Karatepe,"Evaluation for elimination of methylene-orange from aqueous media by using N., Haciyakupoğlu, S., and Baytaş, A. F.membrane." *AIP Conference Proceedings*. Vol. 1809. No. 1. AIP Publishing LLC, (2017).

95) Zheng, Yun, Pan Zhiming, and Wang Xinchen. "Advances in photocatalysis in China." *Chinese Journal of Catalysis* 34.3, 524-535, (2013).

96) Lazar, Manoj A., Shaji Varghese, and Santhosh S. Nair. "Photocatalytic water treatment by titanium dioxide: recent updates." Catalysts 2.4, 572-601 (2012).

97) Hernández-Ramírez, Aracely, and Iliana Medina-Ramírez. Photocatalytic semiconductors. Springer International Pu, (2016).

98) Shieh, K. J., Li, M., Lee, Y. H., Sheu, S. D., Liu, Y. T., and Wang, Y. C. "Antibacterial performance of photocatalyst thin film fabricated by defection effect in visible light." Nanomedicine: Nanotechnology, Biology and Medicine 2.2, 121-126, (2006).

99) K. Michałów, "Flame spray synthesis and characterization of doped TiO2 nanoparticles for photoelectric and photocatalytic applications", Ph.D. thesis, AGH University of Science and Technology, Krakow, Poland (2009).

100) J. Yu, L. Zhang and W. Ho, "Enhancing effects of water content and ultrasonic irradiation on the photocatalytic activity of nano-sized TiO2 powders", *Journal of Photochemistry and Photobiology A: Chemistry*, Vol. 148, 263–271, (2002).

101) J. Tauc, A. Menth and D. Wood, “Optical and magnetic investigations of the localized states in semiconducting glasses”, Phys,Rev.Lett, 25, 749-752, (1970).

102) L. F. Espinosa-Cristóbal, G. A. Martínez-Castañón, J. P. LoyolaRodríguez et, N. Niño-Martínez, F. Ruiz, N. V. Zavala-Alonso, R. H. Lara, and S. Y. Reyes-López, "Bovine serum albumin and chitosan coated

silver nanoparticles and its antimicrobial activity against oral and nonoral bacteria", *Journal of Nanomaterials*, 2015, 9, (2015).

103) Y. Z. Xiu , J. Z. Xin, L. Zhuo, S. Z. Bang and R. C. Rong, "Hybrid effects of zirconia nanoparticles with aluminum borate whiskers on mechanical properties of denture base resin PMMA", *Dental Materials Journal*, 33(1), 141-146, (2014).

104) Abdullah, Omed Gh. "Influence of barium salt on optical behavior of PVA based solid polymer electrolytes." *European Scientific Journal* 10.33 (2014).

105) Y.T. Prabhu, K. V. Rao, B. S. Kumari, V.S.S. Kumar, T. Pavani, Synthesis of Fe3O4 nanoparticles and its antibacterial application. Int. Nano. Lett. (2015).

106) Al-Shamari, A. A., Abdelghany, A. M., Alnattar, H., and Oraby, A. H.. "Structural and optical properties of PEO/CMC polymer blend modified with gold nanoparticles synthesized by laser ablation in water." *Journal of Materials Research and Technology* 12, 1597-1605, (2021).

107) Abdelghany, A. M., E. M. Abdelrazek, and D. S. Rashad. "Impact of in situ preparation of CdS filled PVP nano-composite." Spectrochimica Acta Part A: Molecular and Biomolecular Spectroscopy 130,302-308(2014).

108) M. Muthuvinay, K. Sundara, D. Vanitha and M. Vahini, "Structural and electrical properties of ammonium thiocyanate doped poly ethylene oxide/poly vinyl pyrrolidone blend polymer electrolytes", Vol. 9, 264-267,(2019).

109) Menazea, A. A., and M. K. Ahmed. "Nanosecond laser ablation assisted the enhancement of antibacterial activity of copper oxide nano particles embedded though Polyethylene Oxide/Polyvinyl pyrrolidone blend matrix." Radiation Physics and Chemistry 174, 108911, (2020)..

110) Atkins, Peter, and Julio De Paula. Physical chemistry for the life sciences. Oxford University Press, USA, (2011).

111) Yu, Ming, C. S. Jayanthi, and S. Y. Wu. "Bonding nature, structural optimization, and energetics studies of SiC graphitic-like layer structures and single/double walled nanotubes." arXiv preprint arXiv:0901.3567 (2009).

112) Ramosa, J. M., Maurıcio, M., Anilton Jr, C. C., Otavio, V., and Claudio, A. T. S. "Fourier transform infrared spectrum: Vibrational assignments using density functional theory and natural bond orbital analysis of the bis (guanidoacetate) nickel (II) complex." ScienceAsia 37.3,247-255(2011).

113) Rasheed, Rashed T., Sariya D. Al-Algawi, and Sahar Z. Tariq. "Preparation and Study of Indium Oxide Nanoparticles." Iraqi Journal of Applied Physics 10.4 (2014).

114) K. H. Norman and L. Allinger, "Molecular Mechanics (MM4) Study of Saturated Four-Membered Ring Hydrocarbons", J. Molecular Structure, 3581, 215-237, (2002).

115) R. Y. Hong, J. Z. Qian and J. X. Cao, "Synthesis and Characterization of PMMA Grafted ZnO Nanoparticles", Powder Technology ,163, 160-168, (2006).

116) Karthikeyan, K., Poornaprakash, N., Selvakumar, N., and Jeyasubrmanian, K."Thermal properties and morphology of MgO-PVA nanocomposite film." J Nanostruct Polym Nanocompos 5.4 ,83-88, (2009).

117) Zhu, H. X., Zhou, P. X., Li, X., and Liu, J. M. "Electronic structures and optical properties of rutile TiO2 with different point defects from DFT+ U calculations." Physics Letters A 378.36 ,2719-2724, (2014).

118) Shi, W., Chen, Q., Xu, Y., Wu, D., and Huo, C. F."Investigation of the silicon concentration effect on Si-doped anatase TiO2 by first-principles calculation." *Journal of Solid State Chemistry* 184.8 ,1983-1988, (2011).

119) Fan, Q., Chai, C., Wei, Q., Yang, Y., Qiao, L., Zhao, Y.,and Yao,. R."Mechanical and electronic properties of Ca1− xMgxO alloys." Materials Science in Semiconductor Processing 40 ,676-684, (2015).

120) Indolia, Ajay Pal, and M. S. Gaur. "Optical properties of solution grown PVDF-ZnO nanocomposite thin films." *Journal of Polymer Research* 20.1 ,1-8, (2013).

121) Hazim, Angham, Ahmed Hashim, and HayderAbduljalil. "Fabrication of Novel (PMMA-Al2O3/Ag) Nanocomposites and its Structural and Optical Properties for Lightweight and Low Cost Electronics Applications." Egyptian *Journal of Chemistry* 64.1 ,359-374, (2021).

122) Ahmed, Hind, Hayder M. Abduljalil, and Ahmed Hashim. "Structural, optical and electronic properties of novel (PVA–MgO)/SiCnanocomposites films for humidity sensors." *Transactions on Electrical and Electronic Materials* 20.3 ,218-232, (2019).

123) Kumar, N. B., Vincent Crasta, and B. M. Praveen. "Advancement in microstructural, optical, and mechanical properties of PVA (Mowiol 10-98) doped by ZnO nanoparticles." *Physics Research International* 2014 (2014).

124) Salman, Sabah A., Nabeel A. Bakr, and Mohammed H. Mahmood. "Preparation and Study of Some Electrical Properties of (PVA-Ni(CH3COO)2) Composites." *International Letters of Chemistry, Physics and Astronomy* 40 (2015).

125) Kadham, A. J., Hassan, D., Mohammad, N., and Ah-yasari, A. H."Fabrication of (polymer blend-magnesium oxide) nanoparticle and

studying their optical properties for optoelectronic applications." *Bulletin of Electrical Engineering and Informatics* 7.1 ,28-34, (2018).

126) Z. Hossein and D. Dorranian, , "Effect of dye concentration on the optical properties of red-BS dye-doped PVA film", J*ournal of theoretical Applied Physics*, Vol. 8, No. 139,117-121 ,(2014).

127) M. Ali, "Dielectric and optical properties of (PVAC-PEG-Ber) biocomposites", *Australian Journal of Basic and Applied Sciences*, Vol. 8, No.13, 623-629, (2014).

128) Kan, Caixia, et al. "Formation of gold and silver nanostructures within polyvinylpyrollidone (PVP) gel." *Journal of Solid State Chemistry* 183.4, 858-865, (2010).

129) Abdullah, Omed Gh. "Influence of barium salt on optical behavior of PVA based solid polymer electrolytes." *European Scientific Journal* 10.33 (2014).

130) Abbas, Nada K., Majeed Ali Habeeb, and Alaa J. Kadham Algidsawi. "Preparation of Chloro Penta Amine Cobalt (III) Chloride and Investigate its Influence on the Structural Properties and Acoustical Parameters of Polyvinyl Alcohol." Journal of Kufa-physics 7.2 English and Arabic (2015).

131) M. Venkatara, S. Kilarkaje, A. Prasad and D. Hundekal, , "Refractive index and dispersive energy of NiSO4 doped poly (ethylene oxide) films", *Journal of Materials Science and Engineering* , Vol. 1, 964-973, (2011).

132) Chapi, Sharanappa, and H. Devendrappa. "Optical, electrical, thermal and electrochemical studies of spin-coated polyblend-ZnO nanocomposites." *Journal of Materials Science: Materials in Electronics* 27.11 ,11974-11985, (2016).

133) Abdullah, Omed Gh, Bakhtyar K. Aziz, and Dler Mohammed Salh. "Structural and optical properties of PVA: Na2S2O3 polymer electrolytes films." *Indian Journal of Applied Research* 3.11 ,477-480, (2013).

134) S. Sun , Y. Wang "In situ synthesis of poly nano composites and their optical properties", springer, polymer science, 59, 630-638, (2017).

135) Hayes, Brian S., and Luther M. Gammon. Optical microscopy of fiber-reinforced composites. ASM international, (2010).

136) Matabola, K. P., De Vries, A. R., Luyt, A. S., and Kumar, R."Studies on single polymer composites of poly (methyl methacrylate) reinforced with electrospun nanofibers with a focus on their dynamic mechanical properties." (2011).

137) Mowade, T. K., Dange, S. P., Thakre, M. B., and Kamble, V. D."Effect of fiber reinforcement on impact strength of heat polymerized polymethyl methacrylate denture base resin: in vitro study and SEM analysis." *The journal of advanced prosthodontics* 4.1 ,30-36, (2012).

138) Modak, Sadhan Kumar, Arup Mandal, and Debabrata Chakrabarty. "Studies on synthesis and characterization of poly (methyl methacrylate)-bentonite clay composite by emulsion polymerization and simultaneous in situ clay incorporation." Polymer composites 34.1 ,32-40, (2013).

139) Roque-Ruiz, J. H., Castillo-Ramírez, D., de Jesús Ruíz-Baltazar, Á., Espinosa-Cristóbal, L. F., & Reyes-López, S. Y. "Preparation of silver-doped alumina spherical beads with antimicrobial properties." *Journal of Nanomaterials* 2018 (2018).

140) Awad, M. A., Mekhamer, W. K., Merghani, N. M., Hendi, A. A., Ortashi, K. M., Al-Abbas, F., & Eisa, N. E."Green synthesis, characterization, and antibacterial activity of silver/polystyrene nanocomposite." *Journal of Nanomaterials* 2015 (2015).

141) Oudah, Husham K. "Antibacterial activity and mechanism of the silver nanoparticle in gram positive and negative bacteria." *Iraqi Journal of Physics* 16.39 ,124-134, (2018).